Modelling the Resin Infusion under Flexible Tooling process: a physical and genetic approach

by

J.F.A. Kessels MSc

Thesis submitted for the degree of

Philosophiae Doctor

in

Mechanical Engineering

in the

School of Mechanical and Materials Engineering

of the

North-West University, Potchefstroom Campus

Promoter: Professor J. Markgraaff
Supervisor: Mr. A.S. Jonker

October 2006
Potchefstroom

Abstract

Resin Infusion under Flexible Tooling (RIFT) is a process by which resin is infused through the fibres through the application of a vacuum. Only a one-sided mould is used and the other side is covered with a flexible bag. In the two parts of this thesis a physically based flow model and a genetically based tool are presented to simulate and optimise the RIFT process in advance, both for complex $2\frac{1}{2}$ dimensional geometries.

The flow model of Part I was based on Darcy's law. Due to the flexible bag, the preform compacts during the process and hence the fibre compaction flux term was taken into account and the process was modelled transient. A stabilisation method was developed, using a thickness prediction for a new time step size. Although this prediction was based on a rather crude assumption, it provided a simple and fast way to overcome stability problems.

Experiments were carried out to establish and model the different wet and dry compaction behaviour of two types of preform. The different dry and wet preform properties were also taken into account. A fluid presence function was used for flow front tracking and for the pressure prediction in the partially filled cells. The model was implemented for the use of $2\frac{1}{2}$ dimensional unstructured meshes.

The model was validated with experiments. The compaction of the preform and the flow front propagation during mould filling were measured. It was found that, in the case of highly compactable fibres, the fibre compaction flux term increased the accuracy of the calculated results significantly.

The genetically based tool of Part II is capable of optimising the different process parameters such as flow pipe position and length, fill-distance and number of vents. The tool consists of a mesh distance-based model coupled with a genetic optimisation algorithm.

The mesh distance-based model was based on the assumption that the resin fills the nodes closest to the inlets first. The genetic algorithm was based on the principles of natural selection and genetics and its effectiveness was improved with a variable cross-over rate. The mesh distance-based model was verified with cases known from literature and with the results from the physically based

flow model. The effectiveness of the genetic algorithm was validated with a number of design cases.

For the simple 2D design cases, the tool provided fast solutions which agreed very well with the obvious solutions. For the more complex cases, the algorithm proved to be a very stable and effective method for finding the optimal flow pipe arrangement on any complex geometry.

Uittreksel

"Resin Infusion under Flexible Tooling" (RIFT) word gedefiniëer as die proses waartydens hars in vesels ingesuig word deur middel van 'n vakuum. Die vesels word in 'n oop gietvorm geplaas en die bokant word met dun plastiek materiaal geseël. Hierdie tesis bestaan uit twee dele. In die eerste deel word 'n fisiese en in die tweede deel, 'n geneties gebaseerde vloeimodel gebruik word om die RIFT proses te simuleer en optimaliseer vir komplekse $2\frac{1}{2}$ dimensionele geometrieë.

Die vloeimodel van Deel I is gebaseer op Darcy se wet. As gevolg van die vakuum, druk die plastiek die vesels saam. Daarom word 'n veselkompakteringsvloedterm in ag geneem. Die proses word ook ongestadig gesimuleer. 'n Stabilisasie metode is ontwikkel wat gebruik maak van 'n dikte voorspelling vir die nuwe tydstap interval. Ondanks die growwe aanname van die voorspelling, blyk dit 'n maklike en vinnige manier te wees om stabiliteitsprobleme te oorkom.

Eksperimente is uitgevoer om die samedrukbaarheidsgedrag van twee tipes voorvorms tydens nat en droë toestande te verkry. Die verskillende nat en droë voorvorm karakteristieke is in die model ge-inkorporeer. Verder is 'n vloeistof aanwesigheidsfunksie gebruik vir die vloeifront bepaling en vir die voorspelling van die druk in die gedeeltelik gevulde selle. Die model is geskik vir die gebruik in $2\frac{1}{2}$ dimensionele, ongestruktureerde roosters.

Die numeriese model is verder eksperimenteel geverifieër. Die vervorming van die voorvorm en die vloeifront beweging gedurende die proses is gemeet. Uit die resultate het geblyk dat die veselkompakteringsvloedterm die akkuraatheid van die simulasie resultate aansienlik verbeter in die geval van hoë samedrukbare vesels.

Die geneties gebaseerde program van Deel II van die studie is in staat om die verskillende proses-parameters soos onder andere vloeipyp posisie en lengte, vlociafstand en aantal uitlate te optimaliseer. Die program bestaan uit 'n roosterafstand gebaseerde model gekoppel met 'n genetiese optimaliseringsalgoritme.

Die roosterafstand gebaseerde model is gebaseer op die aanname dat hars die nodes naaste aan die inlate eerste vul. Die genetiese algoritme is gebaseer op die natuurlike seleksie en genetika beginsels waar die effektiwiteit verbeter is deur

'n veranderlike kruisverhoudingstempo. Die model is geverifieer met bestaande gevalle uit die literatuur en met resultate van die fisies gebaseerde vloeimodel. Die effektiwiteit van die genetiese algoritme is getoets met verskillende ontwerpsgevalle.

Vir die eenvoudige 2D ontwerpsgeval gee die model vinnige oplossings wat goed ooreenstem met voor die hand liggende resultate. Vir meer komplekse gevalle blyk die model baie stabiel en effektief te wees vir die verkryging van die optimale vloeipyp posisies.

Contents

List of Figures

List of Tables

Nomenclature

$A_{n,e}$	Cross-Section of the Face Side, n, of Control Volume e.
β	Typical Span Length/Height of a Fibre Beam.
B%	Begin Node Percentage: Percentage of the Main Pipe where the Flow Pipe begins.
BID	Begin Node ID: Node Number where the Flow Pipe begins.
CV	Control Volume.
ϵ	Linear Strain.
e	Control Volume Number.
E	Bending Stiffness.
EID	End Node ID: The Node Number of the End of the Flow Pipe.
F_i	Fitness of Individual i.
GA	Genetic Algorithm.
h	Preform Height.
h_0	Unloaded Preform Height.
I	Fluid Presence Function.
K	Preform Permeability.
l	Length.
$L_{n,e}$	Distance between Control Volume n and e.
LCM	Liquid Composite Moulding.
LVDT	Linear Variable Differential Transformer.
μ	Resin Viscosity.

n	Control Volume Face Number.
n_{edge}	Edge Nodes.
$\vec{n}_{n,e}$	Normal Vector of Face n.
N_a	Maximum Allowable Number of Vents.
N_{nodes}	Number of Nodes in the Model.
N_{pipes}	Number of Pipe Nodes.
N_{vents}	Number of Vents.
ϕ	Porosity of the Preform.
P	Pipe.
P	Probability.
P_{atm}	Atmospheric Pressure.
$P_{crossover}$	Probability of Cross-Over.
$P_{distance}$	Penalty Function for the Fill-Distance.
P_f	Preform Pressure.
$P_{mutation}$	Probability of Mutation.
P_r	Resin Pressure.
P_{total}	Total Net Pressure on the Preform/Resin System.
P_{vac}	Vacuum Pressure.
P_{vents}	Penalty Function for the Number of Vents.
PDE	Partial Differential Equation.
PopSize	Population Size.
q	Resin Flux.
Q	Voluminal Laminar Stationary Flow.
r	Radius.
r_f	Fibre Radius.
RIFT	Resin Infusion under Flexible Tooling
RTM	Resin Transfer Moulding
s	Kozeny Constant.
t	Time.
t_n	Normalised Time.
t_total	Total Mould-Filling Time.
Δt	Time Step Size.
$\bar{u}$	Local Resin Flux Density
$\bar{v}$	Actual Fluid Velocity.
VARI	Vacuum Assisted Resin Infusion.
VARTM	Vacuum Assisted Resin Transfer Moulding.
V_{f_0}	Unloaded Preform Volume Fraction.
V_f	Preform Fibre Volume Fraction.
VOC	Volatile Organic Compound.

w_{vents}	Weighting Factor for the Number of Vents.
w_{pipes}	Weighting Factor for the Number of Pipe Nodes.
$w_{distance}$	Weighting Factor for the Fill-Distance.
x_{max}	Maximum Fill-Distance in the Model.
$\circ$ / ∞	Pipe Nodes.
$\otimes$	Vent.
$\odot$	Inlet.

Preface

In 2001, a research project was initiated at the North-West University to develop, test and produce different types of wind turbine blades, especially for the Southern-African market. The first blade to be developed and produced was a 1.8 m blade. In this framework, a Ph.D. project was started in 2004 to focus on the production technique, especially for larger blades. The goal was to develop a fast, consistent, worker and environmental friendly and cost effective production technique. This technique should be optimised to further reduce production costs and time. It was soon found that the Resin Infusion under Flexible Tooling (RIFT) was the production technique best suited for the production of these large parts. In order to simulate and optimise the RIFT process in advance, two models were developed and are presented in this thesis.

All the modelling work was carried out at the Faculty of Mechanical Engineering of the North-West University in Potchefstroom, South-Africa. The experimental work to determine the material properties, as described in Appendix A and Appendix B, and the experiments to measure the preform thickness during mould filling were carried out at the Faculty of Mechanical Engineering of the University of Twente in Enschede, The Netherlands. The other experiments, as the infusion of the wind turbine blade, were carried out at the workshop of AeroEnergy, Potchefstroom, South-Africa.

The first part of this thesis has already been published in the journal "Composites Part A: Applied Science and Manufacturing" (available online since 15 March 2006) with the title: "Fully $2\frac{1}{2}$D flow modelling of Resin Infusion under Flexible Tooling using unstructured meshes and wet and dry compaction properties". The second part of this thesis is currently in the process of being published, also in the journal "Composites Part A: Applied Science and Manufacturing".

Acknowledgements

First of all I would like to thank Prof. Johan Markgraaff and Mr. Attie Jonker of the North-West University for their professional support, useful and valuable comments, and interesting discussions. It was a privilege to have them as my promoter and supervisor.

I also would like to thank:

AeroEnergy and Jonker Sailplanes for their support and making the experiments possible.

The group of Production Technology of the Faculty of Mechanical Engineering of the University of Twente and especially Prof. Remko Akkerman, who afforded me the opportunity to do the experimental tests, but most of all for his valuable comments and input, enthusiasm and source of motivation. Heel erg bedankt Remko.

The people of the Mechanical Engineering Department in Potchefstroom, and especially Prof. Jat du Toit, Prof. Peet van Schalkwyk, Mr. Willem van Niekerk and Jan-Hendrik Kruger for their valuable input, their interesting conversations, support and many cups of coffee.

Johan Bosman for sharing his office with me, the many pies and his translations into Afrikaans. Baie dankie Bossie.

Mrs. Cecilia van der Walt for the language editing

Volkswagen Business Unit Braunschweig and especially Hans-Werner Scholz for giving me the opportunity to work on my Ph.D.

My parents, brother and relatives for their never ending support.

Mike and Jenny, Sergio and Andrea and all the friends who visited us or live in Potchefstroom and brought a bit of home to our house.

and

Anita, zij weet waarom.

Chapter 1

Introduction

Composites have emerged as a valuable class of engineering materials because they offer many attributes not attainable with other materials. Light weight, coupled with high stiffness, ease of shaping and selectable properties have fostered their use for many years in high performance products as satellite frames, boat hulls, glider fuselages, and also wind turbine blades (Figure 1.1).

Figure 1.1: A wind turbine with three 1.8 meter blades

The primary reason preventing wider usage of high quality fibre reinforced composites is their price. The high costs are primarily due to the material cost itself, but also owing to the high production costs. A wide range of possibilities to manufacture a fibre reinforced composite exist. The oldest and, especially in South Africa with its relatively low labour costs, most common technique to produce composite parts, is hand lay-up. Dry fibre mats are placed into an open mould and plastic resin is poured and distributed by hand over the fibres as a matrix material. The resin cures and the product, made of this composition of fibres, is taken out of the mould.

Although this process is easy, flexible and has low investment costs, a number of disadvantages are linked to it. One of the major disadvantages can be derived from Figure 1.2. This figure shows the contribution of the different process steps to the total production time of a hand lay-up part. These times were measured during the production of one side of a 1.8 meter wind turbine blade at AeroEnergy. The laminating process makes it a very labour and time intensive process. Therefore the labour costs are high and long pot life resins are required.

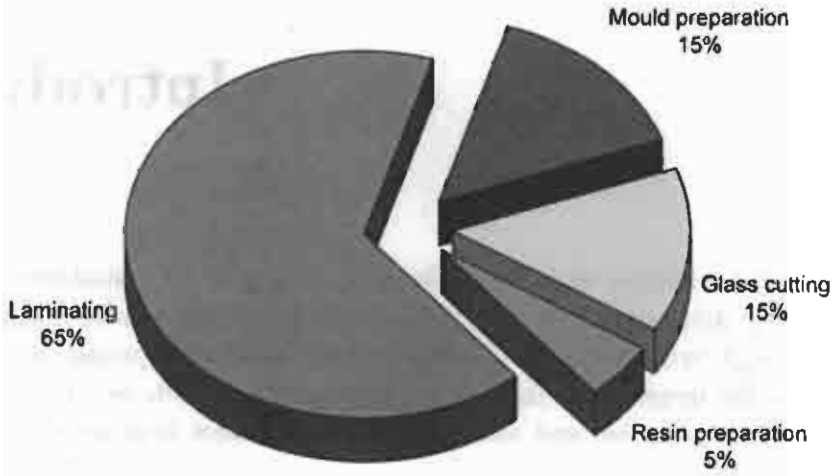

Figure 1.2: Measured hand lay-up process times for one side of a wind turbine blade

Furthermore styrene, a volatile organic compound (VOC), is emitted during this process when polyester-based resins are used. Cases have been reported where this styrene vapour had a detrimental effect on the workers. It can cause depression and fatigue and in severe cases psychiatric symptoms (White *et al.*, 1990; Castillo *et al.*, 2001). New legislation dealing with VOC emissions has identified styrene as the main harmful substance to eliminate. In the UK, the limit has been set at 50 ppm, requiring the users to seek new production methods. Another disadvantage is that the fibre volume fraction and void content are hard to control and hence final product properties may vary largely (Williams *et al.*, 1996).

Closed Liquid Composite Moulding (LCM) processes overcome most of these disadvantages. The two most common ones, Resin Transfer Moulding (RTM) and the Resin Infusion under Flexible Tooling (RIFT), will be discussed in the subsequent sections.

1.1 Resin Transfer Moulding

In the Resin Transfer Moulding (RTM) process several layers of dry continuous strand mat, woven roving, or cloth are placed in the bottom of a two-part mould. The mould is closed, and a catalyzed liquid resin is injected into the mould. Typically, a pressure between 2 and 10 bar is used, but the resin can also be drawn into the mould by a vacuum pressure. As the resin spreads throughout the mould, it displaces the entrapped air through the air outlets and impregnates the fibres. Depending on the type of resin-catalyst system used, curing is performed at either room temperature or an elevated temperature in an oven. Once the cured part is pulled out of the mould, it is often necessary to trim the part at the outer edges to conform to the exact dimensions (Miravete, 1999).

Instead of filling the bottom mould with fibres, a preform, which already has the shape of the desired product, can be used, as depicted in Figure 1.3. Some advantages of using a preform are good mouldability with complex shapes (Mallick, 1988) and the elimination of the trimming operation (near-net-shape production), which is often the most labour-intensive step in a RTM process (Miravete, 1999).

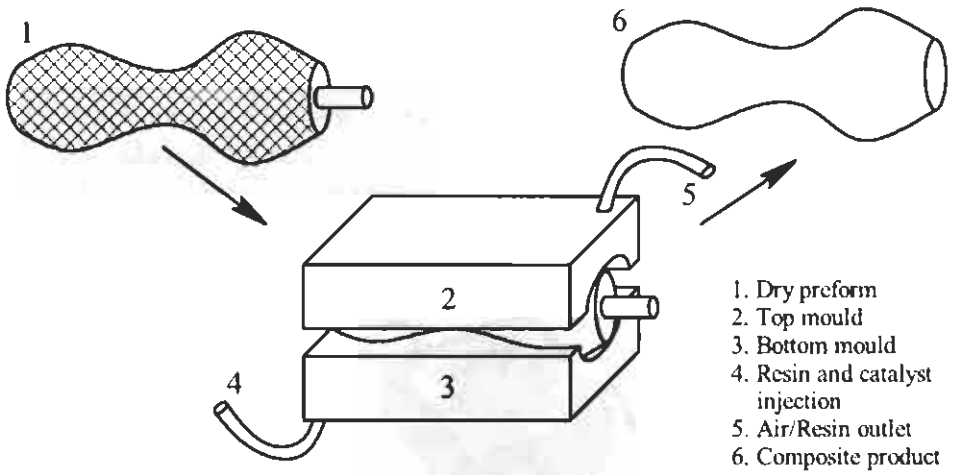

Figure 1.3: Resin Transfer Moulding using a preform

The major advantages of the RTM process compared to the hand lay-up include (Loos, 2001):

- Near net-shape moulded parts;
- Short cycle time;
- Close dimensional tolerances;

- Void-free, structural quality parts;
- Closed mould process, reduced volatile emissions;
- Smooth surface. Finish on both sides of the part can be of class A.

Unfortunately the RTM process requires more expensive double-matching moulds. Handling of the matching mould can become a serious problem, especially for larger products such as big wind turbine blades. The use of a single-sided or even an existing hand lay-up mould is preferred for these cases. Such a process already exists and is called Resin Infusion under Flexible Tooling (RIFT).

1.2 The Resin Infusion under Flexible Tooling Process

In RIFT, existing hand lay-up moulds can be used with only minor alterations. The dry fibre mats or preform are/is draped into or onto the female/male mould and then covered by a semi-flexible plastic sheet (bag). The mould and bag are sealed and placed under vacuum. The resin, which is drawn into the mould by this vacuum, impregnates the fibres. A sketch of the process can be seen in Figure 1.4 and a cross-section of the process in Figure 1.5.

In literature, the RIFT process is often also referred to as Vacuum Assisted Resin Infusion (VARI), or the Vacuum Assisted Resin Transfer Moulding (VARTM) process (Acheson *et al.*, 2004; Correia *et al.*, 2004). The term VARTM is in practice also used for the version of the RTM process, where no injection pressure

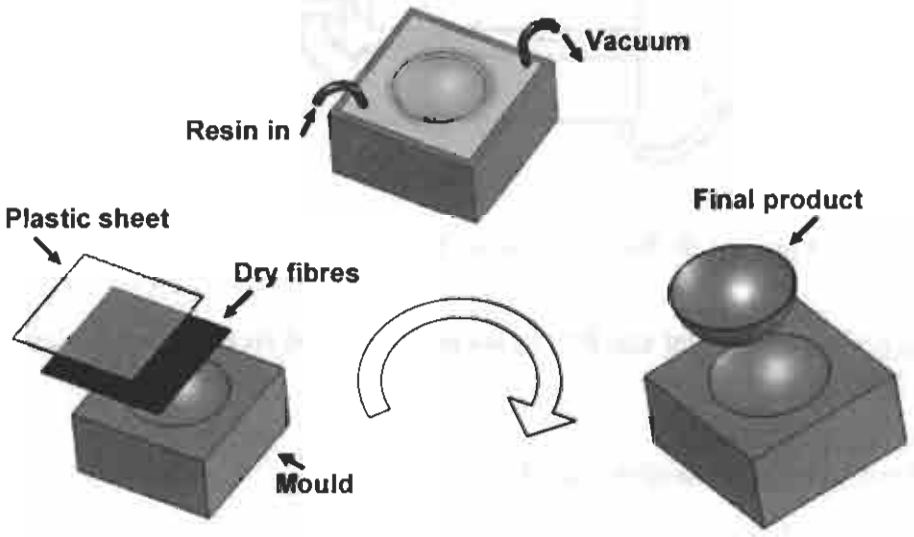

Figure 1.4: Schematical representation of the RIFT process

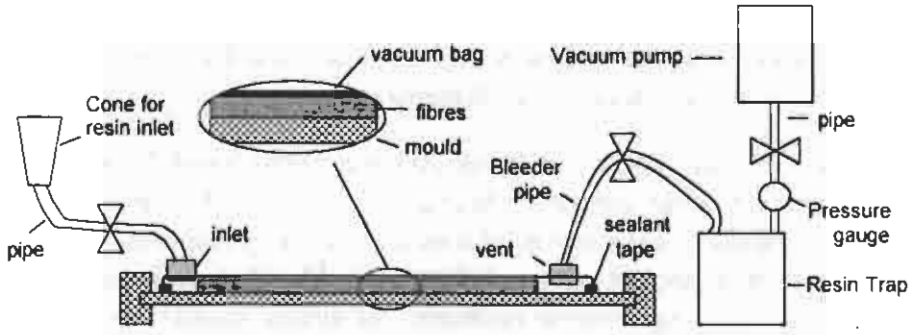

Figure 1.5: Cross-section of the RIFT process on a flat mould

is applied to the inlet, only a vacuum on the outlet. Therefore only the term RIFT will be used here.

Compared to open mould manufacturing, RIFT has various advantages.

- Reduced volatile organic compound emissions. Experimental results show that more than 90% of the VOC emissions from resin is eliminated (Han *et al.*, 2000).
- Reproducible process (Thagard *et al.*, 2003).
- Reduced part weight because less resin can be used as the fibre mats are compressed (Han *et al.*, 2000; Craen *et al.*, 1998). As a result, resin costs are reduced as well.
- Reduced void content and hence higher quality products are produced since gas is expelled by a vacuum (Han *et al.*, 2000). Hand-laid composites always show distinct voids (Summerscales, 2002). Although remaining gas in the resin can also form large voids during RIFT, correct degassing at a lower absolute pressure than the process pressure overcomes this problem.
- Existing hand lay-up moulds can be used with only minor alterations (Thagard *et al.*, 2003).
- Higher production rate versus hand lay-up (Thagard *et al.*, 2003).
- RIFT has the ability to produce very large components and the tooling costs are lower compared to RTM (Thagard *et al.*, 2003).

The first versions of the RIFT process were already described in 1950 as the "Marco Method". It was designed in the USA for manufacturing boat hulls with reduced voidage and tooling costs when compared to RTM (Marco, 1950). In this method, dry reinforcement was laid up onto the solid male tool and a semi-flexible/splash female tool was used for consolidation and to provide a seal for the application of vacuum. It was only in the late 70s that the method became

more widely adopted. Up until then, the composite manufacturing industry was a rather under-regulated industry and resin and reinforcement development favoured open mould lay-up or spray deposition.

In 1974, the Health and Safety at Work Act was introduced to reduce styrene emissions into the work environment. In reaction, Gotch (1978) presented the use of vacuum impregnation using one solid tool face and a silicone rubber diaphragm bag. Liquid resin was poured onto preplaced dry fibre before being enclosed by the bag. Besides reducing styrene emission, moulding quality was higher than that achieved by using hand lay-up.

In the 1980s, the use of a rubber bag as a flexible tool was further investigated and as a result Seemann (1989) patented the "Seemann Composites Resin Infusion Molding Process" (SCRIMP). SCRIMP is very similar to the RIFT process, but it uses a mesh of flow channels, integrated in the flexible bag, to distribute the resin.

Nowadays, many manufacturers of large composite structures such as wind turbine blades and boat hulls use the RIFT process. For these large structures, flow enhancement structures are normally used to speed up the process. Figure 1.6 shows a coarse infusion mesh and a spiral bind infusion pipe which are commonly used. The infusion mesh is a flow distribution medium, while the spiral bind functions as a flow channel. Both have a much better permeability than the preform and are therefore placed between the preform and the plastic bag, improving the overall permeability. With the help of these flow enhancement structures, large components can be infused in a relatively short space of time. Brouwer *et al.* (2003) and Gunnarsson (2004) presented some very impressive examples, e.g. an infusion of an 11.8 m boat hull in only 195 minutes with 340 kg of resin.

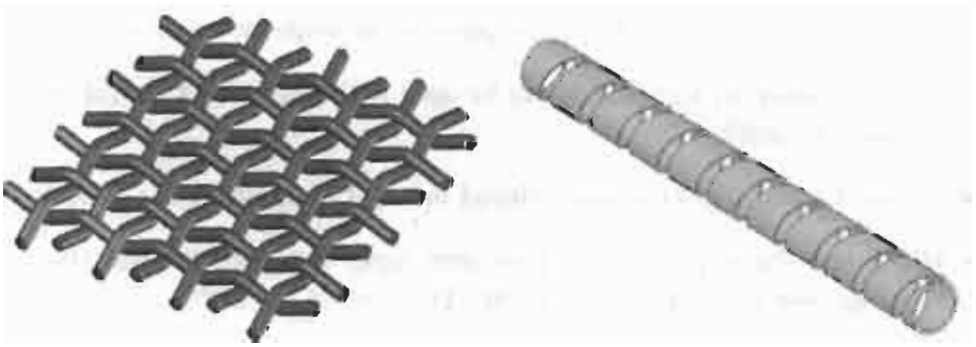

(a) infusion mesh (b) spiral bind

Figure 1.6: Flow enhancement structures.

Although RIFT overcomes most of the problems of hand lay-up, such as styrene emission and reproducibility, a number of disadvantages are also linked to it, which include the following:

1. Product properties and process parameters correlate strongly and hence there is limited direct control over the final product properties (Williams *et al.*, 1996).
2. The risk of failures, compared to hand lay-up, in very large products is often considered to be too high (Brouwer *et al.*, 2003).
3. More consumables are being used compared to RTM or hand lay-up (Summerscales, 2002; Thagard *et al.*, 2003).
4. Surface quality can be a problem (Summerscales, 2002).

The flexible bag allows the preform to compress under the vacuum pressure. Figure 1.7 schematically shows this behaviour during the process. On the left hand side, the resin enters the process with atmospheric pressure and therefore the preform is uncompressed. On the right hand side of the flow front, the pressure equals the applied vacuum pressure, causing the preform to be compressed.

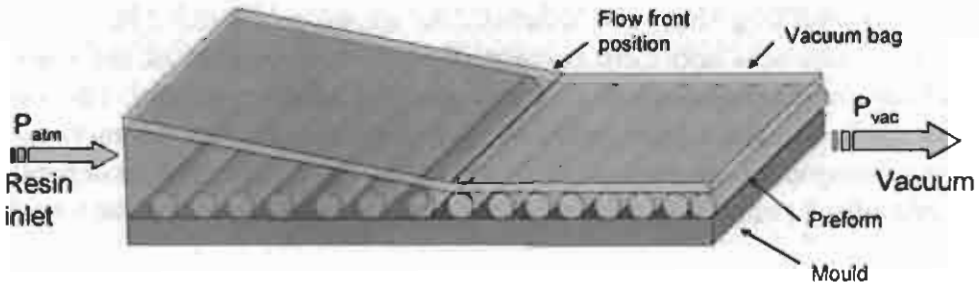

Figure 1.7: Change in preform thickness due to the pressure gradient

Between the resin inlet and the flow front there will be a pressure gradient going from atmospheric to vacuum pressure. This pressure gradient results in a gradient of the preform thickness as well. This reduction and gradient of the preform thickness results in higher fibre volumes compared to hand lay-up, which is desirable in most cases. However, there is limited direct control over the thickness, because it depends on the pressure gradient. Limited direct control over the thickness also means limited control over the fibre content of the final composite laminate and hence final product properties.

The preform compression also causes a reduction of the preform permeability. Hence infusion times are much longer and more unpredictable compared to RTM, increasing the risk of failure significantly.

The process requires single-use ancillary materials such as the bagging film, seals and flow enhancement pipes and/or breather clothes for resin flow enhancement, increasing the costs of consumables (Summerscales, 2002; Thagard *et al.*, 2003).

With respect to the product properties and quality, RIFT can produce laminates with a surface which echoes the topology of the reinforcement fabric. This "print-through" effect is a problem when a good surface finish is required (Summerscales, 2002; Hammami & Gebart, 2000). However, in most practical applications a layer of clear paint or gel coat is applied on the final product making this problem less critical.

1.3 Problem Definition

The previous section explained the great potential of RIFT for the production of large components such as wind turbine blades, but also its disadvantages.

Crucial in a production environment is to exactly know filling times and final product properties in advance in order to prevent expensive failures. If, for example, the fill time is longer than the gel time of the resin used, the process will result in incomplete mould-filling (Hsiao *et al.*, 2004). The previous section revealed that the process parameters and product and process properties (for instance mould-filling time) are related. As shown in Figure 1.8, the mould-filling time, thickness and fibre content depend on a number of variables: the permeability and compressibility of the preform under pressure, the vacuum pressure itself, the resin inlet position, and viscosity and the interactions with the flow enhancement structures (Williams *et al.*, 1996). Due to this dependency, the mould-filling time, final part thickness and fibre content correlate with one another.

Thagard *et al.* (2003) and Hou & Jensen (2004) presented a double-vacuum-bag

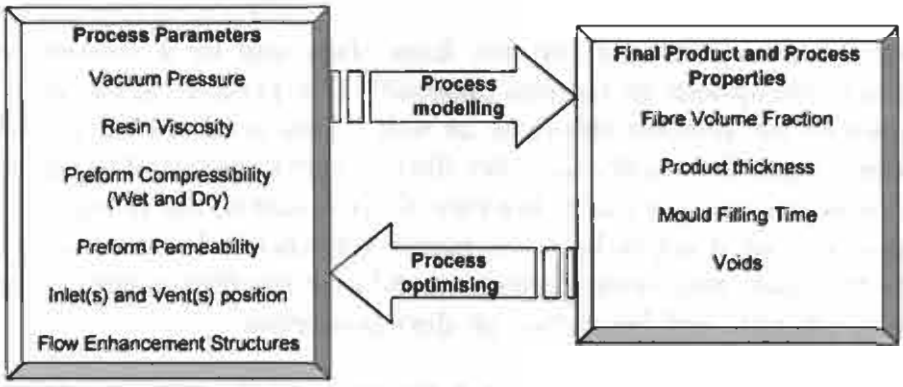

Figure 1.8: Process parameters and final properties

process which overcomes this dependency, but it requires more expensive tooling and is therefore not attractive for smaller production numbers.

A way to know the filling times and final product properties in advance is to develop a full process model and hence develop a full process understanding. Various researchers have worked on these kinds of models and tools (Gutowski *et al.*, 1987; Han *et al.*, 2000; Hammami & Gebart, 2000; Acheson *et al.*, 2004; Correia *et al.*, 2004; Lopatnikov *et al.*, 2004; Grimsley *et al.*, 2001). A detailed overview of this modelling effort will be given in the next chapter. Almost all these models assume a quasi-static process and do not use a different wet or dry preform compaction. Many researchers found, however, that there is a significant difference between the wet and dry preform compaction (Craen *et al.*, 1998; Williams *et al.*, 1998; Andersson *et al.*, 2003). The permeability and hence the fill-time is a function of this preform compaction. Therefore the process should be modelled as fully transient and has to include different wet and dry preform properties.

Once a full process model has been developed, the process parameters can be optimised in order to save process time and costs and achieve optimum product properties.

The ideal process would be fast (short infusion paths and high permeability), give a high fibre volume fraction without any air entrapments and would not require any ancillary goods (for example flow pipes). However, these requirements are conflicting for RIFT processing. A fast process requires the use of flow pipes and flow enhancement layers. Increasing the fibre volume fraction will decrease the permeability of the preform and hence increase the infusion time. Therefore an optimum of the process properties has to be determined by the user, e.g. should the process be fast or have low-cost or result in a product with a maximum fibre volume.

After the optimum process properties are determined, the optimum process parameters need to be established in order to match the optimum process properties. The optimum process parameters could be determined by trial and error, but also here representive computer simulations save significant cost and time.

1.4 Research Objectives

Based on the problems indicated in the previous section, the following research objectives were formulated:

1. Be able to predict the RIFT process, such as filling-time and final product properties.

2. Be able to optimise the RIFT process in advance in order to meet the optimum process properties.

1.5 Research Activities

To obtain these research objectives, the following research activities were planned and carried out:

Process modelling

- Model the RIFT process in order to find the correlation between the process parameters and the process and product properties.
- Experimentally determine the material property data required for the process model.
- Develop, where necessary, new material models to implement the results of these test into the RIFT process model.
- Implement this full process model into a computer simulation tool which can handle arbitrary $2\frac{1}{2}$D geometry.

Verification

- Verify the process model with known analytical solutions.
- Develop an experimental facility to measure the product and process properties such as preform thickness and flow front position during the process.
- Verify the model with experiments using this test facility.

Process optimisation

- Develop an algorithm which optimises the process for the lowest costs (minimal amount of consumables and mould-filling time) and the highest quality products (minimal number of voids).
- Implement this algorithm in a fast computer simulation tool which can handle arbitrary $2\frac{1}{2}$D geometry.

Verification

- Verify the optimisation tool with cases known in literature.
- Verify the optimisation tool with practical design cases.

1.6 Structure of the Research

This research is divided into two parts, corresponding to the two research objectives. Part I deals with the first research objective, Part II with the second objective. Together, the two parts present a full model for both prediction and optimising the RIFT process:

Part I: Physical Approach presents a full $2\frac{1}{2}$D flow model of resin infusion under flexible tooling using unstructured meshes and wet and dry compaction properties.

- **Chapter 2 Modelling the RIFT Process** commences with a literature survey of the previous modelling effort. The governing model equations are presented, as well as the discretisation methods. Finally a method to track the flow front is proposed.
- **Chapter 3 Validation of the Model** presents the verification of the model with known analytical solutions and experimental results.
- **Chapter 4 Discussion of the Physical Approach and its Results** discusses the model, its accuracy and the comparison with the experimental results.

Part II: Genetic Approach will present a tool to optimise the RIFT process in terms of production time and production costs.

- **Chapter 5 Model for Optimising RIFT** starts with an overview of controllable process parameters, followed by a literature survey on the previous modelling effort to optimise the RIFT process. The method of optimisation is presented. A new, mesh distance-based model, is presented to calculate these process properties. This model is specially developed for optimisation purposes and is much faster than the model presented in Part I. This model is coupled with a Genetic Algorithm. The principles of Genetic Algorithms are explained, together with the used optimising algorithm and functions. Finally, the mesh distance-based model is integrated into this genetic optimisation algorithm, providing a tool for optimising the RIFT process.
- **Chapter 6 Simulations and Results** A number of design cases is simulated using the developed optimisation routine. Their results and verifications are presented.
- **Chapter 7 Discussion of the Genetic Approach and its Results** discusses the genetically based optimisation tool, its effectiveness and accuracy and the results of the design studies.

Chapter 8 General Conclusion and Recommendations presents the final conclusions and recommendations of the research.

Part I

Physical Approach

Chapter 2

Modelling the RIFT Process

2.1 Previous Modelling Effort

Many models have been developed in the past to simulate the RIFT process. In order to give a short overview of all these modelling efforts, a number of models will be discussed here in chronological order (Gutowski *et al.*, 1987; Han *et al.*, 2000; Hammami & Gebart, 2000; Andersson *et al.*, 2003; Song *et al.*, 2004; Acheson *et al.*, 2004; Correia *et al.*, 2004).

Almost all models were developed to simulate the RIFT process for 3D parts, for which, logically, 3D models would be required. Since the thickness of composite parts is often much smaller than their length and width, thin film part assumptions were used for these simulation models. For example the resin flow in the thickness direction (here denoted as z) was neglected. Therefore these models, although they describe 3D geometries, are often called $2\frac{1}{2}$ dimensional ($2\frac{1}{2}$D) flow models.

The article of Gutowski *et al.* (1987) is one of the earliest complete mathematical descriptions of the RIFT process. Like all later models, it describes the resin flow through the porous prefom using Darcy's Law. This law was originally derived in 1856 by the French hydraulic engineer Henry Darcy. It was originally derived for water flow through porous soil, but is generally accepted to describe the flow through fibre beds as well. According to this law the relation between the local resin flux density (also called superficial velocity), $\bar{u}$, an isotropic preform permeability K, the resin viscosity μ and the resin pressure gradient ∇P_r, can be written as:

$$\bar{u} = -\frac{K}{\mu}\nabla P_r \tag{2.1}$$

Gutowski *et al.* (1987) also assumed that the fibres make up a deformable, non-linear elastic network. Based on a control volume of length dx, width dy and

height dz (see Figure 2.1) the following resin continuity equation was derived:

$$\frac{\partial}{\partial x}((1+\epsilon)u_x) + \frac{\partial}{\partial y}((1+\epsilon)u_y) + \frac{\partial}{\partial z}(u_z) + \frac{\partial}{\partial t}(\phi(1+\epsilon)) = 0 \qquad (2.2)$$

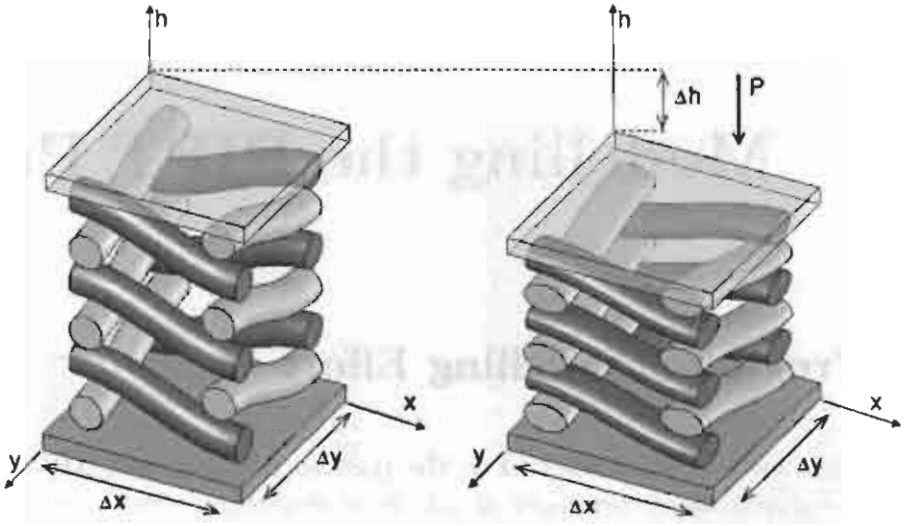

Figure 2.1: The unit cell with deformable fibres.

In this equation, ϵ is the relative change (linear strain) in the z direction and ϕ is the porosity of the preform. The preform compression was modelled by assuming that the preform consists of bending beams of fibres. In later articles, this compression model is referred to as the Gutowski model.

The Kozeny-Carman Theory (Scheidegger, 1974) was used to describe the relation between the fibre volume fraction and the permeability. These basic equations were combined and solved for 1D and 2D compression moulding and for bleeder ply moulding.

Han *et al.* (2000) used these equations to model the flow for the SCRIMP process. As already mentioned in Chapter 1, this process is very similar to the RIFT process, but it uses a mesh of flow channels to distribute the resin. In this case, the mesh was integrated into the flexible bag. Han *et al.* (2000) combined the Navier-Stokes equation for the flow in the channels with Darcy's law for the flow in the preform. The preform compressibility was modelled using a power law function, and the Kozeny-Carman equation was also used to model the permeability. A control volume method was used to solve the continuity equation where the term $\frac{\partial}{\partial t}(\phi(1+\epsilon))$ was kept zero at every time step. This term will later be referred to as the preform compaction flux, because it actually describes the time derivative of the preform height ($\frac{\partial h}{\partial t}$). It should not be confused with the total preform compaction, Δh.

Hammami & Gebart (2000) used the same functions (however, fitted to their own experimental results) but they only looked at the flow in the preform. A significant difference between the wet and dry compression behaviour of the preform was observed but it was not used in the model. A quasi-stationary process was assumed and therefore the preform compaction flux term was neglected, although at that time it was not proven that this approximation was valid.

Andersson *et al.* (2003) also used this assumption. They incorporated the equations for the RIFT process into a commercial 3D CFD software package (CFX-4), taking wet and dry preform compaction into account. It was shown that the thickness of the preform decreased towards the outlet during the filling process. In addition, as Williams *et al.* (1998) also indicated, a thickness minimum was observed instantly behind the resin flow-front because of a change in stiffness due to wetting of the preform.

Song *et al.* (2004) used a similar model to that of Andersson *et al.* (2003) but also modelled the resin curing by taking the resin viscosity as a function of time and temperature. Mould-filling with different types of flow enhancement layers was simulated and validated experimentally. It was shown that the process is significantly faster if these layers are used and that the process can be predicted accurately if these layers are modelled correctly.

Acheson *et al.* (2004) developed a $1\frac{1}{2}$D model to verify the correctness of the assumption to ignore the preform compaction flux term. For the materials used in their article, and because only one preform compaction behaviour was used, this term was very small and hence negligible. A sink term was used to model the fluid flow into the single fibre tows. RTM models were shown to give similar results if an "effective" permeability was used. However, this effective permeability had to be different for the same material being injected under different pressures.

Based on this work, Correia *et al.* (2004) also incorporated this model, like Acheson *et al.* (2004), into existing 2D/3D flow simulating software (in this case LIMS) making it possible to perform $2\frac{1}{2}$D analyses. Also in their case, the preform compaction flux was ignored and the difference between wet and dry preform compressibility not taken into account.

Looking back at all the modelling efforts conducted in the past, it can be concluded that almost all models assume a quasi-stationary process and hence ignore the preform compaction flux term. Furthermore, only Andersson *et al.* (2003) included both the wet and dry preform compressibility and showed that this can have a significant effect on the height distribution during the filling stage. Evidently the process cannot be considered as quasi-static in the general case because of the relatively sudden change in height (hence height flux) at the flow front as soon as the preform wets out. In the subsequent sections a newly developed transient $2\frac{1}{2}$D model is presented that includes the preform compaction

flux term and both the wet and dry preform compressibility.

2.2 Governing Equations

The newly developed RIFT model is based on a number of assumptions. Firstly, the Reynolds numbers are low (laminar flow) for the resin flow, wall effects are ignored, there is no pressure gradient in the z direction and the flow can be described using Darcy's law (Eq. 2.1). Secondly, the resin is incompressible and its viscosity stays constant during the filling stage.

The first assumption restricts the model to preforms with a uniform flow through the thickness. There are two situations in which this occurs: The different plies have a uniform permeability over the thickness, or the flow is dominated by the layer with the highest permeability. An example of the latter is preform packs which consist of a thick flow enhancement core which is covered by only a few single plies of (woven) fabric. In such a preform the single plies of fabric are wetted almost instantaneously as the resin reaches the underlying core; hence the flow can be assumed to be uniform (Grimsley *et al.*, 2001). The CoreTEX fabric, which will be presented later is an example of such a preform.

As for all other models, Terzaghi's law is assumed in the wetted region (Terzaghi & Peck, 1963). It states that the total pressure is distributed over the resin, P_r, and the compactible preform, P_f, as given by the following equation:

$$P_{total} = P_{atm} - P_{vac} = P_f + P_r \tag{2.3}$$

In this equation, P_{total}, is the total net pressure on the preform/resin system, which is the difference between the atmospheric pressure, P_{atm}, and the pressure achieved by the vacuum pump, P_{vac}.

The compaction of the preform under a pressure P_f causes a reduction of the height preform from h_0 to $h_0 - \Delta h$, as depicted in Figure 2.1. It is assumed that the volume of the fibres in the control volume is constant, and hence the relation between the initial (unloaded), V_{f_0}, and current fibre volume fraction, V_f, the initial, h_0, and current height, h, is given by the following standard equation:

$$(1+\epsilon) = \frac{V_{f_0}}{V_f} = \frac{h}{h_0} \tag{2.4}$$

The behaviour of the preform under a pressure P_f and the resulting increase of the fibre volume fraction and decrease in permeability can be modelled in numerous ways. A short overview of previous modelling efforts of other researchers for both the compressibility and permeability is given in Appendix A and Appendix

B. Both Appendices also present the experiments, carried out in the framework of this research, to model the material behaviour for the materials investigated here. Appendix A presents the experiments and results used to model the compaction behaviour. Appendix B presents the experiments and results used to establish the permeability behaviour of these materials. The permeability was modelled using a power law function and the compressibility with a power law and a logarithmic function.

Subsequently all the factors in Equation 2.1 are defined. Substituting this equation into the continuity equation (Eq. 2.2), with $u_z = 0$, leads to the following time-dependent partial differential equation:

$$\begin{aligned} \nabla \cdot (1+\epsilon)\bar{u} + \frac{\partial}{\partial t}(\phi(1+\epsilon)) &= \nabla \cdot (\frac{h}{h_0})(-\frac{K}{\mu}\nabla P_r) + \frac{1}{h_0}\frac{\partial h}{\partial t} = 0 \\ &\Downarrow \\ \nabla \cdot (h\frac{K}{\mu}\nabla P_r) &= \frac{\partial h}{\partial t} \end{aligned} \tag{2.5}$$

In the next section, the discretisation of this PDE using a finite volume representation will be discussed.

2.3 Numerical Model

The main advantages of the finite volume method are that it can accommodate any type of grid, which makes it suitable for complex geometries, and all terms which need to be approximated have a physical meaning and hence it is simple to understand (Ferziger & Perić, 1997; Versteeg & Malalasekera, 1995). The solution domain was subdivided into a finite number of contiguous control volumes (CVs), in this case triangles. At the centroid of each CV lies a computational node at which the variable values were calculated (see Figure 2.2). For each of these CVs the PDE of continuity Eq. 2.5 was written with the following integrals:

$$\int_A \vec{n} \cdot (h\frac{K}{\mu}\nabla P_r)\, dA = \int_V \frac{\partial h}{\partial t}\, dV \tag{2.6}$$

The left hand term represents the net rate of flow into the CV and the right hand term represents the increase of the volume of the CV due to a change in height. Hence, for CV e in Figure 2.2, with the net flow over its 3 faces, n, these

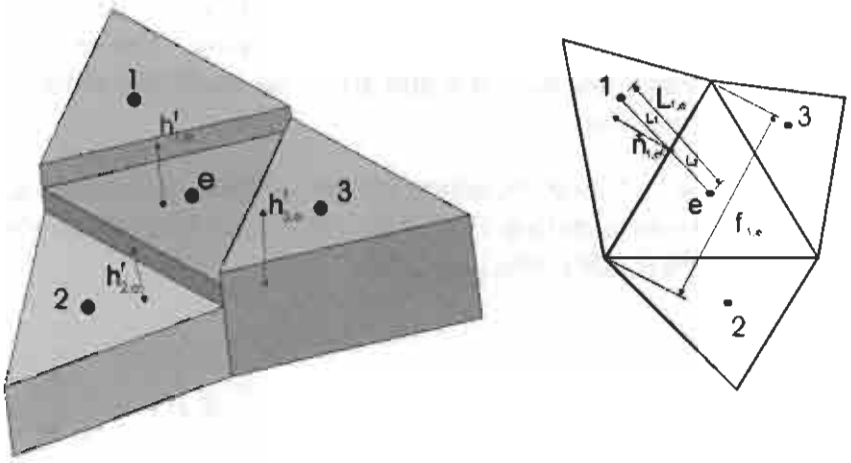

Figure 2.2: Schematical representation of Control Volume e and its neighbours

integrals could be discretised as:

$$\sum_{n}^{1..3} C_{n,e}(P_n - P_e) = \frac{h_e^t - h_e^{t-1}}{\Delta t} V_e \tag{2.7}$$

with

$$C_{n,e} = h_{n,e}^f \frac{K_{n,e}^f}{\mu} \frac{A_{n,e}}{L_{n,e}} \cdot \vec{n}_{n,e} \tag{2.8}$$

In this equation $h_{n,e}^f$ and $K_{n,e}^f$ are, the height and the permeability respectively, of CV e at its face n, $A_{n,e}$ is the cross-section of the face side n, P_n and P_e are the pressures at the neighbour CV n and the CV e itself respectively, V_e is the volume of the CV e , $L_{n,e}$ is the distance between the centroid of CV n and CV e, h_e^t is the height at the CV's centroid at time step t, and finally, $\vec{n}_{n,e}$ is the normal vector of face n. The time step size, Δt, is the difference between the time at calculation step t and $t-1$. The height at the CV faces was interpolated from the values at the centroids using an arithmetic mean (Patankar, 1980). For example in Figure 2.2:

$$h_{1,e}^f = (1-f)h_e + (f)h_1 \tag{2.9}$$

with

$$f = L_2/L_{1,e} \tag{2.10}$$

The permeability at the faces was calculated from these heights using the func-

tion of Table B.1. The cross-section of the faces was calculated by using the length, $f_{n,e}$, of face n of CV e: $A_{n,e} = f_{n,e} \cdot h^f_{n,e}$. The assembly of Equation 2.7 for all CVs led to the following linearised system:

$$\begin{bmatrix} -(C_{i,1} + C_{j,1} + C_{k,1}) & \dots & C_{i,1} & C_{j,1} & & C_{k,1} \\ \dots & & & & & \\ C_{1,c} & & C_{2,c} & C_{3,c} & \dots & -(C_{1,c} + C_{2,c} + C_{3,c}) \\ \dots & & & & & \end{bmatrix} \begin{bmatrix} P_1 \\ \dots \\ P_c \\ \dots \end{bmatrix} = \begin{bmatrix} \frac{h^t_1 - h^{t-1}_1}{\Delta t} V_1 \\ \dots \\ \frac{h^t_c - h^{t-1}_c}{\Delta t} V_c \\ \dots \end{bmatrix} \tag{2.11}$$

Knowing that the resin pressure is equal to the vacuum pressure at the flow front and equal to the atmospheric pressure at the inlet, it was now possible to calculate the pressure field in the wetted region. This pressure field was used to calculate the height and the permeability per CV. The pressure field for the current time step was then calculated again with these new values for h and K until the difference between the previously and newly calculated pressure fields were within a certain tolerance.

2.4 Flow Front Tracking

For the calculation of the pressure field, the position of the flow front was required. For the $1\frac{1}{2}$D case, as presented by Hammami & Gebart (2000) and Acheson *et al.* (2004), the position of the flow front can be found by integrating the fluid velocity over the time t. Note that Equation 2.1 only gives the resin flux density. The actual fluid velocity, $\bar{v}$ is the resin flux density divided by the porosity, ϕ, which equals one minus the fibre volume fraction, V_f:

$$\bar{v} = \frac{1}{(1 - V_f)} \cdot \bar{u} = \frac{1}{\phi} \cdot \bar{u} = -\frac{K}{\mu \cdot \phi} \cdot \nabla P_r \tag{2.12}$$

For the $2\frac{1}{2}$D case, the position of the flow front is more difficult to determine. In many cases, eg. with multiple inlets, even multiple flow fronts may exist.

Although various ways of flow front tracking exist, there are two main approaches: moving and fixed grid techniques. The moving grid technique is based on remeshing of the saturated part of product as the fluid propagates. The accuracy is generally better than fixed mesh techniques, but due to the frequent remeshing, CPU time is much higher (Garcia *et al.*, 2002).

For the fixed grid approach, there are also a number of ways to keep track of the flow front (Hirt & Nichols, 1981; Ferziger & Perić, 1997; Versteeg & Malalasekera,

1995; Garcia *et al.*, 2002). Here the Volume of Fluid technique was chosen (Hirt & Nichols, 1981; Garcia *et al.*, 2002). This technique uses CVs as well. There are different ways to define these CVs. A common method is to associate one CV with each node of the finite element mesh. In case of a triangular mesh, the control volume itself is then defined by lines that go through the centroids of the elements, associated with that node point. For example Koorevaar (2002) and Lee *et al.* (1994) use a control volume method to simulate the RTM process with one mesh for the computation of the pressure field and another (staggered) to update the flow domain. The advantage of this control volume method is that the values at the nodal points are automatically known, but it adds to CPU time and -storage requirements because track needs to be kept of 2 meshes. Therefore the same mesh for the pressure and fluid domain was used here.

The main advantage of the Volume of Fluid technique is that only one value (the fluid presence, I) has to be stored. This fluid presence function, I, represents the relative volume of fluid in a cell increasing from zero for an empty volume to one for a fully saturated volume. Furthermore, also only one scalar convective equation, like other transport equations, needs to be solved. Unfortunately, it has the disadvantage that for most solution schemes, for example first order upwind, the position of the flow front tends to smear out over several CVs. To overcome this problem, different techniques have been presented in the past, for example the donor-acceptor formulation (Hirt & Nichols, 1981). Here a central difference scheme with variable time steps (Patankar, 1980; Davis, 1994) was adopted, which is easily implemented, less diffusive and suitable for low Reynold numbers.

The fluid presence was also used to calculate the pressure field in the flow front itself. For the empty control volumes $P_r = P_{vac}$. In the fully saturated columes, Eq. 2.5 is valid. A combined equation was used for the partially filled ($0 < I < 1$) volumes (Hirt & Nichols, 1981; Garcia *et al.*, 2002).

$$I \cdot \left[\nabla \cdot h\frac{K}{\mu}\nabla P_r\right] + (I-1)\left[P_r\right] = I \cdot \left[\frac{\partial h}{\partial t}\right] + (I-1)\left[P_{vac}\right] \tag{2.13}$$

The volume of resin into each CV volume at the flow front (where $0 < I < 1$) was calculated from the velocity field at every time step. This calculation is similar to any fluid quantity in the flow (such as density, pressure, etc.) and can be written as (Ferziger & Perić, 1997):

$$\frac{\partial I}{\partial t} + \bar{v} \cdot \nabla I = 0 \tag{2.14}$$

Care had to be taken that $I \leq 1$ for every CV, when solving Eq. 2.14, especially for the flow front CVs. If the time step, Δt, becomes too large, it can happen that, for this time step, the flow front moves over more than one CV and hence I

becomes larger than unity for this certain (flow front) CV. Several methods have been developed in the past as flux and slope limiters (Garcia *et al.*, 2002) and also the previously mentioned donor-acceptor method overcomes this problem (Hirt & Nichols, 1981). The method used here was to select at each iteration the shortest time step, Δt, to fill exactly a single CV. This method is widely used and gives good results (Gutowski *et al.*, 1987; Koorevaar, 2002).

By changing Δt to fill exactly one single CV, the term $\frac{h_c^t - h_c^{t-1}}{\Delta t} V$ of Eq. 2.11 changes also. This term is defined here as b_c. In order to prevent stability problems when solving Eq. 2.11 with this new Δt, a prediction of h_c^t is made. The following prediction schemes could have been used:

- The b_c from the last iteration step is being used. Besides not making any physical sense, stability problems occur during the solving of Eq. 2.11.
- The h_c^t is assumed to be h_c^{t-1} and hence the right hand term of Eq. 2.11 is 0. This could lead to higher calculated pressure on the fibres for certain CVs than the previous time step, resulting in negative Δh and hence a change of sign of the right hand term of Eq. 2.11. Due to the highly non-linear behaviour of the fibres under compression, this may lead to stability problems as well. Furthermore, the results of the previous pressure field calculations as K and V_f are no longer used and have to be found again, leading to longer calculation time.
- A prediction of the new h_c^t is made.

The latter was chosen here. It would have been logical to make a prediction of the new height, based on the height of the CVs at previous time steps. However, especially for the newly formed flow front CVs, these data cannot be used, because they had a constant, compacted height at all previous time steps. A different prediction was made here, based on the assumption that the right hand term of Eq. 2.11 stays constant. This assumption is only close to reality if $t \to \infty$ and the preform has similar dry and wet compressibility. Although not close to reality, it ensured, even for the flow front CVs, at least a correct order of magnitude of the height, h_c^t, with the new time step size. Therefore it provided a simple and fast way to overcome the stability problems. The approximation of h_c^t for the new time step size Δt_{new}, based on this assumption, can be written as:

$$\left.\begin{array}{r} b_c = \frac{h_c^t - h_c^{t-1}}{\Delta t} V_c \\ V_c = A_e h_e^t \end{array}\right\} \; h_c^t = \left(h_c^{t-1} + \sqrt{(h_c^{t-1})^2 - 4 \frac{b_c \Delta t_{new}}{A_e}} \right) /2 \qquad (2.15)$$

In this equation, b_e is the right hand term of Eq. 2.11 for CV e, and A_e is the area of CV e. This prediction of h_c^t is only used for the first iteration step

after the time-step Δt is changed into Δt_{new}. After this first iteration step, the preform height can again be derived from the calculated pressure field, using the preform compaction models, as presented in Appendix A.

A full set of equations to solve the pressure, height and volume fraction distribution over the filled region and a way to keep track of the resin flow front position were presented. In the next chapter, the validation of this model will be presented.

Chapter 3

Validation of the Model

The model presented in the previous chapter was implemented in the MATLAB programming environment. The developed program was validated in a number of ways:

- **Closed Form Solution**: The numerical accuracy of the model was validated with a known closed form solution for the RTM case, where preform compaction is neglected.
- **Flow Front Propagation**: The model itself and the used assumptions were validated by comparing the measured and simulated flow front propagation during the filling of flat plates.
- **Preform Thickness during Mould Filling**: The measured and simulated preform thickness was used to validate the assumption that the different wet and dry preform compaction have a significant influence on the mould filling.
- **Infusion of a Wind Turbine Blade**: Finally, the filling of half a wind turbine blade was simulated and compared with experimental results.

The results of these validations will be discussed in Chapter 4.

3.1 Closed Form Solution

Before the model was verified with practical experiments, the numeric code was compared with a known analytical solution in closed form. For the case of resin transfer moulding (RTM), where no preform compression occurs, the mould filling time, t, of a 1D mould with length, x, was derived from the resin continuity equation and Darcy's law:

$$\nabla \cdot \bar{u} = \nabla \cdot (\frac{K}{\mu} \nabla P) = 0 \Rightarrow \nabla^2 P = 0 \tag{3.1}$$

The pressure gradient is hence constant over the wetted length and can be written as:

$$\nabla P = -\frac{P_{atm} - P_{vac}}{x} = -\frac{P_{total}}{x} \tag{3.2}$$

Using this equation in Darcy's law for the actual velocity (see Eq. 2.12), the following closed form solution for the mould filling time t was obtained:

$$\begin{aligned} \bar{v} = \frac{dx}{dt} &= \frac{K}{\mu \cdot \phi} \frac{P_{total}}{x} \\ &\Downarrow \\ \int x dx &= \int \frac{K}{\mu \cdot \phi} P_{total} dt \\ &\Downarrow \\ t &= \frac{x^2 \phi \mu}{2 P_{total} K} \end{aligned} \tag{3.3}$$

The mould filling for the RTM process with a 0.25 m long mould was simulated with $\phi = (1 - V_f)$=0.5, K/μ=1e-13 m^2/Pa·s and P_{total} = 100kPa.

Figure 3.1a shows the simulated flow front propagation for different numbers of elements along the length of the product. Since at every time step exactly one element is being filled, the calculation time increases linearly with the number of elements used. The position of the flow front at a certain time in the model was defined as the maximum x coordinate of the centers of the CVs which had a fluid presence function larger than 0 ($I > 0$). All the results presented here will have the resin inlet on the left hand side (at distance 0) and the vacuum outlet at the right hand side.

Figure 3.1 shows that the more elements were used, the closer the simulated results were to the closed form solution. The error between the closed form solution and the simulated results was plotted against the number of elements which were used, obtaining Figure 3.1b. The line in this figure shows a slope of 1, which corresponds with the first order scheme used in the model.

As soon as preform compaction is taken into account and hence the permeability changes during the mould filling, this closed form solution will not give accurate results. Acheson *et al.* (2004) suggested that for this case an "effective"

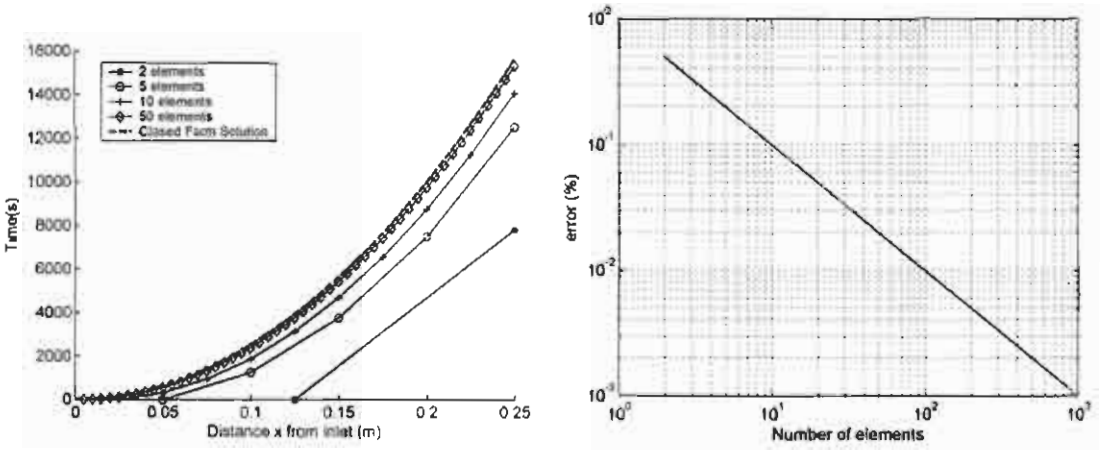

(a) Flow front propagation

(b) error %

Figure 3.1: Simulated flow front propagation for different numbers of elements.

permeability could be used. This effective permeability will, however, be different for the same material being injected under different pressures and may not be accurate in filling complex geometric parts. In order to solve this problem, Lopatnikov *et al.* (2004) presented "a closed form solution to describe infusion of resin under vacuum in deformable fibrous porous media". They modelled the deformable preform as a linearly elastic medium with permeability depending on porosity according to the Kozeny-Carman equation where the preform compaction flux term is neglected. However, the results of the compression test, as presented in Appendix A, showed that the materials used here do not show such a linear elastic behaviour.

3.2 Flow Front Propagation

The easiest way to validate the model was to look at the predicted progression of the flow front during the mould filling process and verify it with experiments. Two types of preforms were used, both supplied by Texglass:

- 10 Layers of twill-weave: This preform consisted of 10 layers of 280 gram/m^2 glass twill-weave, stacked at $(0/90)_{10}$. The 280 gram/m^2 glass twill-weave has a fabric construction of 0.6($\pm$0.02) warp ends/mm and 0.78($\pm$0.02) weft picks/mm.
- 2 Layers of CoreTEX: The CoreTEX fabric consisted of a 280 gram/m^2 glass fibre twill-weave, a 180 gram/m^2 polypropylene fibre core, which functioned as a flow enhancement layer, and a 400 gram/m^2 glass fibre

randomly chopped strand mat layer (denoted as 280TW/ 180PP/ 400C). This preform consisted of 2 symmetrically stacked plies of this fabric where the 400C layers were in the middle, hence $(280TW/\ 180PP/\ 400C)_s$.

Different types of resin and vacuum pressures were used for the different types of preform, as shown in Table 3.1. The viscosity of the resin was measured using a Brookfield viscometer.

Table 3.1: The resin/preform systems used and the applied vacuum pressure

	10 layers Twill	2 layers CoreTEX
Used Resin	Araldite LY 1564 SP	NCS 236
Viscosity of Resin μ $(Pa \cdot s)$	0.346	0.182
Used Vacuum Pressure P (Pa)	87000	57500

The progression of the flow front for these two preform types was measured on a turnable glass plate. On one side of the glass plate the preform, vacuum bag, pipe work and other required materials were mounted. The other side of the glass plate was used for measurements of the flow front position. Figure 3.2 schematically displays this experimental set-up.

The flow front positions were recorded along the centreline of the preform, while the resin was infused over its full width (line infusion). Figure 3.3 shows a recording during one of the experiments and the position of the flow front.

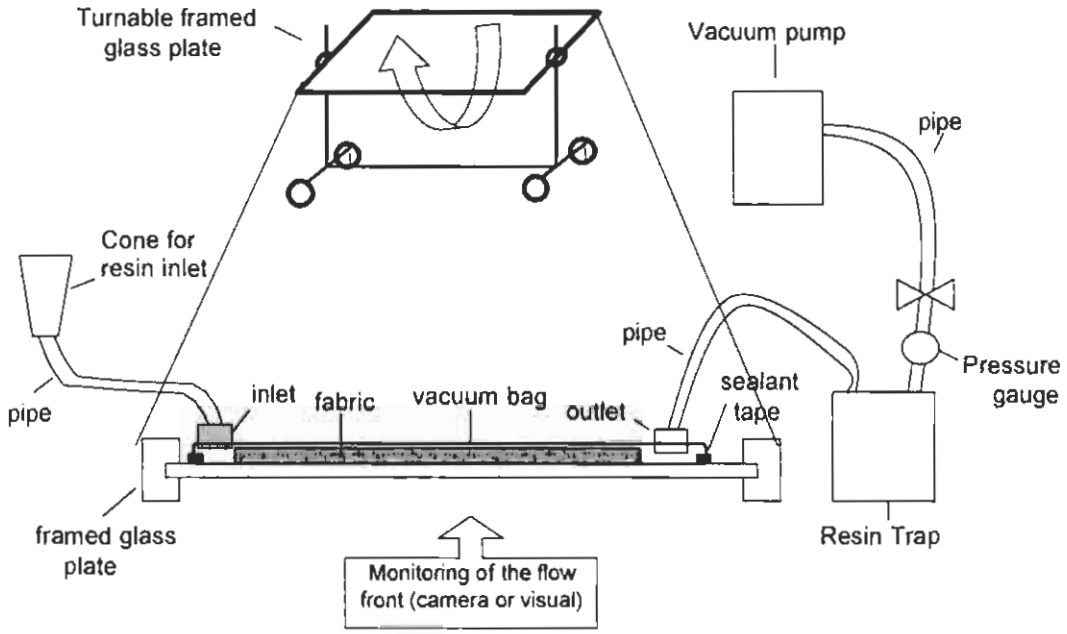

Figure 3.2: Sketch of the experimental set-up.

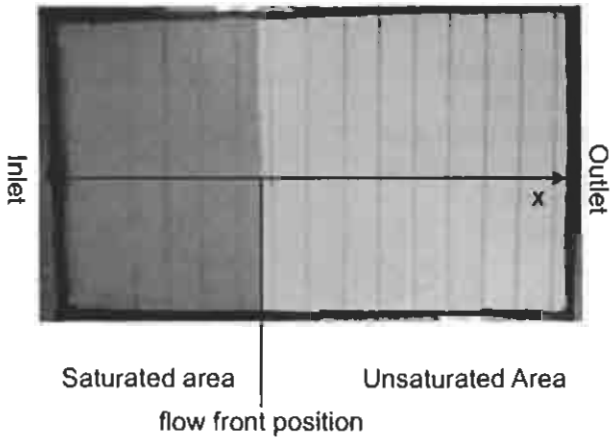

Figure 3.3: The position of the flow front during line infusion

3.2.1 10 Layers of Twill-Weave

Firstly, the flow front propagation for a 0.2 m x 0.2 m flat plate with 10 layers of twill-weave was simulated. For the simulation, 100 CVs were used in the length direction. With these 10^2 CVs in the length direction, the numerical error for the RTM case without preform compaction, should be approximately 1% according to Figure 3.1b.

For the simulations, an isotropic permeability was assumed. This is a valid assumption, especially since the preforms, used to verify the model, were much longer than wide and a line infusion was used. As Cai (1992) already indicated, the flow in these cases is dominated by the flow in the length direction.

Using the experimental set-up depicted in Figure 3.2, the flow front propagation was measured during mould filling of this preform. The simulation and experimental results of the flow front propagation for this preform are presented in Figure 3.4.

The lower line shows the results if only dry preform properties were taken into account ("Dry preform properties"). The next line ("Without flux term") shows the simulated results where the preform compaction flux term was not taken into account. The line of stars (*) shows the results of experiment 1 ("Experiment 1") and the line of diamonds (◇) shows the results of experiment 2 ("Experiment 2"). Between those lines, the solid line shows the simulated results where both dry and wet preform properties and the preform flux term were taken into account ("With flux term") and the dashed line ("Wet preform properties") shows the simulated results where only wet preform properties were used.

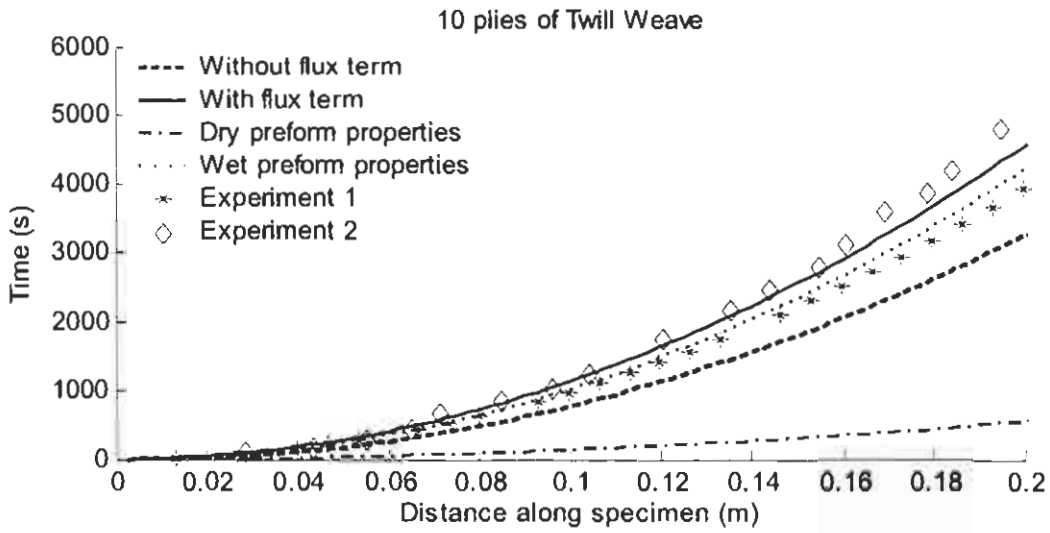

Figure 3.4: Flow front propagation for 10 layers of Twill-Weave

3.2.2 2 Layers of CoreTEX

The same experiment was carried out for a 0.45 m x 0.45 m flat plate with 2 symmetrically stacked layers of CoreTEX. The process parameters are listed in Table 3.1. For the simulation also 100 CVs along the length direction were used. The experimental and simulated results are presented in Figure 3.5. In this figure, the same line styles as for the 10 plies of twill-weave (Figure 3.4) are used.

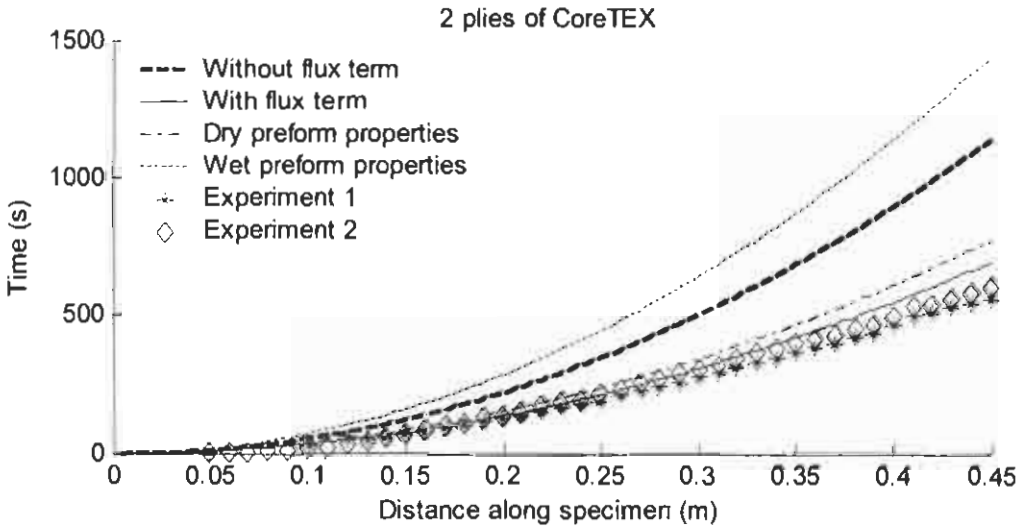

Figure 3.5: Flow front propagation for 2 layers of CoreTEX

3.3 Preform Thickness during Mould Filling

The model was based on the assumption that the different wet and dry preform compressibility would cause a sudden change in preform thickness at the flow front. Therefore the model took the preform compaction flux into account. In order to validate this assumption, the preform thickness during mould filling was measured.

Furthermore, the thickness of the preform was a more direct way to verify the model. The position of the flow front depended on many factors: the viscosity of the resin, the permeability, the compressibility and the vacuum pressure level. The thickness of the preform depended only on the compressibility and the pressure profile[1]. Also, when the compaction behaviour is known, the preform thickness can be used to measure the pressure distribution in the preform indirectly.

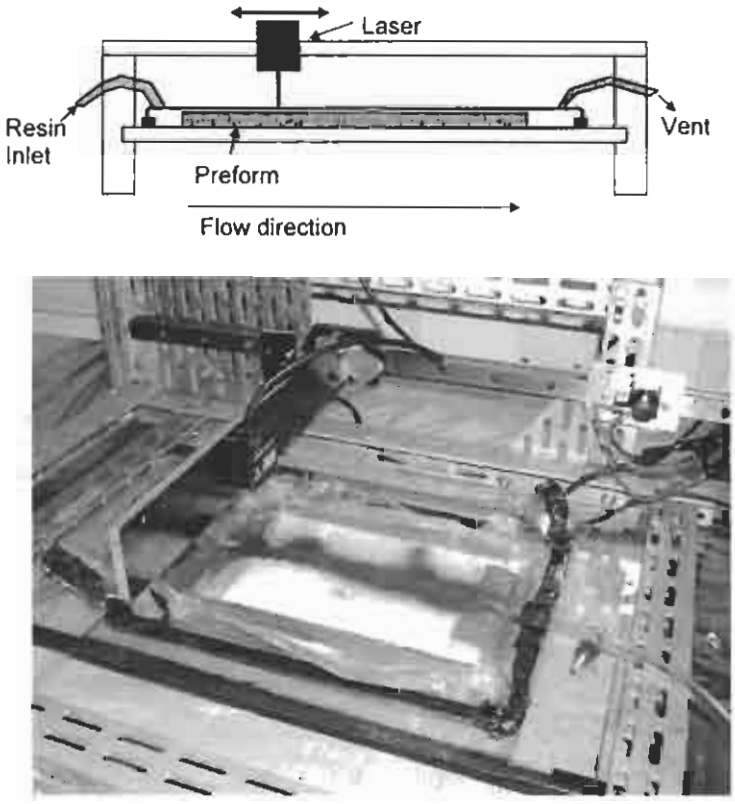

Figure 3.6: A sketch (top) and picture (bottom) of the experimental set-up used to measure the thickness of the preform during the process

The height of the top surface of the 10 layers of twill-weave was measured during

[1]Although a gradient in permeability influences the pressure profile, the permeability itself does not.

mould-filling. A laser, mounted on a sliding rail, was used for this height measuring. Since the height of the bottom (mould) surface was known, the preform thickness could be derived from this height measurement. The laser scanned the surface of the product along a straight line. The scanning of 0.2 m took about 0.5 s which was considered negligable compared to the process times. A graphite spray was sprayed on the vacuum sheet to provide a diffusive reflecting surface. Still, this surface produced significant noise in the measured signal. The sample rate was 1000 Hz allowing an averaging filter to remove this noise without loosing too much data. The experimental set-up is depicted in Figure 3.6.

The results of the thickness measurement at two different times are presented in Figure 3.7.

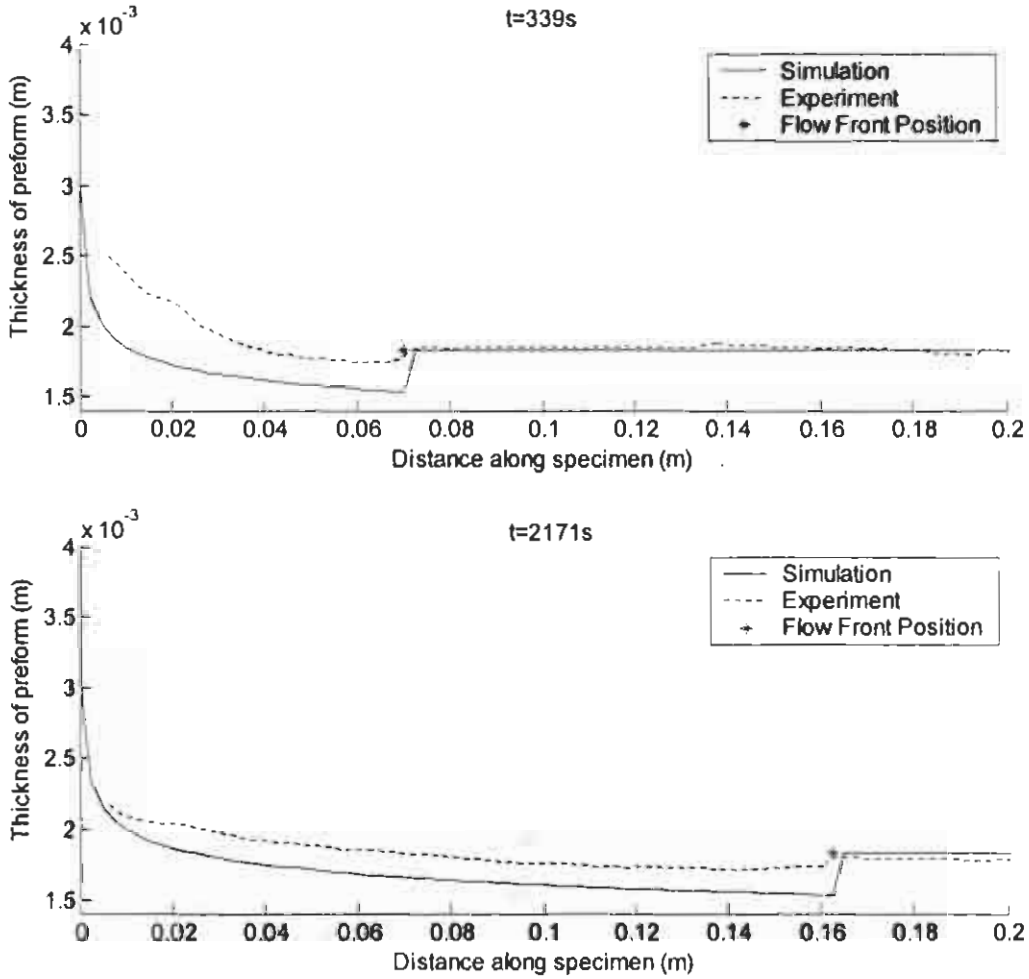

Figure 3.7: Measuring the preform thickness during the filling of 10 plies of twill-weave. Top: The measured and calculated thickness at t=339 s. Bottom: The measured and calculated thickness at t=2171 s.

The first 5 mm of the experimental results are not shown, because in this area a flow pipe, used to allow the line infusion, lifted up the vacuum bag and gave

incorrect thickness results. In Figure 3.7 also the calculated thicknesses of the preform are presented. using the simulation of Section 3.2.1.

3.4 Infusion of a Wind Turbine Blade

Finally the infusion of one side of a 2.0 metre wind turbine blade was simulated and tested. The CoreTEX/NCS256 preform/resin system of Table 3.1 was used, but the infusion pressure was 80 kPa. The resin inlet was at the root of the blade and the vacuum outlet at the tip. The flow front position was taken as the maximum distance between the inlet and the flow front along the x-axis (as defined in Figure 3.3).

The infusion of this wind turbine blade was simulated using a mesh with 1043 triangular CVs. The mesh was generated by PATRAN and imported into the flow model. The calculation time of the complete mould filling was 17 minutes on a 2.01 GHz PC with 512 MB of RAM. The simulated and experimentally measured flow front propagations are presented in Figure 3.8.

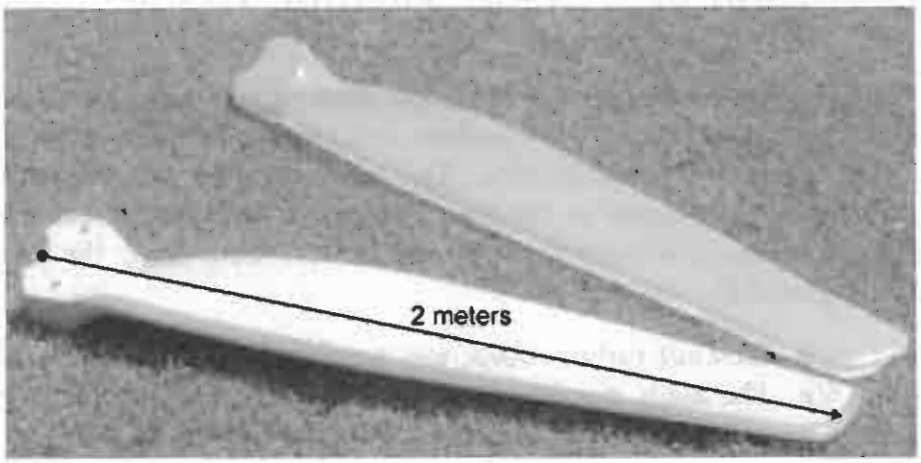

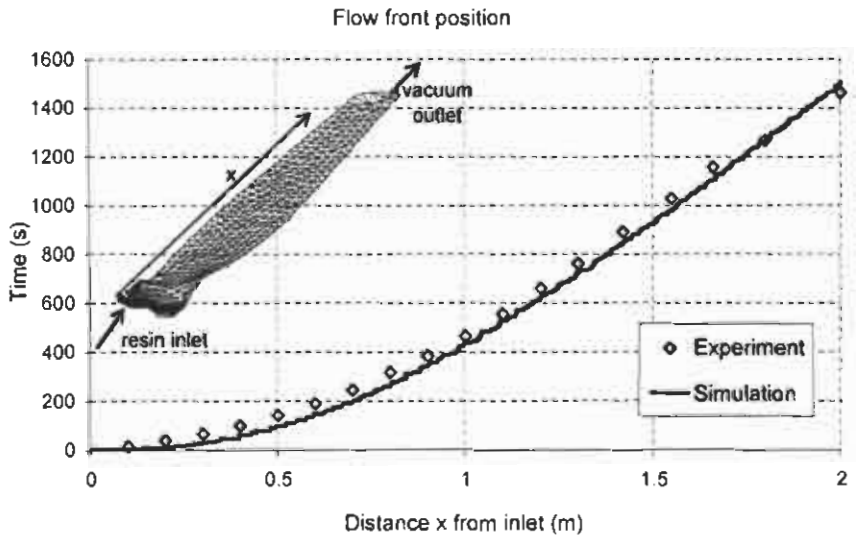

Figure 3.8: Top: One side of a wind turbine blade after infusion and the final product after it is bonded to the other side and finished. Bottom: Simulated and experimental results of the flow front propagation for one half of a wind turbine blade.

Chapter 4

Discussion of the Physical Approach and its Results

4.1 Discussion

4.1.1 Flow Front Propagation

Figures 3.4 and 3.5 show that if the different wet and dry preform properties are taken into account ("With flux term"), the simulation results agree well with the experiments. If only the dry (for the CoreTEX) or wet (for the Twill-Weave) preform compaction properties are included, the simulation results also agree well. However, because the wet properties give good results for one material and dry properties for another material, the model cannot be simplified by using only one compaction behaviour.

Figures 3.4 and 3.5 show the importance of the fully transient process model, without ignoring the flux term. The thickness measurements of the preform in Figure 3.7 illustrate the reason behind this. As Andersson *et al.* (2003) showed, a thickness minimum was observed instantly behind the resin flow front. From this minimum, the preform thickness changed quite suddenly to the larger dry compacted thickness and the flux term, $\frac{\partial h}{\partial t}$, is significant. This results in a different pressure profile, as depicted in Figure 4.1. In this figure the calculated normalised pressure fields from the resin inlet (0% on the x-axis) up to the flow front (100% on the x-axis) for the two types of preform are presented. The continuous line represents the pressure profile if the flux term is taken into account, the dotted line represents the case where this term is ignored. Acheson *et al.* (2004) and Correia *et al.* (2004) presented similar figures. Looking at the pressure field at the flow front (100% on the x-axis) and bearing Darcy's Law in mind, which states that the resin speed depends on ∇P at the flow front, it is easily derived that the resin speed (and hence flow front propagation speed)

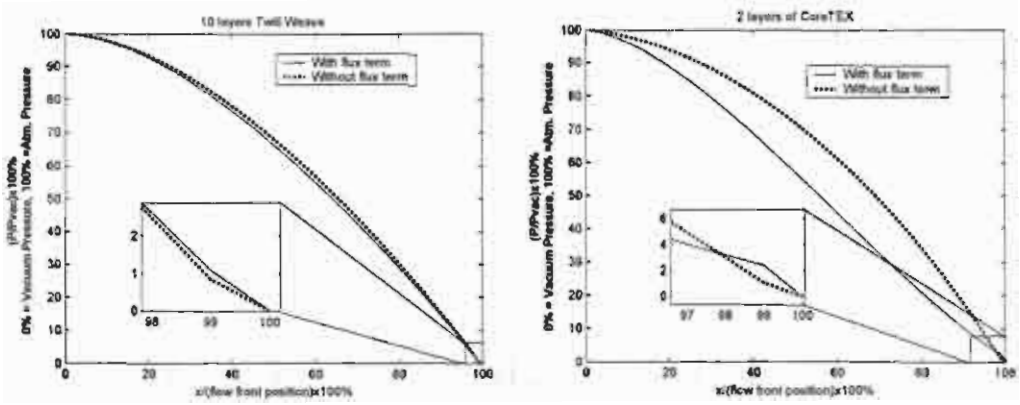

(a) 10 layers Twill (b) 2 layers CoreTEX

Figure 4.1: Normalised pressure fields for RIFT with the flux term $\frac{\partial h}{\partial t}$ and without the flux term.

will be different for both cases. A quasi-static process, as employed previously (Gutowski *et al.*, 1987; Han *et al.*, 2000; Hammami & Gebart, 2000; Andersson *et al.*, 2003; Acheson *et al.*, 2004; Correia *et al.*, 2004), is definitely not valid if different dry and wet preform properties are taken into account.

If the fibre compaction rates and/or resin speeds are lower, the pressure profiles will be closer together, resulting in similar flow front speeds. In these cases, it is valid and even advisable to ignore the flux term. It will give similar results, existing RTM software with only minor alterations can be used (Lee *et al.*, 1994; Andersson *et al.*, 2003; Correia *et al.*, 2004) and it saves significant calculation time.

4.1.2 Preform Thickness during Mould Filling

The measured values for the thickness of the wet region in Figure 3.7 (the left side from the flow front) are larger than the calculated ones. The thickness minimum behind the resin flow front is therefore less pronounced than in the simulation. Possible explanations can be found in the way the compaction tests were carried out. The single plies of the preform could not move as freely in the process compared as they could in the compaction tests. In the tests the single plies were wetted out, stacked and uniformly compressed. In the mould-filling process, the fibres in the preform were still connected to the fibres in the dry region and hence transverse shear accompanied the compaction. In addition, rigid plates were used in the compression tests whereas compaction during the RIFT process was induced by the flexible bag. Looking at Figure 2.1, only a small area of the fibres could actually touch these rigid plates. Therefore the

local pressure on the fibres was much higher compared to the global pressure on the preform. In the RIFT process, the flexible bag distributes the pressure more uniformly over the fibres. These higher local pressures could lead to a higher global preform compaction. This does not explain why there is only a difference in the wetted region between the compaction tests and the experiments. It could be that, due to a lubrication effect, wet fibres are more sensitive to local pressures than in a dry state. However, further research should validate this assumption.

4.1.3 Infusion of a Wind Turbine Blade

Figure 3.8 shows the results of the simulation of a wind turbine blade. Although only 1043 CVs were used, it took relatively long to simulate the infusion of such a simple product, even if the flux term was ignored. Some adaptions were made to speed up the process, for example a prediction of the length of the next time step when an element is filled. Still, this implementation is not very suitable for optimisation purposes, where many different concepts of in and outlet positions have to be calculated. For such a case, it is questionable whether a high accuracy is required. Standard RTM software, with altered values for the permeability to compensate for the preform compaction, would probably be accurate enough and in any case much faster.

Without ancillary goods, such as flow channels and the flow enhancement layers, the RIFT process is quite a slow process. The experiments showed that with those flow enhancement layers, such as the CoreTEX fabric, high flow front speeds were obtained and, even without additional resin inlets, material infusion lengths of over 2 metres were reached. In this case, the flow was dominated by the layer with the highest permeability and the adjacent single plies of fabric were wetted almost instantaneously as the resin reached the underlying core.

If thicker or more plies are used, 3D flow effects will occur. The computational technique presented by Han *et al.* (2000) could work with this model. Han *et al.* (2000) introduced a second fluid presence function for every CV which represents the flow in the flow enhancement layer (or even flow channels as used in SCRIMP). Using this extra function, the through-the-thickness flow at every time step can also be calculated. In these cases there will be a flow front area where the flow enhancement layer is completely filled while the underlying woven fibres are only partially filled. This behaviour cannot be predicted with the fill-one-CV-at-a-time technique, presented here. Furthermore, the compaction behaviour in this area will have to be determined as well.

Another shortcoming of the model is, as mentioned in Section 3.2, that the permeability of both preforms is assumed isotropic. In cases where the permeability can no longer be assumed to be isotropic, the model can be modified to accommodate a permeability tensor. This is relatively straightforward: The

permeability at every cell face, $K^f_{n,e}$, in equation 2.8, can be calculated based on the orientation of the face out of the permeability tensor. This tensor should be obtained from permeability tests, as done in Appendix B, for different stacking angles.

4.2 Conclusion

The validation showed that the presented model is able to predict the flow front propagation and the preform thickness very well during mould-filling. The accuracy of the model depends largely on the material data used, which is quite time consuming to acquire. The different predictions of the flow front propagation and the preform height during infusion showed the importance of taking the different wet and dry preform properties into account. By doing so, the preform compaction flux term becomes significant, especially at the flow front, and the process cannot be modelled as quasi-static, as is the case in all previous modelling attempts.

The accuracy gained by taking wet and dry preform properties into account and modelling the process transient comes with a significant time penalty. Therefore this model is less suited for optimisation purposes.

Part II

Genetic Approach

Chapter 5

Model for Optimising RIFT

The model presented in the previous chapters is able to predict the RIFT process with the process parameters, such as product shape, resin inlet and outlet, preform permeability, preform compaction, vacuum pressure and resin viscosity known. However, in practical design cases, the requirements of the process are known in advance rather than these process parameters. These requirements are normally quite simple: The process should produce the highest quality products at minimum costs.

A reduction of the production costs can mainly be achieved by minimising:

- Process time;
- Amount of consumables, e.g. flow enhancement pipes and infusion mesh.

Although the final product quality and properties depend on a number of factors such as materials used (fibres, resin and gel-coat), curing time, temperature and mould surface, the main factors which can be influenced by the process parameters are:

- The fibre volume fraction;
- The number of voids due to air entrapments.

In this part, a genetically based tool will be presented to optimise the controllable production parameters for producing the highest quality products with minimum costs. This part is introduced by a literature overview of previous modelling efforts to optimise the RIFT process. Most researchers focused on optimal positions for the inlet(s) and vent(s). The reason can be found by looking at the controllable process parameters in more detail. Hence an in-depth overview of these parameters will firstly be given. The literature overview is

followed by a section where a mesh distance-based model is developed. This model, although not physically based, is much faster and therefore much better suited for optimisation purposes than the model presented in Part I. This model is coupled with a genetic algorithm, which will be presented in the final section, forming the genetically based optimisation tool.

5.1 Process Parameters

As presented in Chapter 1, Figure 1.8, the adjustable process parameters are:

- Vacuum Pressure
- Resin Viscosity
- Preform Properties
- Inlet(s) and Vent(s) positions
- Flow Enhancement Structures[1]

For an ideal process, some of the product and production properties require contradictory process parameters and an optimum is not always obvious. The influence of the different process parameters on the product and process properties and how they can be optimised will be explained in more detail:

The **Vacuum Pressure** influences the process time and fibre volume fraction in quite a straightforward manner: The lower the pressure used (more vacuum), the higher the fibre volume and faster the resin flow will be. Therefore in most cases maximum vacuum pressure is used. An exception is made where resins are used with a volatile compound, as in most polyester resins. Here a higher pressure (less vacuum) is used (normally a minimum of 0.4 bar absolute pressure) to make sure this compound does not out gas during the process, causing gas bubbles in the final product.

The **Resin Viscosity** has a linear relationship with the mould-filling time. As can be derived from Darcy's Law (Eq. 2.1): the lower the viscosity the faster the resin will flow. Low viscosity resins are therefore favoured for liquid composite moulding processes, making the choice of the resin quite easy. The resin should have an acceptable price and a viscosity as low as possible, while still having acceptable chemical and mechanical properties when cured.

[1] Although the flow enhancement structures and the preform properties are directly related, they will be discussed separately.

The **Preform Properties**, influencing the RIFT process, are the preform permeability and compressibility. The preform permeability has a linear relationship with the mould-filling time: The lower the permeability, the slower the resin flows. The permeability of the preform depends on the types of fibres, the weaving, stacking or stitching pattern, but also, as shown in Appendix B, on the fibre volume fraction. In general, a maximum fibre volume fraction is desired since this will give the best mechanical properties for the final product with minimum weight. A high fibre volume fraction will reduce the permeability and hence increase processing time and cost. In the RTM process, this problem can be overcome. Only a slight pressure (enough to keep the preform in place) is applied to the preform during infusion and hence the fibre volume fraction will be low and the permeability and resin speed will be high. After infusion, the mould cavity is made smaller, which increases the pressure on the preform, resulting in a higher fibre volume fraction without slowing down the process. In RIFT, the infusion pressure and pressure on the preform are coupled, as presented in Section 2.2, Equation 2.3. Therefore an optimum has to be found between the fibre volume fraction and the permeability of the preform, depending on the desired process time, final product properties and costs.

A way to largely improve the permeability of the preform is by using flow enhancement layers. These flow enhancement layers can be integrated into the preform. An example of such a preform is the CoreTEX fabric used for this research. This textile preform consists of a thick, open structured flow enhancement core which is covered by a few single plies of woven fabric. Although relatively easy to use, the major drawback of these preforms is that an excess amount of resin stays in the flow enhancement core after the process. Because this core is integrated into the preform, it cannot be removed from the product, causing an extra weight penalty to the final product.

Another possibility to improve the permeability is the SCRIMP method. In the 1980s this method was patented by Seemann (1989). It uses a rubber bag as a flexible tool which can have an integrated mesh to distribute resin within the tool; eliminating the need for an infusion mesh or a breather cloth and reducing the amount of consumables. This rubber bag should be tailor-made for the product, making it unattractive for small production numbers.

The preform compressibility influences the final product thickness and fibre volume fraction. The more the preform compresses, the higher the fibre volume fraction and the lower the product thickness will be. The choice of the preform and hence its compressibility properties is mainly determined by the desired mechanical properties of the final product. Therefore the preform compressibility is normally not used to optimise the process itself.

The **Inlet(s) and Vent(s) positions** are considered the most important variables in the process design. The inlet and vent arrangement must ensure that the resin fills the entire preform, preventing dry spots in the final product. In

order to reduce filling-time, it is furthermore preferred that the distance from inlet to vent be short. The optimal position of the inlet and vent was therefore a subject of much research (Cai, 1992; Young, 1994; Boccard *et al.*, 1995; Luo *et al.*, 2001; Jiang *et al.*, 2002; Gokce & Advani, 2004). Whereas the position of the inlet can almost be chosen freely, the position of the vents depends on the position of the inlet and the geometry of the product. As Jiang *et al.* (2002) stated in their article, vents should be positioned at every area which, during some stage of the filling process, does not connect (without passing a saturated area) to a vent. In these areas the vents should be located at the position which is filled last. An example can be seen in Figure 5.1 and will be discussed in more detail in Section 5.4.

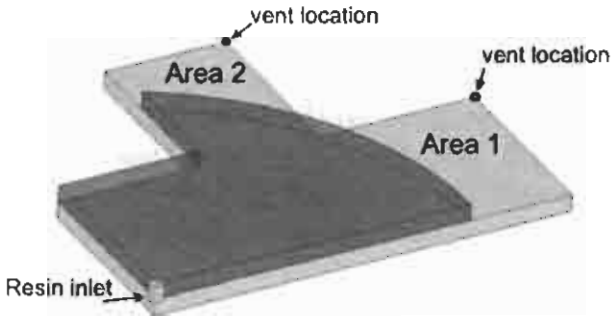

Figure 5.1: The flow front creating two non-communicating areas.

Flow Enhancement Structures can significantly improve the flow filling-times. As already mentioned, they can be integrated in the preform. Another solution is to put the flow enhancement structures on top of the preform with a peel-ply in between. This peel-ply allows the flow enhancement structures to be "peeled-off" after infusion, solving the problem of the extra weight penalty associated with integrated structures. Two types of flow enhancement structures were already presented in Figure 1.6: the infusion mesh and the spiral bind. Figure 5.2 shows the tip of a wind turbine blade, after production, using these flow enhancement structures. A peel-ply was used as well, thus the spiral bind (flow pipe) and the infusion mesh could be peeled-off the final product, leaving a clean product surface.

The use of the infusion mesh is straightforward: nearly the entire top surface of the preform can be covered. Because the flow through the infusion mesh is much faster than in the preform, care has to be taken that the resin gets time to flow through the thickness. If this is not the case, the resin in the infusion mesh can arrive at the vent prematurely, causing a dry spot under the vent location, as demonstrated by Hsiao *et al.* (2004).

The great effectiveness of the spiral bind can be demonstrated by comparing its permeability with the permeability of a preform. The effective permeability of a pipe can be found by using the Poiseuille's law (or the Hagen-Poiseuille law,

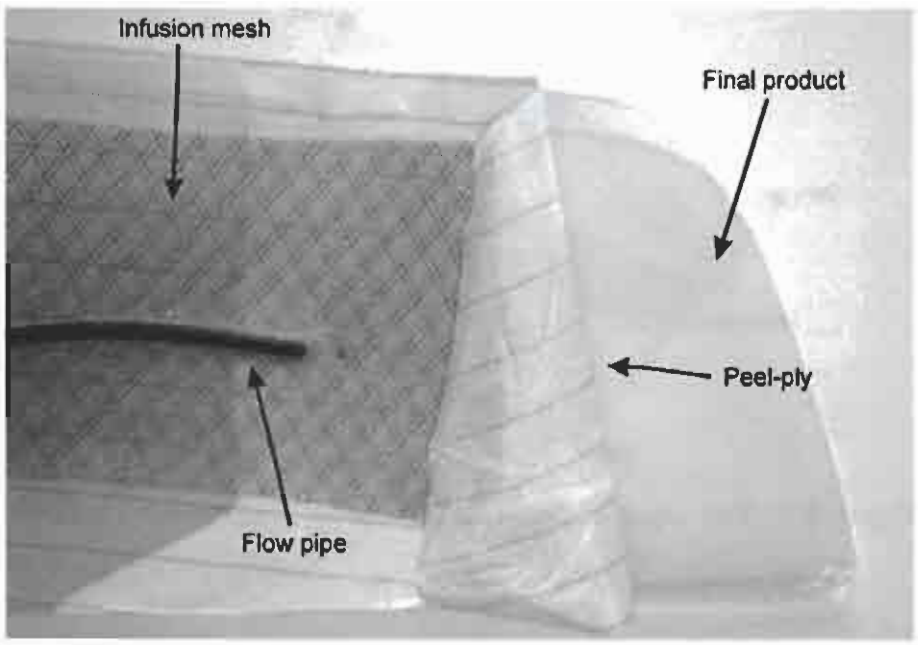

Figure 5.2: A tip of a wind turbine blade after production, using flow enhancement structures and a peel ply.

also named after Gotthilf Heinrich Ludwig Hagen for his experiments in 1839). This physical law describes the flow of an incompressible uniform viscous liquid through a narrow cylindrical tube. According to this law, the voluminal laminar stationary flow Q through a pipe with a constant circular cross-section radius r and a length l can be written as (Sutera & Skalak, 1993):

$$Q = \bar{u}\pi r^2 = \frac{\pi r^4}{8\mu}\frac{\Delta P}{\Delta l} \tag{5.1}$$

Combining this equation with Darcy's law (Eq.2.1) gives an effective permeability for a pipe with radius r:

$$K = \frac{r^2}{8} \tag{5.2}$$

Consider a pipe with $r = 12\text{x}10^{-3}$ m. It has an effective permeability of $K = 1.8\text{x}10^{-5}m^2$. As shown in Appendix B, even preforms with an optimal flow behaviour, like CoreTEX, only have a permeability between $0.1\text{x}10^{-8}m^2$ and $1\text{x}10^{-8}m^2$. If these permeability values are compared, it is clear why flow pipes are such an effective way of reducing the infusion time.

Although the use of flow pipes reduces the process time and hence costs, it increases the amount and costs of consumables. Another disadvantage of using infusion pipes is that its use is not as straightforward as e.g. the infusion mesh. There is a great risk of creating dry spots. Figure 5.3 shows a T-shaped flow

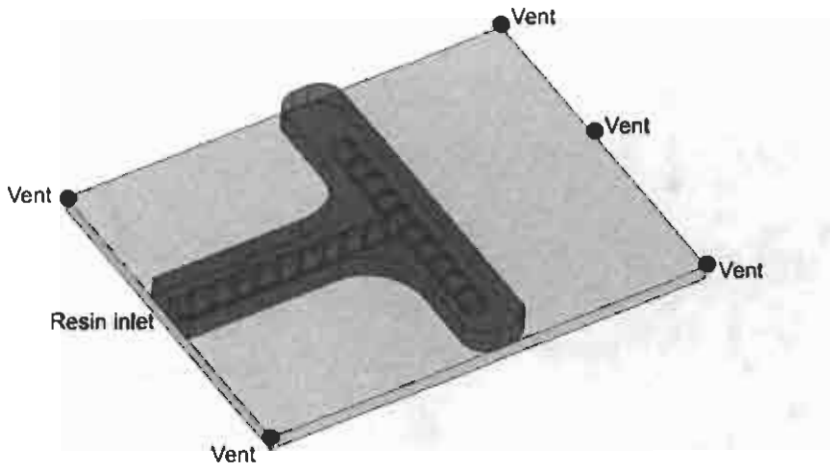

Figure 5.3: Two pipes causing the flow front to disconnect 3 areas.

pipe on a rectangular plate.

Since the permeability of the flow pipes is much higher than the permeability of the surrounding preform, the resin will first fill the spiral bind. As a result, the three areas in the figure no longer connect and air can be entrapped in one of these areas, causing dry spots. This can be prevented by adding more vents (as shown in the figure) or changing the positioning of the pipes. In case of Figure 5.3, 5 vents would be required in order to prevent dry spots, whereas without the pipe and a positioning of the resin inlet in one of the corners, only one vent would be sufficient.

Looking at the adjustable process parameters, it can be concluded that, for an optimal process, the vacuum pressure is chosen maximally and resin viscosity minimally. The preform properties will mainly depend on the desired mechanical properties of the final product, leaving only the inlet, vent and flow pipe position as variables to optimise.

5.2 Previous Modelling Efforts

The number of optimising tools developed for the RIFT process is significantly lower than those for the RTM process (Hsiao *et al.*, 2004). A fast model is preferred over high accuracy for optimising purposes. RTM models, with an "effective" permeability, which accounts for the change in permeability due to compression, can therefore also be useful (Andersson *et al.*, 2003). For this reason, some RTM optimisation models will also be discussed.

Cai (1992) was one of the first to look at the optimal location of the inlet and vent. He came up with some useful closed-form solutions for the wet length,

mould filling time and pressure distribution of rectangular, trapezoidal and circular sections. These closed-form solutions were used to calculate the mould-filling time for different scenarios of the inlet/vent positions on 2 different 2D shapes (rectangular and trapezoidal). It was concluded that for the shortest infusion times, inlets and gates should be arranged in such a way that shortest paths can be achieved. Furthermore the resin flow direction should be from the larger sides to smaller sides (e.g. with a trapezoidal shape), or from the outside mould perimeter to the inside.

Two years later, Young (1994) published one of the first algorithms to optimise the inlet location on any $2\frac{1}{2}$D geometry. A previously developed non-isothermal flow simulation program was coupled with a genetic search algorithm. Genetic algorithms belong to a category of stochastic search techniques, where only the fittest (best objective function) will survive during the artificial evolution process. A detailed description will be given in Section 5.5. The genetic algorithm gives the flow simulation software inlet positions as input variables and, depending on the results of the simulation, the algorithm optimises the inlet positions. These optimised positions are again given to the simulation tool until a near global optimum is found. Two applications were presented: a flat rectangular mould, with 98 nodes and 156 elements and a more complex automotive part with 264 nodes and 448 elements. In the latter case, the disadvantage of using a physically based flow model was shown: the calculation of only 600 generations with a population size of 30 was over 75 hours. Still, it was shown that a genetic algorithm has a better chance to locate the near global optimum than a gradient based search method.

Boccard *et al.* (1995) addressed the issue of excessive calculation times when numerical simulations are used to optimise the RTM process. Therefore a fast geometrically based model was presented to determine the vent location of flat (2D) RTM moulds which may contain impermeable inserts. An isotropic preform permeability was assumed. The geometric model used the distance from the inlet to the perimeter of the mould (or sub-domain in case of multiple inlets). A vent should be positioned at the distance furthest from the inlet. By assuming a partial channel/partial radial flow, the mould-filling time was calculated based on the distance the resin has to travel from the inlet to the vent. The model was verified with 6 different mould shapes and good agreement was found between actual and calculated fill-times (generally within 10%) in a much faster way than with a numerical simulation. However, the major drawback of the model is that it is limited to 2D shapes and the calculation of the distance for complex parts is very difficult (Jiang *et al.*, 2002).

In their article, Lin *et al.* (2000) evaluated the strength and weaknesses of genetically and gradient based algorithms for optimising the RTM process. It was concluded that the strength of genetic algorithms is the handling of discrete variables and discontinuous functions and that it is a global search method which is

less likely to be trapped in a local optimum. Since the object function used by Lin *et al.* (2000) was smooth, they preferred a quasi-Newtonian method because it converged faster and hence calculation times were shorter. Like Modi *et al.* (2003) also did later, the faulty finite element model used by Young (1994) was addressed: the model used by Young (1994) had a non-uniform element size, and because a single node was used to model the inlet, the equivalent inlet radius was linearly proportional to the size of the adjacent elements. Consequently, the fill-time differed significantly if the element size was varied near the inlet. Lin *et al.* (2000) presented the example of inlets of 0.04 m and 0.05 m for a 1 m radial mould. The difference in fill-time was larger than 10%. In the optimisation algorithm uniformly meshed geometries were therefore used with constant element size. A flat as well as an uneven plate were optimised with areas of different permeability and the x and y coordinates of the resin inlet were taken as optimising parameters to optimise the fill-time. A significant improvement in fill-time was achieved, but neither the calculation times nor the position of the vents were mentioned.

Luo *et al.* (2001) used a neural network and genetic algorithms to optimise the inlet and vent position for the RTM process. They defined a resin flow index which characterized the resin flow front shape. Their objective function was a short filling-time and a desirable resin flow pattern (small distance standard deviation). Although they showed that their neural network process model was much faster than a genetic algorithm, the neural network required a training of simulated experiments, reducing the time advantage significantly.

Jiang *et al.* (2002) also used a genetic algorithm to, again, optimise the inlet and vent position for the RTM process. The novel aspect of their research was that a genetic algorithm was coupled with a mesh distance-based model, which is a geometrically based flow model. Such a model is fast and can accommodate any type of mesh (e.g. the mesh of a structural analysis). It is based on the assumption that the node closest to the inlet is filled first, then the 2nd closest, etc. A more detailed description is given in Section 5.4. The model could only optimise 2D geometries. An extension to the use of $2\frac{1}{2}$D geometries will be presented in the next section. Although not mentioned explicitly in the article, it was shown how ineffective a genetic algorithm can be. In a case where one inlet was allowed on a model with 930 nodes, it took the algorithm 1000 trials. It would have been even faster to try all 930 nodes successively! Due to the mesh distance-based model, optimising times in order of minutes instead of hours, like Young (1994), were still achieved. Unfortunately, no reference was made to the hardware used. A decade of computer hardware development alone could already be the reason for this improvement.

Hsiao *et al.* (2004) were some of the few researchers who tried to optimise the RIFT process. RTM software and a genetic algorithm were used to find the optimum for the diameter of the flow runner channels and the number of layers of a

flow distribution medium. Because these values could be zero, solutions without these flow enhancement structures could also be found. For the flow calculation they used the same software as Correia *et al.* (2004) (LIMS). The flow distribution medium and flow channels were modelled with 2D elements, which only had an in-plane permeability, but 3D elements were used to model the preform, which also took the through-the-thickness permeability into account. Good agreement between simulation and experiments was achieved and the void content was reduced by a smart choice of the flow enhancement structures. The arrangement of the flow distribution medium corresponded with the obvious solution, as already presented in Section 5.1: the distribution medium had to cover the entire top surface of the preform, except close to the vent. This allowed the resin to flow through the thickness before reaching the vent and hence preventing a dry spot under the vent. Unfortunately only one design case, where the position of the flow channels/pipes and flow distribution medium were fixed and determined by the user in advance, was presented. Especially with larger and more complex structures, the optimal position of these flow enhancement structures is not always straightforward and should be included in the adjustable production parameters, which have to be optimised by the routine.

Gokce & Advani (2004) focused on the optimal gate and vent location for the RTM process. Race-tracking along the mould perimeter was taken into account as an extra factor. Race-tracking is the phenomenon in which resin flows faster through undesirable flow channels than in the rest of the part. These flow channels occur due to disturbances in the preform or (most commonly) because the preform does not fit tightly into the mould, creating flow channels at the perimeter of the product. Race-tracking can be an issue in the RIFT process, but undesired open channels are more likely to be closed off by the flexible bag. The cascades optimisation method was used to find the optimal inlet/vent configuration and they verified their results in a Virtual Manufacturing Environment.

Summarizing all these modelling efforts, it is obvious that most authors focussed on optimising the inlet/vent positions for the RTM process. These algorithms can also be used for the RIFT process, in which an optimal inlet/vent position has importance similar to RTM. The tools based on physically based flow models were more time consuming than geometrically based ones. Some authors tried to reduce calculation costs by rather using other optimising algorithms than genetic algorithms, but were then limited to continuous objective functions (Lin *et al.*, 2000) or had to train a neural network (Luo *et al.*, 2001).

Hsiao *et al.* (2004) showed that significant improvements can be made to the RIFT process by a "smart" choice of the flow enhancement structures besides choosing the position of the inlet/vent correctly. Better improvements should be possible if also the positioning of the flow enhancement structures would be included in the optimising parameters. As already presented, the positioning of the distribution medium is quite straightforward and does not need to be opti-

mised. The model presented here will therefore optimise the inlet/vent position as well as the positioning of flow pipes.

5.3 Method of Optimisation

Based on the desired process properties (as process costs and time) the inlet/vent and flow pipe arrangement have to be optimised. As already presented in Section 1.3, the optimum process properties need to be determined by the user, e.g. should the process be fast or have low-cost, etc.

A newly developed mesh distance-based model is used here to simulate the process, based on a given inlet/vent and flow pipe arrangement. This mesh distance-based model is much faster and hence better suited for optimising purposes. It is similar to the model developed by Jiang *et al.* (2002) and will be explained in the next section (5.4). The output parameters of the mesh distance-based model are:

- x: The fill-distance;
- N_{vents}: The number of the vents;
- N_{pipes}: The length of the flow pipe, represented by the number of nodes on the pipe (pipe nodes).

These output parameters are coupled to the process properties, such as process costs and process time, using weighting functions. With the weighting factors, the output parameters are fitted into an objective function. For the optimisation of this objective function, a genetic algorithm (GA) will be used, since the design space is non-uniform and discrete. Young (1994) and Lin *et al.* (2000) showed that although other algorithms can be faster, GAs are stable and able to find the global optimum.

In genetics, the objective function is called the fitness function. Young (1994); Jiang *et al.* (2002) and also Gokce & Advani (2004) came up with similar objective or fitness functions to fit the output parameters into a fitness value F.

Generally, the fitness function has the following structure:

$$F = w_{vents}(1 - \frac{N_{vents} - 1}{N_{nodes}}) + w_{distance}(1 - \frac{x}{x_{max}}) + w_{pipes}(1 - \frac{N_{pipes}}{N_{nodes}}) \quad (5.3)$$

where

$$\sum w = 1 \tag{5.4}$$

In Eq. 5.3, w represents the weight functions with w_{vents} for the number of vents, $w_{distance}$ for the fill-distance and w_{pipes} for the number of pipe nodes respectively. N_{nodes} is the number of nodes in the model and hence the maximum number of pipe nodes and vents. The last parameter, x_{max}, is the maximum calculated distance (by the mesh distance-based model) between any two nodes in the model. The optimum of the fitness function is 1. This represents the case where there is only one vent, no pipe is being used and the fill-distance is 0.

The values for the weight functions are chosen according to the objective of the optimisation and the desired optimum process properties. If a short fill-time and hence fill-distance is important, the weight function $w_{distance}$ will be larger than in the case where the number of vents have to be reduced or the costs of consumables has to be reduced. In the next chapter, different fitness functions will be used for the different design cases which have different objectives, but firstly the developed mesh distance-based model and the genetic algorithm will be presented.

5.4 Mesh Distance-Based Model

The mesh distance-based model is based on the assumption that the resin first fills the nodes which are closest to the inlet(s), then the next closest, etc. Although locally true, Cai (1992) already showed that this assumption is not globally true for the RIFT or RTM process. If different types of flow exist (radial or linear/channel), it is possible that a node further away from the inlet is filled earlier than a closer one. Still it is valid to make this assumption when the objective of the optimisation is only to minimise the distance between inlet and vent with the minimum number of flow pipes (and an accurate estimation of the fill-time is of second order importance) (Jiang *et al.*, 2002).

The distance between the inlet and a certain vent is defined here as the fill-distance for that vent and the minimum distance between the inlet and a certain node is defined as the fill-distance for that node. The process of calculating the fill-distances for all nodes is presented in Table 5.1 and depicted in Figure 5.4. On 2D parts, the direct distance, as depicted in Figure 5.4, could be used, as Jiang *et al.* (2002) did, but it will restrict the model to the use of geometrically described surfaces. For parts where only a $2\frac{1}{2}$D unstructured mesh is given, this direct distance cannot be used.

Before the fill-distance for every node can be calculated, it should be known which nodes are the flow pipe nodes. The definition of the flow pipe nodes will

be discussed in the next paragraph.

Table 5.1: Method to calculate the fill-distances

Step	Procedure
	Initiation
1	The neighbour nodes of the inlet(s) are identified as flow front nodes and the inlet nodes are defined as distance known nodes with distance 0.
	Calculation
2	The distance of the flow front nodes to the distance-known-nodes is calculated. In case of a triangular mesh, as used in this research, the distance between two neighbouring nodes equals the edge length of the element they both belong to.
3	The minimum of the calculated distances for every flow front node is taken as the distance from this node to the inlet.
4	The distance of the flow front nodes is now known and therefore these nodes are defined as distance known nodes. Their neighbours are defined as flow front nodes.
	Termination
5	With this new set of flow front nodes the calculation continues with step 2 until the distances of all nodes in the model are known.

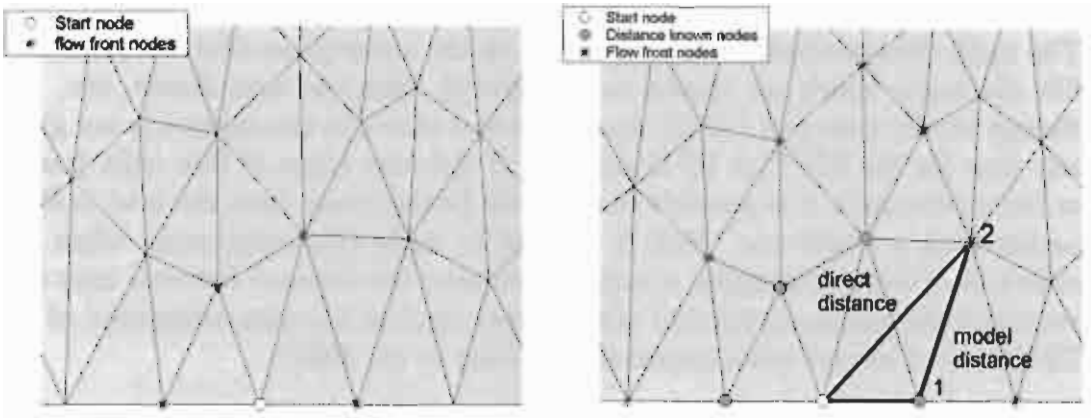

(a) First step (b) Second step

Figure 5.4: Calculation of the distance from the start node.

5.4.1 Definition of the Flow Pipes

The flow pipes can be defined in various ways. As Lin *et al.* (2000) indicated, for an accurate flow simulation the pipe should be modelled using more than one

node over its width. In most cases this would require a re-meshing of the product if different scenarios of flow pipe positioning are simulated, causing a significant time penalty. Because the mesh distance-based model is purely geometrically based, a single node can be used to represent the width of the pipe, without causing singularities.

The most straightforward way to define the pipe would be to define a chain of connecting nodes, which represents the shape of the pipe most accurately. In the case of Figure 5.5a, the definition would start with node 1, end with node 4 and include all the marked nodes in between. The disadvantage of this definition is that the number of possibilities is enormous should the optimal pipe position be unknown. In a simple model with 100 nodes where all nodes can be part of the pipe, there are 1.2E+30 possibilities for the positioning of the pipe, making it almost impossible to find an optimum.

Here another approach is used: the pipe is defined by its starting node and end node. The pipe itself lies on a geodesic path between the starting and end nodes along the element edges. This reduces the solution space significantly. For the same 100 node model, where the optimum starting and end node of the pipe have to be found, there will "only" be 10,000 possible solutions for such a pipe. This approach reduces the flexibility of the flow pipe: the flow pipe follows a geodesic path along the element edges, whereas with the other approach they can follow any path. If, in practice, more flexible pipes are desired, one or more extra points on the pipe can be defined, like in Figure 5.5b, giving this approach much more flexibility.

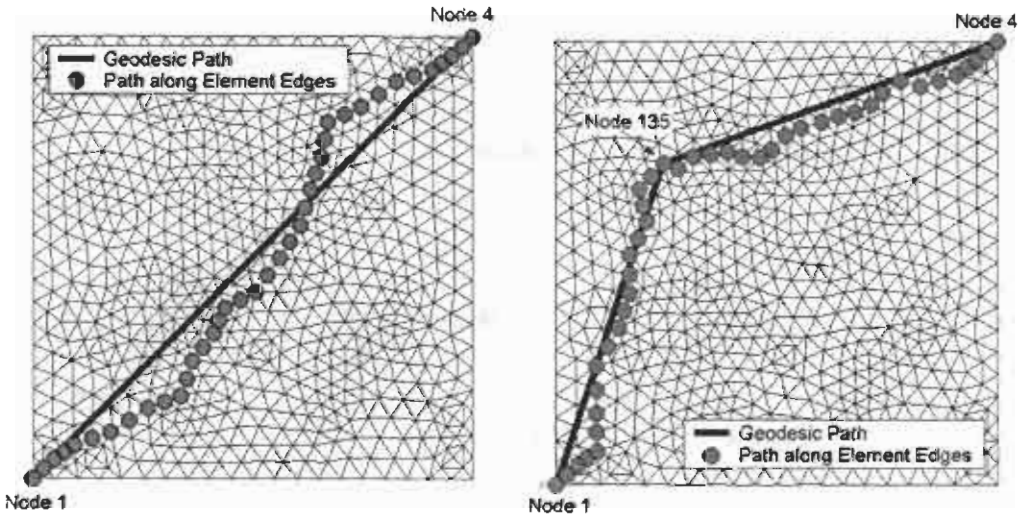

(a) To node 4 (b) To node 4 via node 135

Figure 5.5: Geodesic paths along the element edges of a pipe starting in node 1.

The geodesic path between two points on a surface is defined as the shortest

path on the surface between these points. Since the flow pipe has to follow the element edges, the geodesic path of the flow pipe is defined as the shortest path between its starting and end points along the element edges. An example is depicted in Figure 5.5. The actual path of the flow pipe is longer than the geodesic path between the starting and end point: Assume the width and length of the square in Figure 5.5 are both one metre, then the geodesic path has a length of 1.4142 m whereas the flow pipe along the element edges has a length of 1.5026 m.

The path of the flow pipe is easily found with the routine described in Table 5.1. The starting node of the flow pipe is defined as the inlet. For every node the shortest distance to the inlet is stored but also a "bread-crumb" containing the neighbouring node ID from where it gets its shortest distance. For example, assuming that the starting node in Figure 5.4b is the beginning of a flow pipe, then for Node 2, its shortest distance to the starting node is being stored, but also the bread-crumb where it gets its distance from: in this case Node 1.

At the end of the calculation routine of Table 5.1, this trail of bread-crumbs is traced back, starting at the end node and ending at the beginning of the pipe. This gives the shortest distance from the end node to the starting node, but also gives the inter-lying nodes on the pipe. These nodes, including the begin and end nodes, are defined as pipe nodes and define the path of the pipe along the element edges, as shown in Figure 5.5. For example, assuming again, that the starting node in Figure 5.4b is the beginning of a flow pipe and Node 2 is the end node of the flow pipe, then the trail of bread-crumbs will go from Node 2 to Node 1 and end at the starting node.

As already mentioned, extra flexibility is obtained by defining extra points / nodes on the pipe. This is especially necessary when modelling curved surfaces, for example spheres. The geodesic path on a curved surface is not always obvious or desired. An example is shown in Figure 5.6.

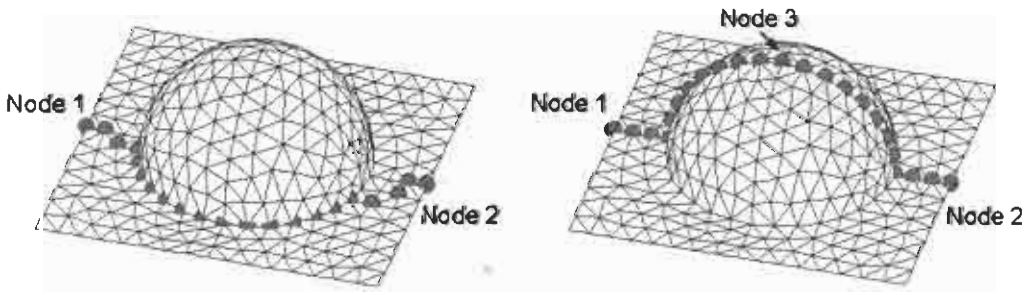

(a) To node 2 (b) To node 2 via node 3

Figure 5.6: Geodesic paths on a half sphere starting at node 1.

Assume that the pipe should go from node 1 to node 2 over the top of the sphere.

This is a direct path, but not the geodesic path between nodes 1 and 2. If only 2 nodes are defined, the model takes one of the 2 geodesic paths, as can be seen in Figure 5.6a. For this desired path a third point, on top of the sphere, has to be defined, as shown in Figure 5.6b.

As soon as all the pipe nodes are known, the fill-distance for every node is calculated, again by using the routine presented in Table 5.1. Because the permeability of a pipe is much higher than the permeability of a fibrous preform (as shown in Section 5.1), it is assumed that as soon as the process starts, all pipes are filled before any part of the preform wets out.

Figure 5.7 shows a practical example of the infusion of a 20 foot boat hull. All the pipes are already filled and the amount of wet preform can be ignored. Therefore the distance between the pipe node is divided by a large number (here 1000), making sure the pipe nodes are filled before any other node.

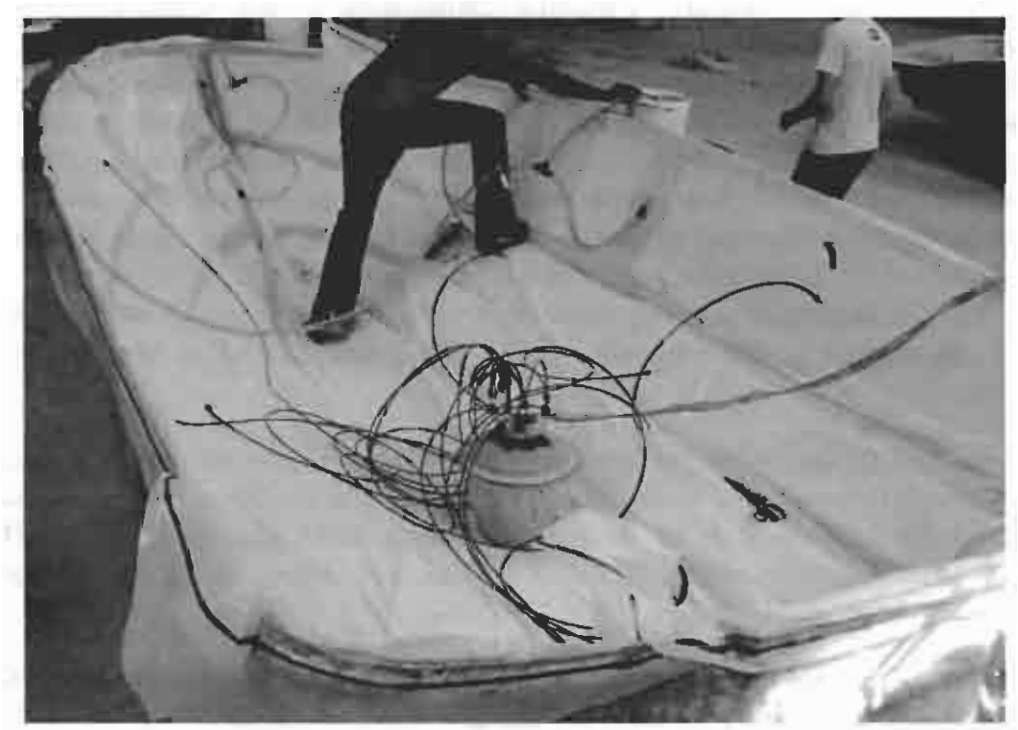

Figure 5.7: Infusion of a 20 foot boat hull.

5.4.2 Determination of the Vents

Based on the fill-distance of every node, the position of the vents is determined. Vents should be placed in such a way that all the air can evacuate during the process and no air gets trapped in a region. This is ensured when the vents are

positioned at the points which are filled last, while all their neighbouring nodes are already filled.

Boccard *et al.* (1995) as well as Jiang *et al.* (2002) used this definition for their geometrical models and placed the vents at the maximum distance in a region from the inlet. Jiang *et al.* (2002) also searched for these regions by checking, during the filling process, whether all areas were still connected. As soon as certain unsaturated areas were disconnected by the resin (as depicted in Figure 5.1 and 5.3), these areas were defined as groups where a vent should be placed. These groups are concatenated (all nodes in the group neighbour to one or more other nodes in the group) but cannot be connected with the other groups without passing the resin. The area of the groups was also calculated. The node with the maximum distance in every group was then defined as the vent position for that group.

From the article of Jiang *et al.* (2002) the reason for defining these groups and their areas remains unclear. A possible explanation is that it can function as an extra parameter of the objective function for the optimising routine. Their main objective was to reduce the number of vents. The area of the groups was a more continuous function than the function of the number of vents, which was discrete. Optimising continuous functions is much easier than optimising discrete ones (Lin *et al.*, 2000). Better convergence could be achieved if the area of one group is minimised instead of merely looking at the number of vents. However, the definition of the groups comes with a serious calculation time penalty because an extra calculation loop is required. As will be indicated in the next chapter, good convergence is also achieved without this extra calculation loop and time penalty.

The method to determine the vent positions developed and used here is simple and straightforward: the vents should be positioned at the nodes which have a larger fill-distance than all their neighbouring nodes (local maxima). This reduces the determination of the vent to a simple matrix operation, reducing calculation costs significantly.

As soon as all pipe defining nodes and inlets are known, the maximum fill-distance and the number of vents for the model is calculated, using the method described in Table 5.1. With these parameters and the fitness function, the fitness value for this pipe arrangement is calculated. As already explained in Section 5.3 a genetic algorithm is used for the maximisation of the fitness function, which is explained in the next section.

5.5 Genetic Algorithm

The mesh distance-based model calculates the infusion length (fill-distance) and the positions and number of vents as a function of the inlet and pipe positions. Using the weighting functions, these output parameters are fitted into an objective function. In this section, the optimisation of this objective function is presented.

Generally, traditional algorithms for function optimisation are limited to convex regular functions. They use characteristics, such as gradients, linearity and continuity of the problem to determine the next sample point. However, many functions are multi-modal, discontinuous and non-differentiable, like the one in this study. For this kind of design space, stochastic sampling methods can be used: the next sample point is determined, based on stochastic sampling/decision rules rather than on a set of deterministic decision rules (Houck *et al.*, 1998). Genetic Algorithms (GAs) belong to this group of stochastic methods.

The basic principles of GAs were proposed by Holland (1975). It is based on the mechanism of natural selection and natural genetics for which the English philosopher, Herbert Spencer coined the phrase "Survival of the fittest" (Man *et al.*, 1999). The combination of design parameters is represented by a single bit string analogue to the genes of a chromosome. Several of these bit strings, generated by the different combinations of design parameters, form a population.

The degree of "goodness", or how well the chromosome fits into the environment, is represented by a fitness value, which is calculated using a fitness function, as already presented in Section 5.3. Throughout a genetic evolution, the fitter chromosome has a tendency to yield better quality offspring, meaning a better solution to the problem. Hence, through natural selection and reproduction, the population improves and only those who fit in the environment best (highest fitness value) will survive and represent the optimal solution (Young, 1994; Man *et al.*, 1999).

The main strength of GAs is that they are robust, can deal with a wide range of problem types and generally produce global optimal solutions in a large search space. As Goldberg (1989) stated: the reason GA's are still robust in a multi-modal, discontinuous and non-differentiable design space is that they differ in four ways from normal optimisation:

1. GAs work with a coding of the parameter set, not the parameters themselves.
2. GAs search from a population of points, not a single point.
3. GAs use objective function (fitness-function) information, not derivatives or other auxiliary knowledge.

4. GAs use probabilistic transition rules, not deterministic rules.

Therefore, as shown at the beginning of this chapter, most researchers used GAs to optimise the mould-filling process (Young, 1994; Lin *et al.*, 2000; Luo *et al.*, 2001; Jiang *et al.*, 2002; Hsiao *et al.*, 2004). Other methods, such as cascaded optimisation (Gokce & Advani, 2004) or the quasi-Newtonian method presented by Lin *et al.* (2000), can obtain faster results, but because of its stability and other advantages, a GA is also used here. Furthermore, the proposed model is much faster than conventional flow models, allowing large numbers of iterations in a relatively short period of time.

The different steps **Initiation, Selection, Reproduction** and **Termination** of the GA developed here will be discussed in more detail in the subsequent sections.

5.5.1 Initiation

The algorithm starts with the initiation of a random population. Traditionally, binary digits are being used to represent the design parameters, e.g. a pipe at node position 10 could be represented with the binary digits 00001011. Real or integer values can also be used, allowing a wider range of operators. Goldberg (1989) recommended "the principle of meaningful building blocks". For this optimisation problem, an integer representation of the pipe positions is more meaningful and therefore used. The number of the node has no physical relationship with its position: Similar numbers do not have to be close to one another.

The definition of the individuals depends on the number of pipes to be allowed in the process and how the pipes should be defined. If only one pipe is allowed, its definition is straightforward and defined by its start and end points. For example: if the pipe starts at the node with the node ID number 15 and ends with node ID number 12, the individual representing this pipe will be defined with the "chromosome" [15 12].

In case more pipes are allowed, the individuals describing these pipes can be defined in numerous ways. Table 5.2 shows a few examples in case two pipes are present. In case the pipes do not have to connect, they both have to be defined by their Beginning node ID (BID) and End node ID (EID). In case the pipes are connected at their end points, only the beginning of the first pipe and the end of the first and the second pipe have to be defined, because the end of the first pipe is the same as the beginning of the second pipe. The last case of Table 5.2, which will also be used here, is when the second pipe connects to any position on the first pipe. The beginning of the second pipe is not defined by a node ID, but by a length percentage of the first pipe (B%). The node on the first pipe,

which is closest to this length percentage of the first pipe, is chosen as a begin node of the second pipe.

Table 5.2: Three examples of the definition of the individuals for two pipes

No Connection				Pipes connect by Ends			Second connects to First			
BID	EID	BID	EID	BID	EID/BID	EID	BID	EID	B%	EID
[15	12	24	14]	[15	12	14]	[15	12	90%	14]

5.5.2 Selection

Once the population has been defined, a selection is made of which individuals will produce offspring. One of the most common proportionate selection techniques, and also the technique used here, is the Roulette Wheel Selection scheme (Man *et al.*, 1999).

In this scheme, the fitness of all the individuals in the population is added up, giving the total fitness. A random number is generated between 0 and the total fitness. The individual whose fitness, added to the fitness of the preceding individuals, is equal or larger than the random number, is selected as a parent. In Figure 5.8 the circumference of the circle is the total fitness of the population with 5 individuals.

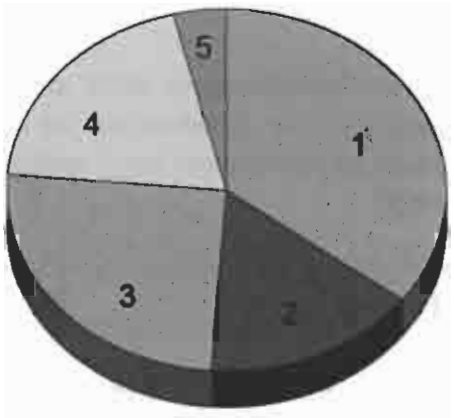

Figure 5.8: Roulette wheel selection.

The size of the interval of each individual i in the pie chart represents its fitness F_i. In this figure, individual 1 is the fittest and occupies the largest interval and therefore has the highest probability to be chosen. More general: the probability, P_i, that individual i, with fitness F_i is chosen out of a population with $PopSize$ individuals is:

$$P_i = \frac{F_i}{\sum_{j=1}^{PopSize} F_j} \tag{5.5}$$

This shows that the use of roulette wheel selection limits the GA to maximisation since the evaluation function must map the solutions to a fully ordered set of real positive values ($\Re^+$). Other methods, such as ranking methods, allow minimisation and negativity (Houck *et al.*, 1998). In this case the fitness-evaluation function can be declared in such a way that the GA only has to maximise the fitness function, overcoming this limitation of the roulette wheel selection.

5.5.3 Reproduction

The generation of offspring is controlled by two fundamental operators: Cross-over and Mutation. One-point cross-over (also called simple cross-over) is depicted in Figure 5.9. With a probability $P_{cross-over}$, an arbitrary cross-over point is chosen and the portions of the two individuals behind that point are cut off and exchanged to form the new offspring.

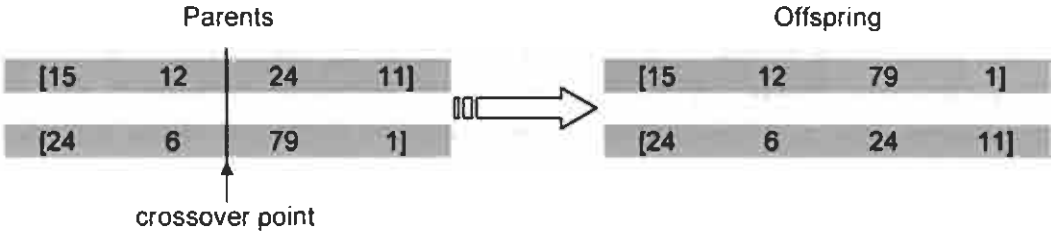

Figure 5.9: Example of one-point cross-over.

Multi-point cross-over can be introduced to allow more sections of the parents to exchange. Here the length of the chromosome for each individual is limited (the maximum is the number of pipes times two), making multi-point cross-over less useful (Man *et al.*, 1999).

The use of real values, to represent the design parameters, allows more operators, such as (Beasley *et al.*, 1993):

- Average: take the arithmetic average of the two parent genes.
- Geometric mean: take the square-root of the product of the two parents
- Extension: take the difference between the two values, and add it to the higher, or subtract it from the lower.

As already mentioned, the node IDs in the model only depend on the way the mesh was generated and do not have a physical meaning or relationship with its position. An example are the meshes generated by the PDE-Toolbox of Matlab: The first node IDs are positioned at the corners of the meshed geometry. Any kind of averaging or extending makes no physical sense and is similar to a random

mutation or creation of the offspring. These types of operators were therefore not used.

After cross-over the offspring is exposed to mutation. A similarity can be found in natural genetics: a spontaneous change in the DNA sequence can be caused by deamination of certain bases, hydrolysis of base-sugar, radiation damage and oxidative damage (Man *et al.*, 1999, 6). In a GA, mutation is applied to each offspring individually and randomly with a small probability $P_{mutation}$. This principle of mutation is depicted in Figure 5.10.

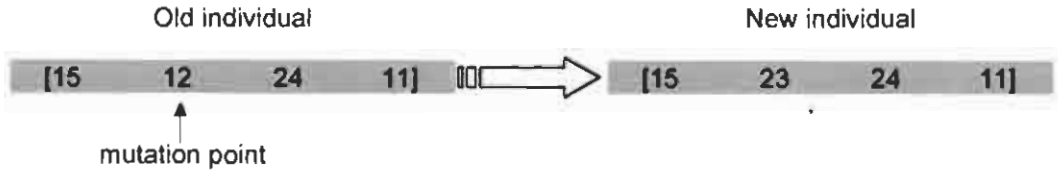

Figure 5.10: Example of one-bit random mutation.

Beasley *et al.* (1993) also present two extra mutation operators for real value representation:

- Creep: add or subtract a small, randomly generated amount.
- Geometric creep: multiply by a random amount close to one.

For the same reason the extra cross-over operators were not used, these extra mutation operators were also not used.

The probability of cross-over ($P_{cross-over}$) and mutation ($P_{mutation}$) are normally fixed values. The problem with fixed values is that after the population evolves, it becomes quite homogeneous and offspring produced by cross-over become clones instead of new samples. Booker (1987) presented a variable cross-over rate, depending on the spread of fitness. When the population converges, the cross-over rate is reduced to give more opportunity for mutation to find new variations. De Jong & Spears (1990) showed that having such an "adaptive" cross-over operator enhances long-term performance significantly. In our case, the mutation rate was set to 0.2 and the cross-over rate varied linearly from 1 to 0.3, depending on the spread of the population.

Due to cross-over and mutation, it is possible that the best individual is not conserved. Many researchers reinsert the best parent(s) after mutation to ensure that the best solution is conserved. An example is given by Man *et al.* (1999, 19) where the best half of the parent population and the best half of the offspring population are combined to form the new population. The disadvantage of this method is that it gives less possibilities for the algorithm to find better solutions different from the known solutions, since they have a higher probability

of selection. Another solution, the method used here, is to reinsert the best individual after n-steps. If after n-steps no individual had a better fitness than the best individual, this best individual is inserted in the algorithm again.

5.5.4 Termination

The termination of the GA is controlled by the convergence and a maximum number of iteration steps. The solution is considered to be converged, if the fitness of the best individual in the population did not improve during the last m iteration steps, where m has to be determined for every case. To prevent excessive calculation times when the solution does not converge, a maximum number of iteration steps is set as a safety limit. If this maximum number of steps is reached, the iteration cycle is ended, but it is less likely that the optimum solution is found.

5.5.5 Implementation

The combination of the mesh distance-based model and the Genetic Algorithm forms the model for optimising the RIFT process. The mesh distance-based model and the GA were implemented in the MATLAB programming environment. The structure of the model for optimising RIFT is schematically represented in Figure 5.11.

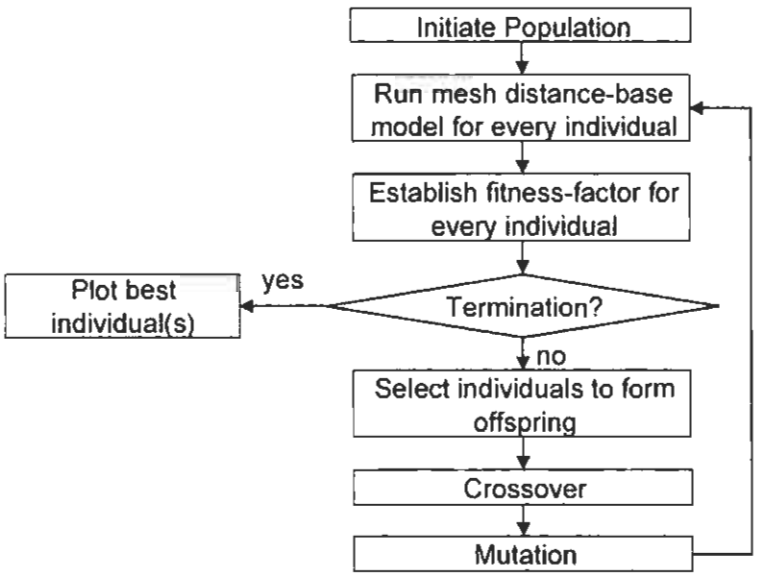

Figure 5.11: Diagram of the Model for Optimising RIFT.

Chapter 6

Simulations and Results

The mesh distance-based model together with the genetic algorithm were, like the physically based flow model of Part I, also implemented in the MATLAB programming environment, forming a genetically based optimisation tool for the RIFT process. The two components of this tool, namely the mesh distance-based model and the genetic algorithm, were validated successively. The results of the verification will therefore also be presented successively.

The mesh distance-based model is solely geometrically based and the following aspects were therefore compared with known geometric formulas:

- **Calculated Distance**: The distances calculated by the model were compared with known geometric distances.
- **Position of the Vents**: The predicted positions of the vents were validated with cases known from literature.

Having verified the mesh distance-based model, the effectiveness of the genetic algorithm and the influence of different fitness functions were analysed with a number of design cases. Finally the results of one of the design cases was compared with the results of the physically based model of Part I.

The results of all the verifications, presented in this chapter, will be discussed in Chapter 7.

6.1 Calculated Distance

The model uses the method depicted in Figure 5.4 to calculate the distances between the nodes. Significant errors can occur between this calculated distance

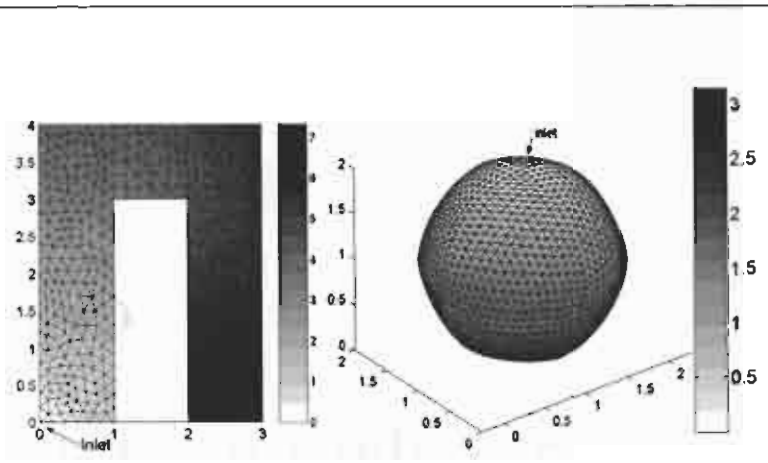

(a) direct (b) direct

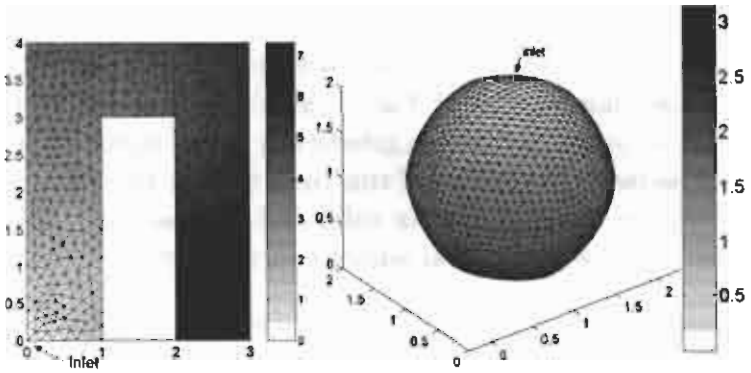

(c) mesh based (d) mesh based

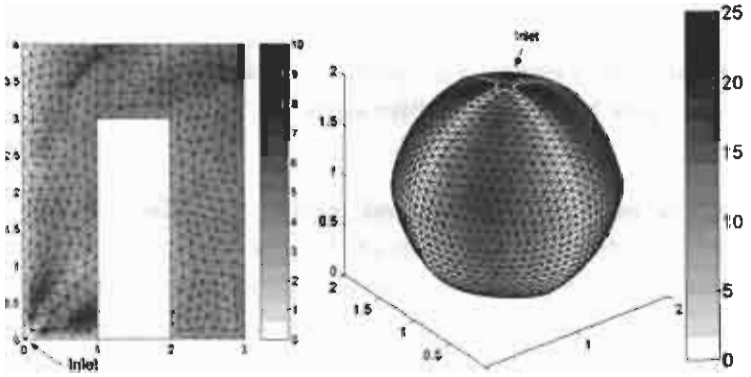

(e) error % (f) error %

Figure 6.1: Distances from the top to any node on a sphere and the distances from the bottom left corner to any node on a U-shaped plate and the error between the two approaches.

and the geometrical, direct distance. The direct distance from the starting node to node 2 in Figure 5.4 differs quite considerably from the calculated distance via the interlying node 1. As already presented in Section 5.4, the direct distance could be used in case the surfaces of the product are geometrically described. The model, developed here, has to handle any $2\frac{1}{2}$D unstructured mesh and hence the direct distance cannot be used.

The error between the geometrical, direct distance and the mesh-based distance for respectively a sphere and an U-shaped plate is presented in Figure 6.1. The intensity of the grey scale represents the fill-distance in metres or the error in percentage. The figure shows that especially close to the inlet, the relative error is quite large (up to 25%) and that the relative error between the geometrical distance and the mesh-based distance for a certain node decreases if the number of nodes between the inlet and that node increases. The relative error near the inlet on the U-shaped plate is approximately 10%, whereas the relative error on the point furthest away from the inlet is more or less 3%.

6.2 Position of the Vents

The method to determine the location of the vents, presented in Section 5.4.2, was verified using the results of Boccard *et al.* (1995) and Jiang *et al.* (2002). They extensively verified their method to determine vent locations with a number of design cases. In these design cases, the user determined the shape of the (2D) products and the position of the inlet(s). The models of Boccard *et al.* (1995) and Jiang *et al.* (2002) had to find the desired location of the vents for these design cases in order to prevent dry spots. The forecasted vent locations were validated with the practical experiments of Boccard *et al.* (1995) and showed good agreement.

The same design cases of Boccard *et al.* (1995) and Jiang *et al.* (2002) were used here to verify the method to determine the vent locations of Section 5.4.2. The most critical cases, where multiple flow fronts and inserts in the product exist, are depicted in Figure 6.2.

The fringes in the figure represent the fill-distances from the inlet(s). The location of the vents were determined by the mesh distance-based model of Section 5.4. The positions and the number of vents all agree very well (100%) with the results from Boccard *et al.* (1995) and Jiang *et al.* (2002).

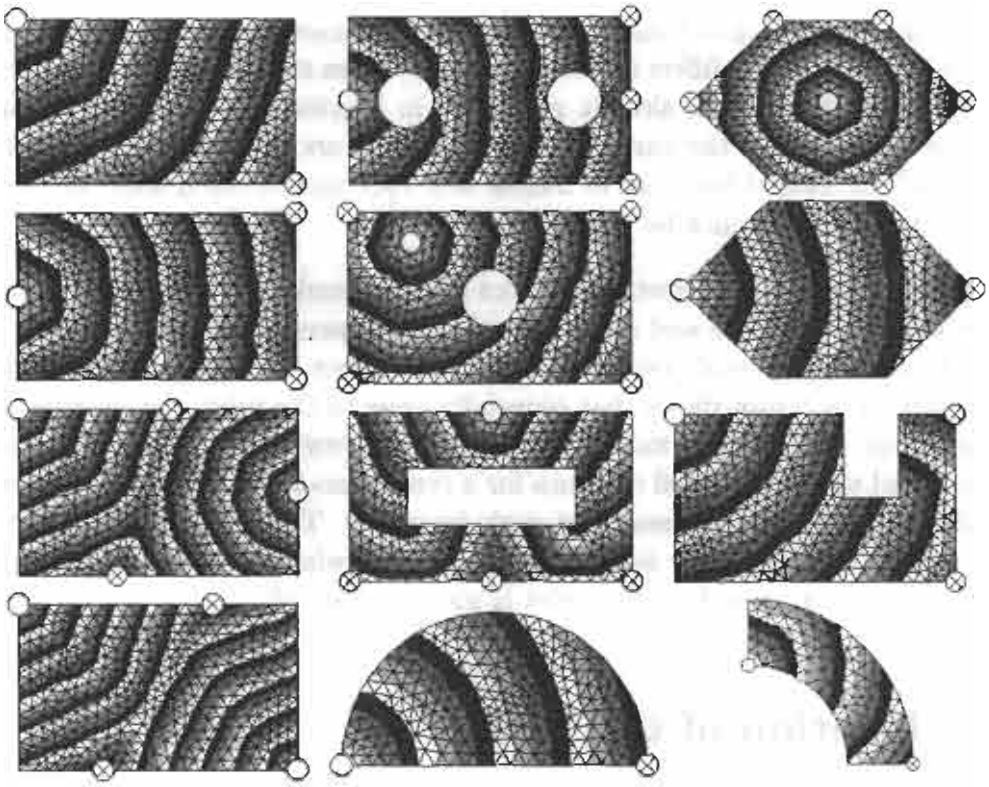

Figure 6.2: Vent (⊗) and inlet (◯) positions for different shapes.

6.3 Design Cases and Model Settings

The effectiveness of the genetic algorithm was validated with a number of design cases. The optimisation tool had to find the optimal pipe and vent location in order to minimise the maximum fill-distance. The model was allowed to locate the pipe(s) and vent(s) anywhere on the product. The begin node of the first flow pipe was considered to be the resin inlet. The pipe and vent arrangement was optimised for the following products:

- A flat rectangular plate;
- A flat T-shaped plate;
- A glider seat.

The flat plates were used to examine the influence of different fitness-functions. Furthermore, the optimal solutions for these plates were easier to recognize, since they are 2D products.

The glider seat is a 3D complex part and was used to validate how the optimisation tool handles these kinds of shapes. Different numbers of flow pipes

were allowed on the product to show the influence on the optimal solution. The final solution of the genetically based optimisation tool was verified with the physically based model of Part I.

For all design cases, the following model settings, as described in Section 5.5, were chosen:

- **Population size**: was set at 20. This number was based on the recommendations of De Jong & Spears (1990) as well as Man *et al.* (1999, 10).
- **Probability of Mutation**: was set at 0.2, as also recommended by De Jong & Spears (1990).
- **Probability of Cross-over**: was varied linearly between 1 and 0.3, depending on the spread of the population.
- **Reinsertion rate**: the best individual was reinserted after every 20 generations, unless a better individual had been found in the meantime.
- **Convergence**: if the fitness did not improve during the last 200 steps, the solution was considered to be converged. This was based on experience: The solution of the cases used here did not improve further if more than 170 generations were calculated since the last best solution.
- **Maximum number of iteration steps**: was set at 1000. This number was never reached for the results presented in the following sections.

Finally the fitness function was defined. The function used here gives the fitness, F, as a function of the fill-distance, x, and the maximum distance in the model, x_{max}:

$$F = (1 - \frac{x}{x_{max}})/P_{vents} \tag{6.1}$$

The variable P_{vents} works as a penalty in case an individual has more vents, N_{vents}, than the maximum allowable number of vents, N_a, and was defined as:

$$P_{vents} = \max \begin{Bmatrix} N_{vents} - N_a + 1 \\ 1 \end{Bmatrix} \tag{6.2}$$

6.4 Rectangular Plate

The first design case was a rectangular, flat plate with dimensions 0.6 x 1.0 m, meshed with 1581 nodes and 3000 first-order triangular elements.

Four scenarios were simulated. For the first three scenarios, the objective of the optimisation was to minimise the maximum fill-distance. For the last scenario, the number of consumables had to be minimised as well.

6.4.1 Scenario 1

For the first scenario, the optimisation tool had to find the minimum fill-distance (thus maximising the fitness function F of Eq.6.1) using one pipe only. The pipe was defined by only its Begin- and End node ID-number, or as defined in Table 5.2: [BID EID]. One vent was allowed and hence in Eq. 6.1, N_a=1.

Convergence was reached after 17 minutes on a 2.01 GHz PC with 512 MB of RAM. The best solution, after convergence was reached, is presented in Figure 6.3. In this figure, and also in the following figures, ∞ are pipe nodes, $\otimes$ marks the position of a vent and $\odot$ is the beginning of the flow pipe and also the inlet. The intensity of the grey scale represents the fill-distance in metres.

The solution presented in Figure 6.3a confirms the obvious result and corresponds with the design rules of Cai (1992). Figure 6.3b shows the maximum, minimum and average fitness of the population during the optimisation cycles.

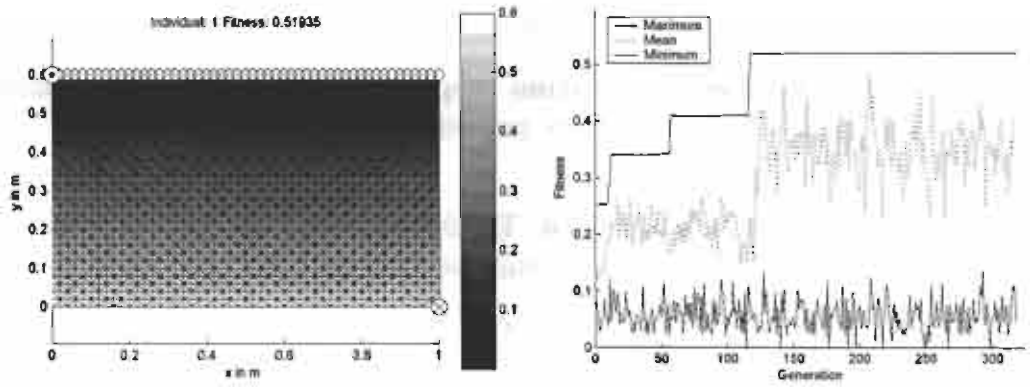

(a) Best solution (b) Development of the population

Figure 6.3: Optimising the fill-distance if 1 vent and 1 pipe are allowed.

After approximately 120 generations (117 to be exact), the optimal solution was found. Every generation consisted of 20 individuals, thus 2340 individuals (or iteration steps) were calculated to obtain the optimal solution. With 1581 nodes in the model, there were 1249780 possibilities to position this pipe. This shows that the genetic algorithm is over 500 times more effective than trying all possibilities successively. However, as shown in Figure 6.3b, after the optimal solution was found, the algorithm calculated another 200 generations to ensure

convergence, and the solution obtained was the optimal solution. This resulted in a total of 318 generations (6360 individuals), which is still almost 200 times less than the total number of possibilities.

6.4.2 Scenario 2

The objective of the second scenario was the same as the first, and again only one pipe and vent were allowed. However, the pipe was defined using an extra central point, making the definition of this pipe according to Table 5.2: [BID EID/BID EID]. In this case, there were approximately $4x10^9$ possibilities for the positioning this pipe.

The best solution after convergence is depicted in Figure 6.4.

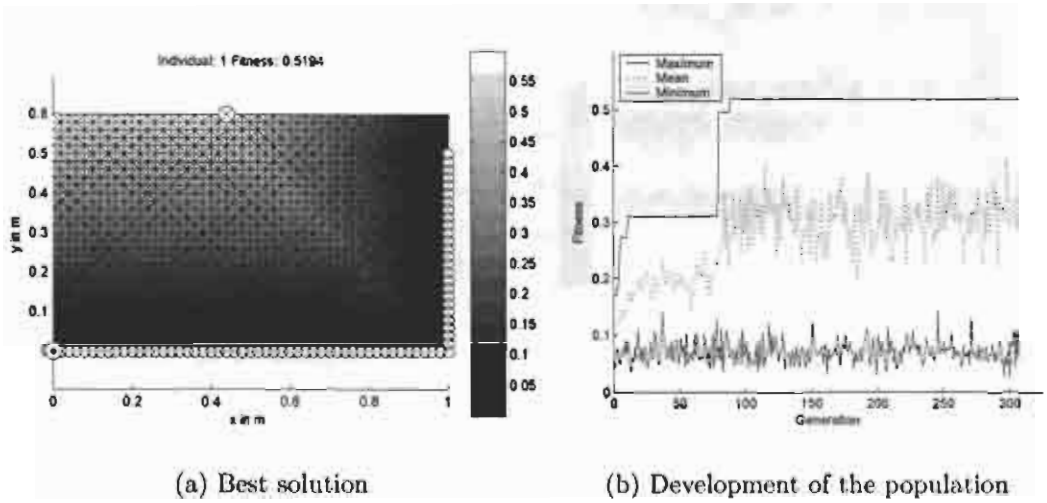

(a) Best solution (b) Development of the population

Figure 6.4: Optimising the fill-distance if 1 vent and 1 pipe with a central point are allowed.

The solution shown in Figure 6.4 has the same fitness as the solution of scenario 2. One would probably expect that the pipe would go all the way up to the upper right corner. However, this would not reduce the maximum fill-distance, since 0.6 m will still be the maximum distance from any pipe. More interesting is the development of the population: the algorithm needed more or less the same number of individuals to come to convergence compared to the first scenario, although the number of possible solutions was much larger. The genetic algorithm became more effective as the number of design parameters increased. Of course the figure only shows one case. Therefore the first scenario was simulated 50 times, as well as the second scenario. On average, the first scenario converged after 326 generations and the second after 353 generations.

6.4.3 Scenario 3

The objective of the third scenario was, like the other scenarios, to minimise the maximum fill-distance. However, a total of 3 pipes and 2 vents were allowed on the product. The first pipe was defined by an extra central point and two other pipes had to connect to this main pipe. The definition, according to Table 5.2, for these pipes is: [BID EID/BID EID B% EID B% EID]. The same fitness function was used, but in order to allow 2 vents on the product $N_a = 2$.

The results after convergence are presented in Figure 6.5. Also here the algorithm did not need significantly more calculation time than with the first scenario.

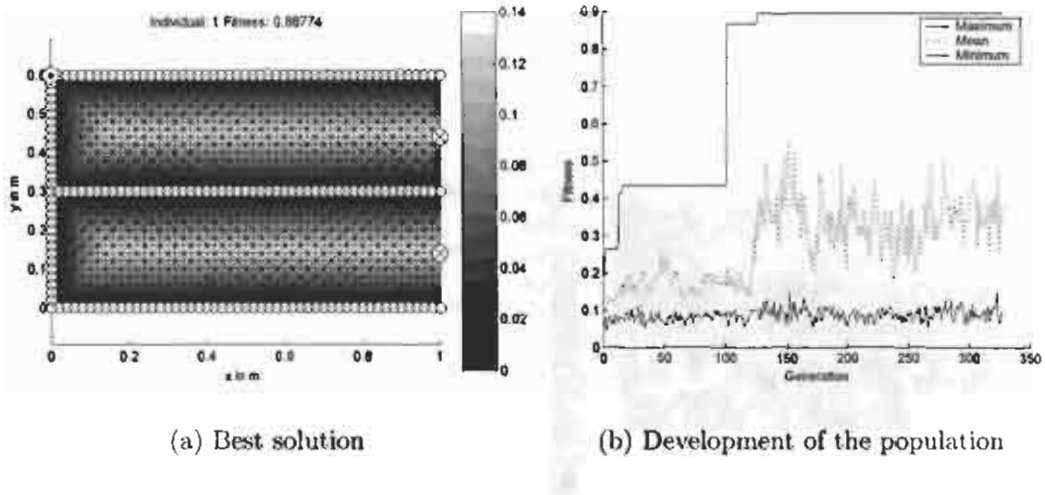

(a) Best solution

(b) Development of the population

Figure 6.5: Optimising the fill-distance if 2 vents and 3 pipes are allowed.

The result of this scenario also confirmed the obvious solution, but also gave rise to the question: Is this the optimal solution with the minimum number of pipe nodes required? It can be expected that, for example, the middle pipe could be shorter without reducing the maximum fill-distance of 0.14 m. Therefore the amount of consumables was minimised as well as in the fourth and final scenario.

6.4.4 Scenario 4

The objective of the fourth scenario was to minimise both the fill-distance and the flow pipe length. The same boundary conditions (number of pipes and vents) applied as for scenario 3. By reducing the pipe length, the amount and cost of consumables as well as the amount of resin needed to fill the product will be reduced. If, for example, a spiral bind with a diameter of 12 mm is used, every meter of this flow pipe will consume an extra 112 ml of resin.

In case a reduction of consumables and costs is desired, the genetic algorithm can easily be adjusted to minimise the flow pipe length, simply by modifying the fitness function. The total length of the flow pipes could be calculated by adding up the lengths of the edges of the elements between the pipe nodes. It is much faster to look at the number of pipe nodes, N_{pipes}, which also gives a fair indication of the total pipe length, provided the lengths of the element edges are more or less uniform. The following fitness function was therefore used to also minimise the pipe length:

$$F = \frac{w_{distance} \cdot (1 - \frac{x}{x_{max}}) + w_{pipes} \cdot (1 - \frac{N_{pipes}}{N_{nodes}})^4}{P_{vents} \cdot P_{distance}} \tag{6.3}$$

In this fitness function, N_{nodes} is the total number of nodes in the model. Because the total number of nodes in the model is usually much larger than the number of pipe nodes, N_{pipes}, the term N_{pipes}/N_{nodes} is not very sensitive to a change in the number of pipe nodes. A 4th power was therefore applied to the pipe evaluation. Hsiao *et al.* (2004) also used this 4th power to distinguish the good results from a batch of results more clearly.

The factors $w_{distance}$ and w_{pipes} are the weighting factors for the evaluation of the fill-distance and the number of pipe nodes respectively. These weighting factors have a huge influence on the final solution: If $w_{distance}$=1 and w_{pipes}=0, the solution will be as depicted in Figure 6.5a. If $w_{distance}$=0 and w_{pipes}=1, the optimal solution will be that no pipes are placed on the product. Here, $w_{distance}$ and w_{pipes} were set at 0.1 and 0.9 respectively in order to emphasise the optimisation of the flow pipe length. Still, it had to be ensured that the total fill-distance is not larger than the allowable fill-distance, which was arbitrarily set at 0.2 m. For this reason, an extra penalty function, $P_{distance}$, was introduced, which reduced the fitness if the fill-distance is larger than 0.2 m:

$$P_{distance} = \begin{cases} 10, x > 0.2 \\ 1, x \leq 0.2 \end{cases} \tag{6.4}$$

The result with the highest fitness factor after convergence is depicted in Figure 6.6. All three horizontal pipes were shorter and the length of the flow pipes was reduced by 0.34 m compared to the previous case. The maximum fill-distance was 0.2 m, as could be expected due to the penalty function.

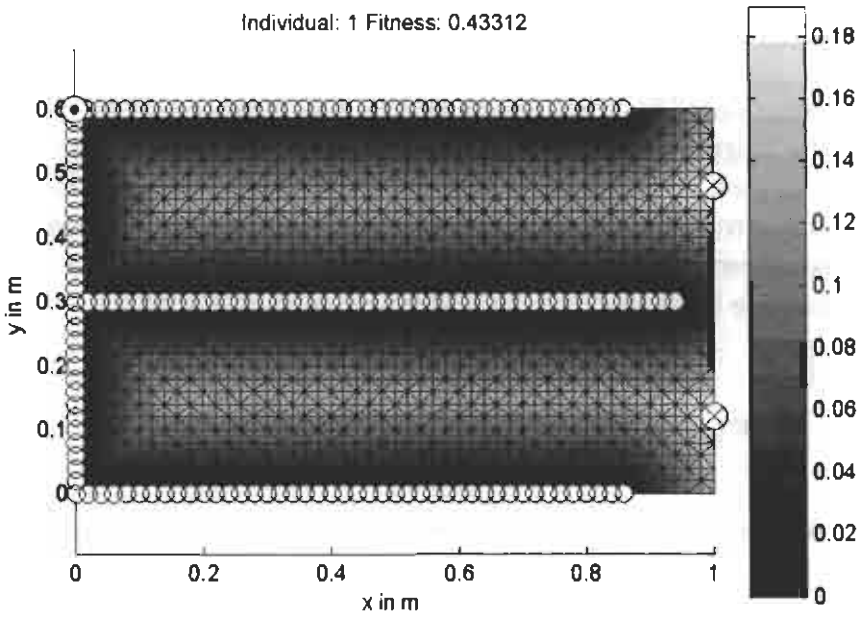

Figure 6.6: Optimising the fill-distance and the amount of consumables if 2 vents and 3 pipes are allowed.

6.5 T-Shaped Plate

The optimal positioning of the flow pipes on the rectangular plate was quite straightforward. Therefore the pipe positioning on a 1 x 1 m T-shaped plate was also optimised. The objective was the same as for the rectangular plate: minimising the maximum fill-distance. One main pipe and one pipe attached to this main pipe were allowed on the plate, so the definition of the pipes was: [BID EID B% EID]. The amount of consumables was kept free, so Eq. 6.1 was used to calculate the fitness for every individual.

6.5.1 Scenario 1

In the first scenario, the number of vents was kept free as well, so $N_a = \infty$. For this case, the best and second best solution after convergence are presented in Figure 6.7

The number of vents in Figure 6.7, especially for the best solution, was quite large. In a production environment this is undesirable, especially if the vents are located on the product and on the perimeter. Therefore a second scenario was simulated.

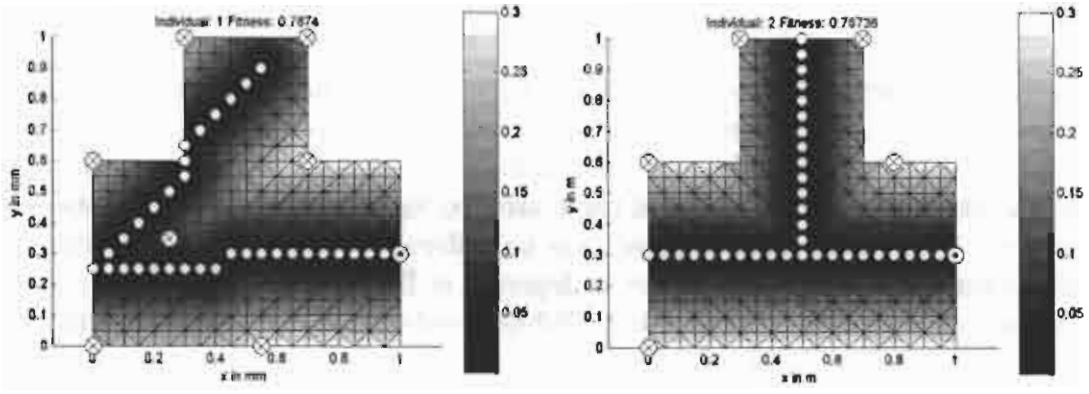

(a) best solution (b) second best solution

Figure 6.7: Fill-distance of the two best solutions for a T-shaped plate if the number of vents may be infinite.

6.5.2 Scenario 2

In this scenario, the allowable number of vents was set at 1 ($N_a = 1$) and the objective was still to minimise the maximum fill-distance. The best and second best solution after convergence for this scenario are presented in Figure 6.8. No optimal solution was found with only one vent. Interestingly, the second best solution even had 3 vents, but because the fill-distance was significantly smaller than that of the best solution, it still had a comparable value for the fitness.

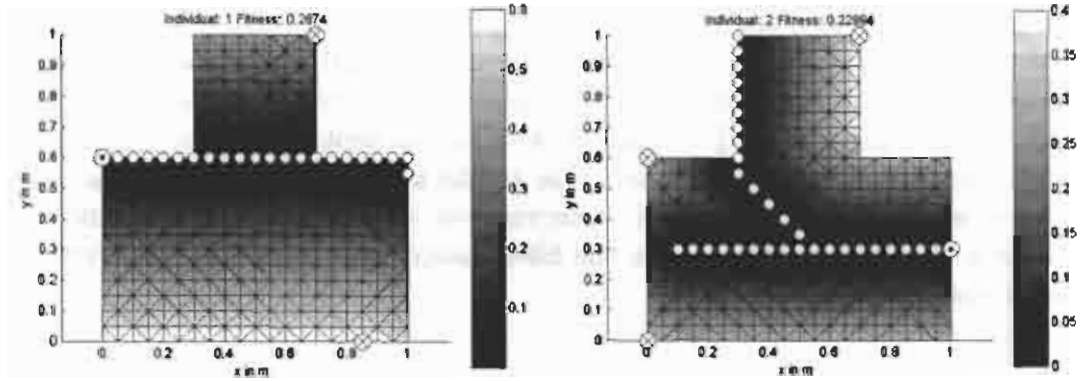

(a) best solution (b) second best solution

Figure 6.8: Fill-distance of the two best solutions for a T-shaped plate if the number of vents should be one.

6.6 Glider Seat

The following design case was a pilot seat for a glider. Where the previous design cases were only 2D, this product was 3D and had a more complex shape. The seat is basically a bath-tub shape with a back rest and armrests on either side. On the other side of the back rest there are two leg rests with a gap in between for the control stick. The arm rests are on different levels, thus the product is not symmetrical. The CAD model is depicted in Figure 6.9a. This CAD model was meshed with MSC-Patran using 1463 first-order triangular elements and 807 nodes. The meshed FEM model is presented in Figure 6.9b.

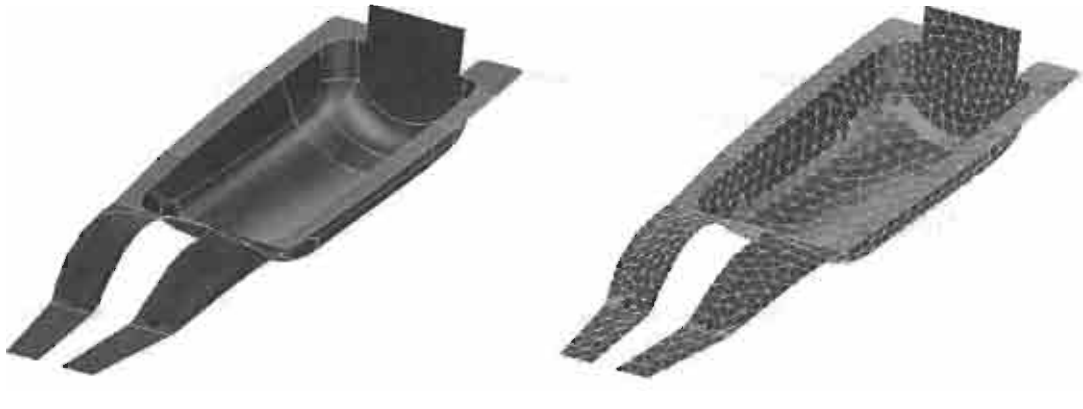

(a) CAD (b) FEM

Figure 6.9: The CAD and FEM model of the glider seat

The seat consists of a combination of carbon-and-Kevlar fibre and production numbers are only a few per year. Since the permeability of this carbon/Kevlar combination is quite low, infusion times and thus the maximum fill-distance had to be as short as possible. The number of vents was kept free ($N_a = \infty$) and the fitness function of Eq.6.1 was used. Due to the two leg rests, it was clear that at least two pipes should be used, otherwise one of the two leg rests would not contain a pipe which will increase the fill-distance by at least the full length of the leg rest (approx. 0.5 m)

6.6.1 Scenario 1

For the first optimisation scenario, 2 pipes were allowed, where the second pipe had to connect to the first pipe. Both pipes were defined using three points, as described in Section 5.4.1, to allow the pipes to be more flexible on the curved surfaces.

The result with the best fitness factor, after the optimisation routine converged, is presented in Figure 6.10. Convergence was reached after 382 generations and 10 minutes of calculation time. The solution with the best fitness factor had both pipes leading to the end of each leg rest, where the second pipe connected right at the beginning of the first pipe. The maximum fill-distance was 0.26 m and the number of vents was 8.

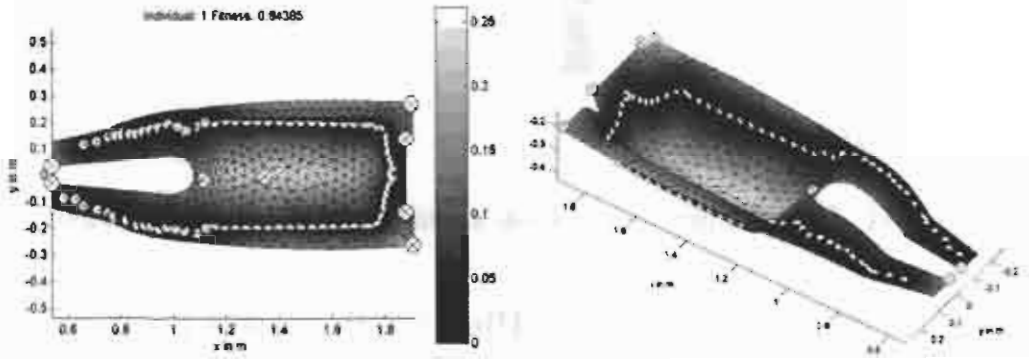

(a) Top View (b) 3D view

Figure 6.10: Optimal pipe position on a glider seat if 2 pipes are allowed. (○ is a pipe, ⊗ is a vent and ⊙ is the inlet)

6.6.2 Scenario 2

In order to reduce the fill-distance even further, a second scenario was simulated where a third pipe was allowed. Convergence was reached after 551 generations and 14 minutes of calculation time. The solutions with the best and second best fitness after convergence are depicted in Figure 6.11.

The fill-distance was further reduced to 0.21 metre. The solution with the highest fitness required a total of 9 vents, whereas with the solution with the second best fitness only 8 vents were necessary. Therefore, the second best solution was preferred to the best solution.

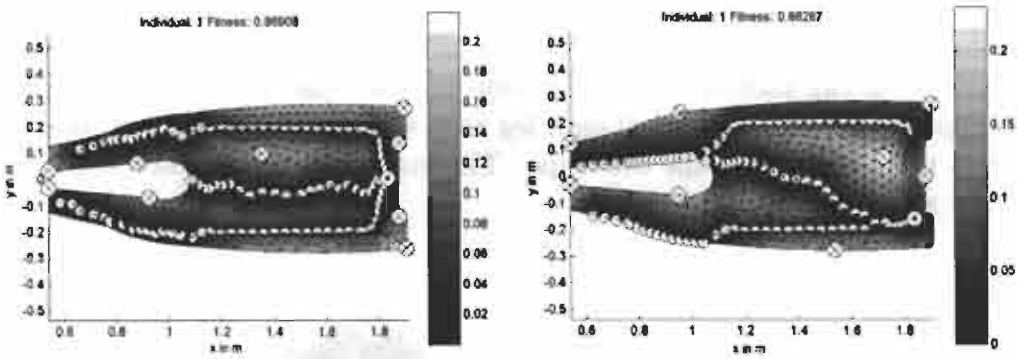

(a) Best solution (b) Second best solution

Figure 6.11: Optimal pipe position on a glider seat if 3 pipes are allowed.

6.6.3 Verification with the Physically Based Flow Model

Figure 6.11b shows the required position of the vents for this flow-pipe set-up. Since the mesh distance-based model is only geometrically based, the position of the vents should be verified with a simulation, using a physically based flow model. Here the flow model presented in Part I was used, without the preform compaction. The preform permeability and resin viscosity were both normalised to unity. The genetically based optimisation tool defines the flow pipes by nodes, whereas the physically based model uses the centroids of the control volumes. Therefore the physically based flow model was extended to accommodate the 2D flow pipes. A detailed description of this extension can be found in Appendix C. Figure 6.12 shows a 3D view of the seat with the 2D flow pipes and Figure 6.13 shows the meshed model.

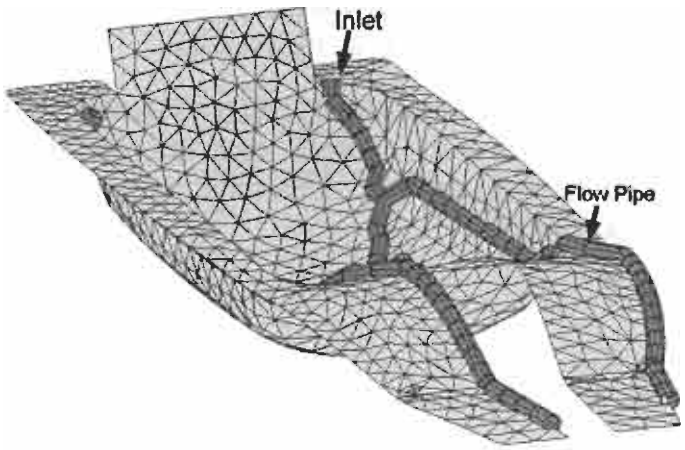

Figure 6.12: 3D view of the used model for the flow simulation.

The flow pipe had a permeability which was a factor 1000 higher than the rest of

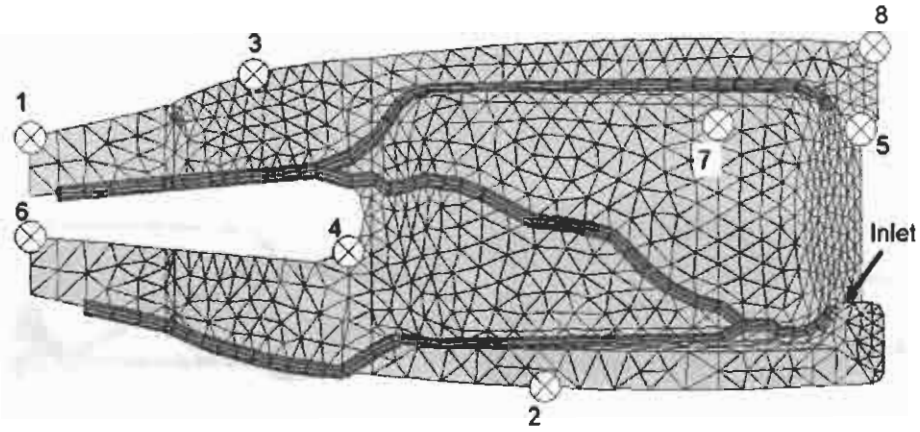

Figure 6.13: Flow pipe and inlet position used by the flow model and predicted vent position calculated by the flow model of Part I.

the preform. This is the same factor as used by the genetically based optimisation tool. The simulation of the mould filling with the physically based flow model took 32 minutes. The simulated propagation of the flow front is depicted in Figure 6.14, where t_n is the normalised time, which is defined by the time at that moment, t, divided by the total filling time, t_{total}.

The prediction of the position of the vents by the physically based flow model can be derived from this flow-front propagation, but is also presented in Figure 6.13. The number of vents and the area where these vents had to be positioned agreed quite well with the results of the mesh distance-based model. Only the exact positions differed slightly compared to the predicted positions by the genetically based optimisation model.

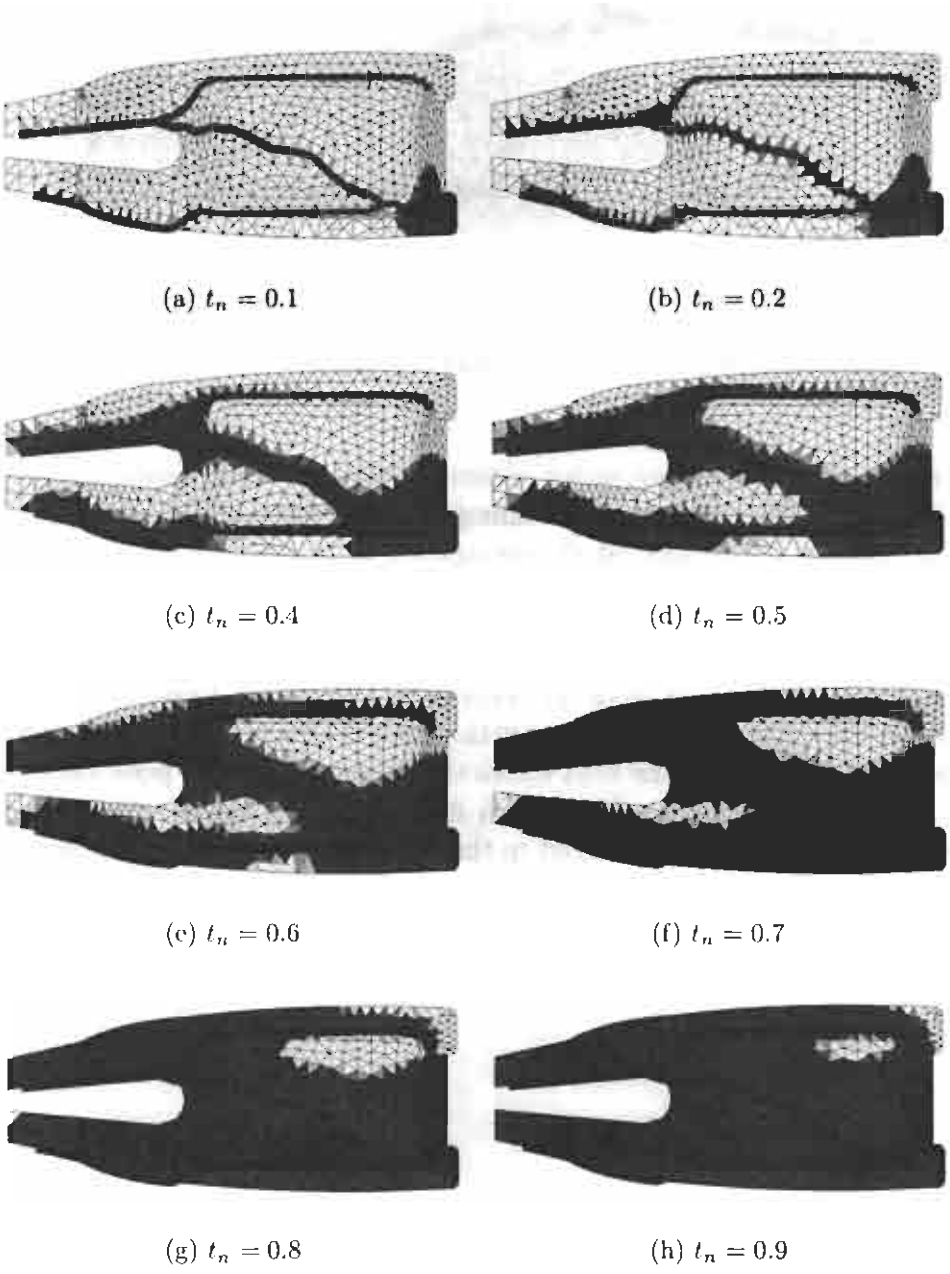

(a) $t_n = 0.1$ (b) $t_n = 0.2$

(c) $t_n = 0.4$ (d) $t_n = 0.5$

(e) $t_n = 0.6$ (f) $t_n = 0.7$

(g) $t_n = 0.8$ (h) $t_n = 0.9$

Figure 6.14: Simulated mould filling of a glider seat at different times, where $t_n = t/t_{total}$.

Chapter 7

Discussion of the Genetic Approach and its Results

7.1 Discussion

7.1.1 Calculated Distance

The distances calculated by the model, as presented in Section 6.1, differed up to 25% from the geometrical, direct distance in some areas. This error depends largely on the structure of the mesh. One extreme, where the relative error is zero, is the left side of the U-shaped plate of Figure 6.1 and at 0, 90, 180 and 270 degrees on the sphere. The nodes along these lines are on a straight line and therefore the error is, obviously, zero. Another extreme, where a maximum error occurs, is depicted in Figure 7.1.

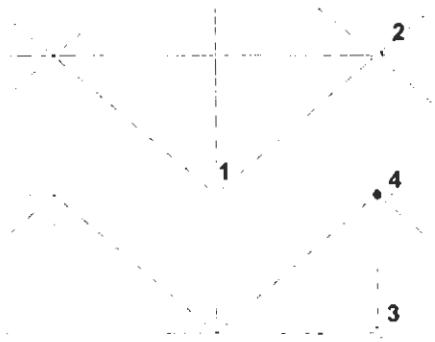

Figure 7.1: A structured mesh in which the nodes do not connect in every quadrant.

Assume the distances from node 1 to node 4, 2 to 4 and 3 to 4 are all 1. In that case, the geometric and mesh-based distance from node 1 to node 2 are both

$\sqrt{2}$. However, the mesh-based distance from node 1 to node 3 is 2 (via node 4), although this distance should also be $\sqrt{2}$. An error of 41% occurs, which is also the maximum error of the model.

This mesh-structure dependent error should be borne in mind when creating the mesh for a model. The nodes in the mesh should have one or more connections to other nodes in every quadrant and not be as node 4, for example. This node has only connections in the quadrants 3 and 4. Modern preprocessors, such as MSC-PATRAN as used here, have the possibility to generate such meshes, which reduces this error significantly.

As also shown, the error of the distance between two points reduced if the number of nodes between these points increased. Only the distance to the vents (maximum fill-distance) and the position and number of vents is of importance for the optimisation. Since the vents are positioned at the points furthest away from the inlet, the distance at the vents is relatively accurate (with the presented cases within 3%). The mesh distance-based model is therefore very well suited for minimizing the maximum fill-distance.

7.1.2 Position of the Vents

The position and the number of vents were also predicted well by the mesh distance-based model. For the scenarios presented in Section 6.2, the number of vents and their positions agreed 100% with the results known from the literature. In all these cases, the resin was injected from one or more points causing only a radial flow in the product. If the resin is injected using a flow pipe, the flow will be partially radial and partially linear. If these two different types of flow exist, the assumption that the point furthest away from the inlet or flow pipe is filled last may not be true. The mould filling of the glider seat, simulated by both the physically based model and the genetically based optimisation tool, showed that the position of the vents can be different. Although the number of vents and the region, where these vents should be placed, was predicted well by the mesh distance-based model, the exact position differed from that of the physically based model. Once an optimal solution is found and a more accurate location of the vents is desired, an extra simulation with a physically based flow model should therefore be performed.

7.1.3 Rectangular Plate

In the first design case, the flow pipe position on a rectangular plate was optimised. A total of 2340 individuals were calculated to come to convergence. The best solution after convergence agreed very well with the obvious optimal solution. It also showed that the genetic algorithm, used here, had a higher ef-

fectiveness than the one used by Jiang *et al.* (2002). They needed 3071 trials to optimise the position of 2 inlets (which is similar to a pipe defined by its begin and end point) for a 1036 node model. This is mainly due to the variable cross-over rate which allowed the solution to converge faster to the optimal solution (De Jong & Spears, 1990).

This design case also showed that the genetic algorithm became more effective if the number of design parameters, i.e. number of pipes, increased. The reason lies in the nature of the genetic algorithm and the problem itself: the begin and end positions of the pipes can be optimised independently from one another and, due to cross-over, the solutions found for the different pipes can be interchanged as well.

In the last optimisation scenario of the rectangular plate, the length of the flow pipes was also optimised. The calculation of the total pipe length was simplified by taking the number of flow pipe nodes as an indication for the total flow pipe length. Although this assumption saves significant calculation time, it requires a constant element edge length in the model. In the case of the rectangular plate, the diagonal element edges were a factor $\sqrt{2}$ longer than the horizontal and vertical ones. Therefore it can be expected that the model will favour flow pipes along the diagonal edges since more distance is covered with less flow pipe nodes. In the presented case, this phenomenon did not occur, which justified the simplification.

7.1.4 T-Shaped Plate

The optimisation of the T-shaped plate showed the influence of the fitness function. The number of vents could drastically be reduced (from 7 to 3) with the the fill-distance only increasing by 0.1 m. Although, in the second scenario, the objective was to find a solution with only 1 vent, the optimisation tool only found solutions with two and more vents. This correlates with the results of Boccard *et al.* (1995). They showed, for a similar shape, that at least 2 vents were necessary, since, if the inlet can be on any of the nodes in the model, there will be at least 2 local maximums.

The minimum number of vents can also be useful information for the mould design. The mesh distance-based model can provide this information by calculating the distance from every node to all other nodes. The minimum number of local maximums equals the minimum number of vents. Although this may sound elaborate and time consuming, it took the mesh distance-based model approximately 2 minutes for the 1581 node model to calculate the distance from every node to all other nodes.

7.1.5 Glider Seat

On a more complex shape, like the glider seat, the optimal pipe position is not always obvious and this is where the developed optimisation tool becomes very useful. Especially the second scenario showed that solutions with a fitness close to the optimal solution can be different but still of interest. After an optimisation cycle it is therefore recommended to look at all individuals of the last population, since one of these individuals (like the second best solution in this case) can be better suited for a reason, which cannot be or is not included in the fitness function.

The best solution for the 3-pipe-scenario was basically an extension of the best solution for the 2-pipe-scenario. If the best solution for the 2-pipe-scenario would have been used in the initial population for the 3-pipe-scenario, the optimal solution, as depicted in Figure 6.11a, would have been found within 30 generations. Although this reduces the calculation time significantly (from 351 to 30 generations) it has the disadvantage that the second best solution, as shown in Figure 6.11b, would not have been found. The best solution of the previous optimisation has a fitness which is much better than the other random individuals in the initial population. Due to the roulette wheel selection, the population will converge prematurely and other, sub-optimal solutions will not be found. A solution could be to use more populations simultaneously, as proposed by Pohlheim (1995). One population could start with the best solution of a previous optimisation cycle and the other population(s) with a random population. This would allow the algorithm to evolve different (sub-) optimal design solutions simultaneously. It is, however, questionable, with such a multi-population approach, whether the calculation time advantage still exists.

7.2 Conclusion

The genetically based optimisation tool developed in this part provided a fast method for optimising the different process parameters of the RIFT process. The optimisation tool was based on a mesh distance-based model and a genetic optimisation algorithm.

The genetic algorithm provided a stable and effective optimisation method. A variable cross-over rate increased the effectiveness. Depending on the choice of the fitness function, the algorithm was capable of optimising the different production parameters such as flow pipe position and length, fill-distance and number of vents, where previous models only focused on an optimal inlet/vent arrangement. The genetic algorithm did not only provide the optimal solution, but also the sub-optimal solutions, which were also of interest.

The mesh distance-based model gave a fast prediction of the fill-distance and position and number of the vents and was therefore very well suited for optimisation purposes. Although differences between the geometric distance and the calculated distances occur close to the inlet, the maximum fill-distances at the vents were within an acceptable range. The position and number of vents, predicted by the model, agreed 100% with the test cases known from literature.

As soon as different types of flow exist, as with the glider seat, the predicted positions of the vents differed from the actual ones. This did not influence the optimisation process, since the number and region were still correct, but required a final calculation with a physically based flow model to give a more exact vent position.

Chapter 8

General Conclusion and Recommendations

The main objectives of this research, as presented in Chapter 1, were to be able to simulate and to optimise the RIFT process in advance. Therefore 2 models were developed: a physically based flow model and a genetically based optimisation model.

The physically based flow model took all the process parameters such as the wet and dry compressibility and permeability of the preform, vacuum pressure and the resin inlet position and viscosity into account. The relation between these parameters was determined experimentally using compression, viscosity and permeability tests. New material models were developed to model the different wet and dry preform compressibility and permeability. A significant difference in wet and dry preform compaction was found. Therefore the preform compaction flux was taken into account as well. Finally the model was incorporated into a computer simulation tool which handles any $2\frac{1}{2}$D geometry.

The model was verified with known analytical solutions and experiments where the measured flow front propagation and preform thickness during mould-filling were compared with the simulated results. This verification showed that the model was able to predict the process properties such as fill-time, flow front propagation and preform thickness very well.

The preforms used for this research demonstrated different wet and dry preform compaction behaviour. The accuracy of the predicted flow front propagation and fill-times was significantly increased by taking these different wet and dry preform properties into account. The gained accuracy comes with a significant time penalty, since the process has to be modelled as transient and the fibre compaction flux has to be taken into account. For preforms with very similar wet and dry compaction behaviour, it could be possible that the results with and without the fibre compaction flux term are very similar. It would be advisable, in

these cases, to ignore the fibre compaction flux term and model the process quasi-static, as done in all previous models, since it will save significant calculation time. Further research should reveal whether it is possible to decide, in advance, whether or not the process should be modelled as transient, depending on the type of preform, compaction behaviour, resin speed and desired accuracy.

Determining the process parameters, especially the experimental determination of the preform permeability under different pressures, was quite time consuming. In the cases presented here, an isotropic permeability was assumed. In case anisotropic behaviour needs to be taken into account as well, the experimental effort will be even more intense. There are two ways to solve this problem. The method used in practice is to infuse a test plate of the used preform under a flexible bag. By monitoring the flow-front progression an "effective" permeability for the different directions can be found, as already mentioned in Section 2.1. This effective permeability can then be used to simulate the flow in a complex part. This method is much faster but also less accurate than the method described in Appendix B. Furthermore, the same vacuum pressure should be used for testing and final production. A more fundamental approach is to try to model the permeability and its variance, based on the preform properties such as yarn thickness, bundle size, weave type, stacking pattern, fibre type and stitch characteristics. As discussed in Appendix B, much research has already been done on this subject, but a major problem remains the large variations in measured and predicted permeabilities.

One objective was to be able to predict the final product properties such as product thickness and void content. One reason for voids in the final product is that, during the process, certain areas are closed off by the flow front and no longer connect with a vent. This can be predicted by the model, as shown in Section 6.6. The final product thickness, however, will depend on the pressure profile on the preform during curing. The developed model can be used for this purpose, simply by changing the boundary condition at the inlet as soon as the inlet is closed off. The pressure profile will gradually go from the profile depicted in Figure 4.1 to a flat profile where the pressure on the whole preform equals the applied vacuum pressure. How fast the pressure changes in the product will depend on the viscosity of the resin. The viscosity of the resin will change due to curing; hence the time-dependency of the resin viscosity should be modelled.

The developed genetically based optimisation tool allows for the optimisation of the process for the lowest costs and the highest quality products. The costs were minimised by minimising the amount of consumables and the mould-filling time. The product quality was maximised by placing vents in the required positions; hence reducing the chances of void formation.

The tool was based on a mesh distance-based flow model, which resulted in a fast computer simulation tool, handling any $2\frac{1}{2}$D geometry. The verification of the tool with cases known from literature and practical design cases showed that

the tool provided a stable and effective way to optimise the process in advance.

The choice of fitness function strongly influences the outcome of the optimisation. The weighting factors $w_{distance}$ and w_{pipes} and the penalty functions P_{vents} and $P_{distance}$ were chosen, based on the desired outcome. In practice, these values and functions will have to be coupled to production costs. For example it can be cheaper to use more vents and flow pipe length in order to reduce the fill-distance. Such a direct connection between the process costs and the amount of consumables, number of vents and the mould-filling time should also be the subject of further research.

Appendices

Appendix A

Compressibility of the used Preforms

Van Wijk (1946) was one of the first researchers who studied the elastic deformation behaviour of fibrous materials for the textile industry. Nowadays much of this work is also used in the research of advanced composite materials. The only major differences between textile bundles and advanced composite bundles are the degree of waviness (textile fibres can be very wavy), twist (composite fibres have typically no twist) and lubrication (Gutowski, 1997).

For the out-of-plain compression behaviour (compression in z direction) of fibrous preforms, Gutowski *et al.* (1987) developed a physically based model. This model is widely used and often referred to as the "Gutowski" model. This model is based on the assumption that the preforms consist of a lubricated fibre beam network. The fibres have a slight waviness sinusoidal character with a typical span length/height, denoted as β. The wavy fibres have a bending stiffness of E and a maximum possible fibre volume fraction of V_{max}. With these parameters, the Gutowski model describes the compression pressure as a function of the volume fraction with the following equation (Gutowski *et al.*, 1987):

$$P_f = 3\pi \frac{E}{\beta^4} \frac{(\sqrt{\frac{V_f}{V_0}} - 1)}{(\sqrt{\frac{V_{max}}{V_f}} - 1)^4} \tag{A.1}$$

The Gutowski model was developed for lubricated (saturated) preforms, although it could be fitted to dry preform compaction. Williams *et al.* (1998); Andersson *et al.* (2003); Kelly *et al.* (2004) showed that there is a significant difference between the preform compaction in a wet and dry state. Also Hammami (2001) was aware of this behaviour but did not use it in his model. Williams *et al.* (1998) measured a significant difference between wet and dry compaction while measuring the height during the RIFT process using a LVDT at a fixed

point. They recorded an almost constant compression in the unsaturated area. As soon as the flow front reached the LVDT, a rapid decrease in preform thickness at the resin front was observed, followed by a steady increase after the front had passed. Andersson *et al.* (2003) used different wet and dry preform compaction behaviour in their model account and were able to simulate this behaviour. Williams *et al.* (1998) explained this behaviour by the initial lubricating effect of the fluid, followed by a steady increase in pressure under the bag as the front moves further away from the LVDT.

Another geometrically based model was presented by Lomov & Verpoest (2000). They came up with a full mathematical description using the warp and weft yarn properties and weave structure. With their model, they were able to obtain a good correlation of experimental and computed results. Because their model is geometrically based, it also predicts the internal structure of the fabric in a compressed state, which can, for example, be used for flow calculations. The main drawback of the model is that it needs excessive input data such as yarn cross-section, linear density of warp and weft yarns, diagrams for yarn compression and flattening. Instead of measuring this data, it is often much easier to measure the global compressibility of the used fabrics and try to fit it in some sort of function or model, as in the case of the Gutowski model.

Many authors encountered problems fitting their experimental data into a physically based model, such as the Gutowski model, and found that the compaction behaviour of their materials was best described using empirical expressions. Most commonly, a non-linear elastic power law expression is used in the form:

$$P_f = Ah^n \tag{A.2}$$

In this equation, h is the preform height, P_f is the pressure applied on the preform, and A and n are material parameters to be determined through experiments (Hammami & Gebart, 2000; Andersson *et al.*, 2003; Kim *et al.*, 1991; Song *et al.*, 2004; Kelly *et al.*, 2004). Other authors, such as Robitaille & Gauvin (1999), used a logarithm expression in the form of:

$$P_f = A \cdot ln(P) + B \tag{A.3}$$

Where A and B had to be determined experimentally.

Other formulas were also used if the relaxation of the preform under a constant deformation had to be modelled. Relaxation can be significant. In RIFT, relaxation should not be an issue, since the deformation is not kept constant due to the flexible bag. However, if the material shows relaxation under constant pressure it is most likely to also show creep under constant pressure. Still, neither are taken into account for the materials used here. Robitaille & Gauvin (1998) showed that this relaxation can be significant if deformation speeds and

pressures are high (for example with RTM). However, Craen *et al.* (1998) showed that for the speeds and pressures used by RIFT, relaxation and creep do not play an important role.

A.1 Experiments

For the materials used in this research, there was no data available on either wet or dry preform compaction. Wet and dry compaction tests were performed, similar to the ones of Hammami (2001) and Kelly *et al.* (2004). The preforms were put between two solid plates with known area and then compressed while the used force and height change were measured. The compression speed was manually controlled but in all experiments lower than 5 mm/min. The experimental set-up is presented in Figure A.1.

Figure A.1: The experimental set-up for measuring the compression behaviour of the different preforms.

For the measurement of the wet preform compaction, the preform was wetted out with polyol before the compression experiment. Polyol was chosen because it had a consistency and viscosity (0.3 $Pa \cdot s$) similar to most common resins without having the problem of curing during the experiments.

A.2 Results

The results of the compression test for 2 layers of CoreTEX and 10 layers of 280 gram glass twill weave are presented in Figures A.2 and A.3 respectively.

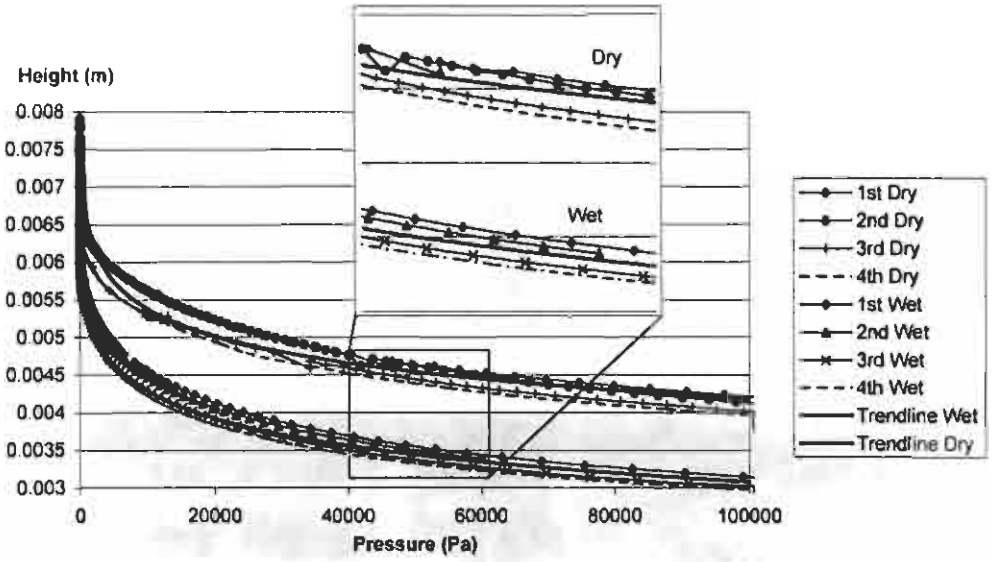

Figure A.2: The compression behaviour of 2 layers of CoreTEX.

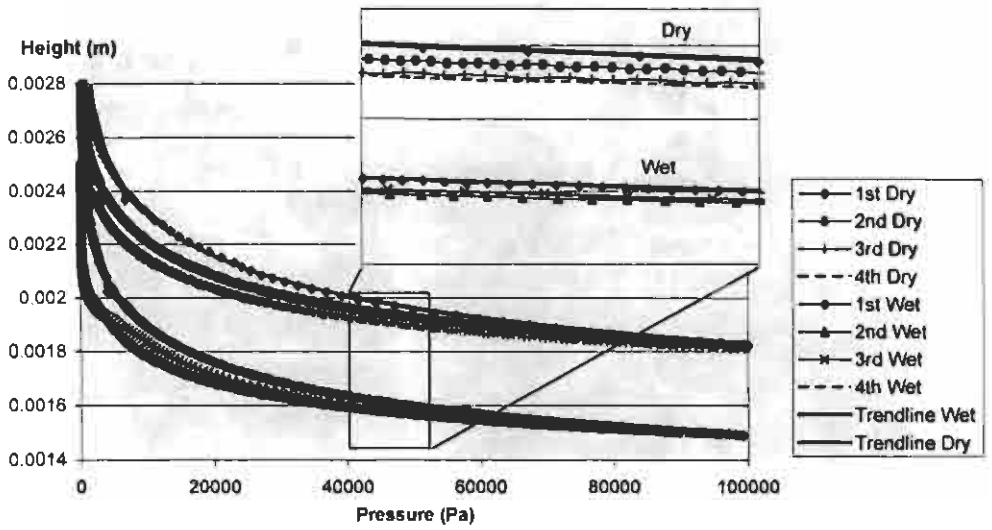

Figure A.3: The compression behaviour of 10 layers of 280gr. Glass Twill.

During the experiments, it was observed that repeating the compression test on the same sample led to a slightly higher compression compared to the first test at equal pressure. This is best demonstrated by Figure A.2. Williams *et al.* (1998) and Craen *et al.* (1998) explained this from a nesting effect of the material. Here, the results of the first tests of every sample were used, because it was assumed

that the preforms were not exposed to any pressure before the beginning of the process.

The results of the first test for the 10 layers of glass were fitted into a power law function and for the 2 layers of CoreTEX into a logarithm function for both wet and dry compaction. For the model presented here, it was desired to have the preform height as a function of the applied pressure instead of the inverse as in equation A.2. These functions are presented in Table A.1.

Table A.1: Functions to model the compression behaviour in a dry and wet state and the limit for the uncompressed thickness.

	10 layers Twill	2 layers CoreTEX
Wet h (m)	$h = 0.002918P^{-0.0559}$	$h = -5.22 \cdot 10^{-4} ln(P) + 0.009098$
Dry h (m)	$h = 0.0058786P^{-0.1013}$	$h = -5.23 \cdot 10^{-4} ln(P) + 0.01023$
Uncompr. h (m)	$h = 0.00287$	$h = 0.00691$

These functions approach infinity if the pressure goes to zero. This was solved by taking into account the maximum uncompressed preform height ("Uncompr. h" in Table A.1). This height was taken as an upper limit for the preform height.

Appendix B

Permeability of the used Preforms

The permeability as a function of the preform height (and hence fibre volume, see Eq. 2.4) is an area of much research. The most commonly used model is the Kozeny-Carman Theory, developed by Kozeny and Carman (Kozeny, 1927; Carman, 1937; Scheidegger, 1974). It describes the permeability as a function of the fibre volume, V_f, fibre radius r_f and the Kozeny constant, **s**, which has to be determined experimentally (Gutowski *et al.*, 1987):

$$\mathbf{K} = \frac{r_f^2}{4\mathbf{s}} \frac{(1 - V_f)^3}{V_f^2} \tag{B.1}$$

This equation was originally developed for granular beds consisting of ellipsoids and it has been assumed that it is also valid for fibrous porous media (Gebart, 1992). The drawback of this theory is that the predicted permeability is isotropic, which is obviously false for a unidirectional reinforcement. Gutowski *et al.* (1987) tried to overcome this problem by introducing different values for r_f for different directions. Another problem with Equation B.1 is that the permeability is still larger than zero for fibre volume fraction larger than the theoretical maximum V_f. Gutowski (1997) solved this problem by proposing the following heuristic model:

$$\mathbf{K} = \frac{r_f^2}{4\mathbf{s}} \frac{(\sqrt{\frac{V_a}{V_f}} - 1)^3}{(\frac{V_a}{V_f} + 1)} \tag{B.2}$$

where V_a also is an empirical parameter. Still, many researchers encountered problems fitting their results to these models and even suggested that the Kozeny constant, **s**, may vary with fibre volume fraction for a given preform. Therefore much research has been done to model the permeability (Gebart, 1992; Robitaille *et al.*, 2002) and its variance (Lawrence *et al.*, 2004; Loendersloot, 2006) on a macro and micro scale using channel-flowlike models to model the flow between the individual fibre tows.

B.1 Experiments

Here a global permeability for different preform thicknesses was established experimentally. A double-sided solid (RTM) mould with adjustable cavity height was used. The bottom mould is depicted in Figure B.1.

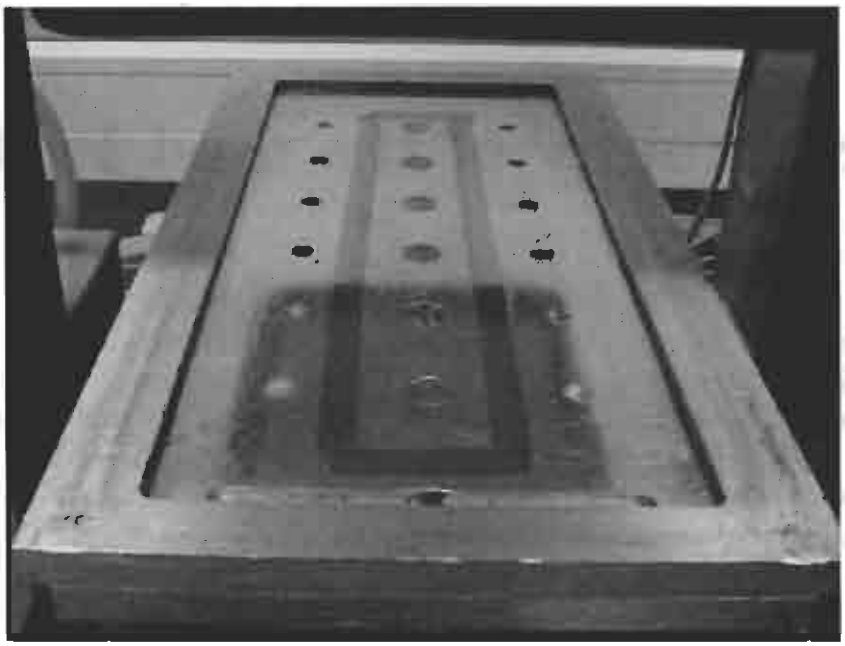

Figure B.1: The bottom mould with flow front and pressure sensors to measure the permeability for different preform thicknesses.

Using flow-front sensors (which basically consist of 2 copper wires which make electric contact when the resin passes), and a weight scale, the unsaturated and saturated flow rates at different cavity heights were measured. The permeability was calculated from the observed flow rates using Darcy's law. Curve fitting subsequently led to an empirical relation between the permeability and the fibre content. A power law was used to fit the experimental results for the materials used here.

B.2 Results

The results are presented in Figures B.2 and B.3 for the 2 layers of CoreTEX and the 10 layers of twill-weave respectively. Table B.1 also shows the power law functions which were fitted to the data in order to model the permeability.

Table B.1: Functions to model the permeability, K.

	10 layers Twill	2 layers CoreTEX
$K\ (m^2)$	$K = 381.84h^{4.8866}$	$K = 8.827 \cdot 10^{-05}h^{1.8375}$

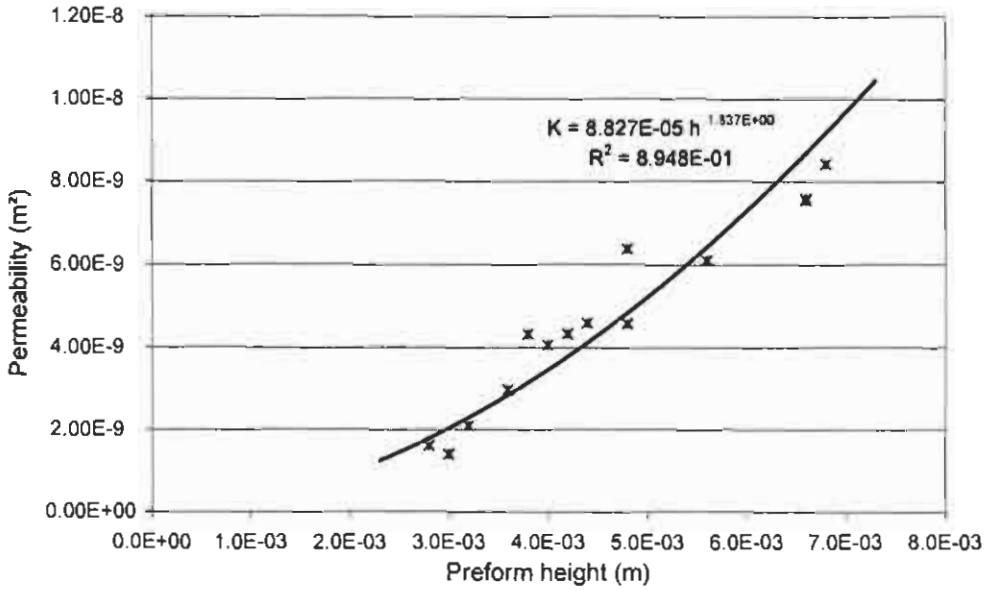

Figure B.2: Permeability as a function of preform height for 2 layers of CoreTEX.

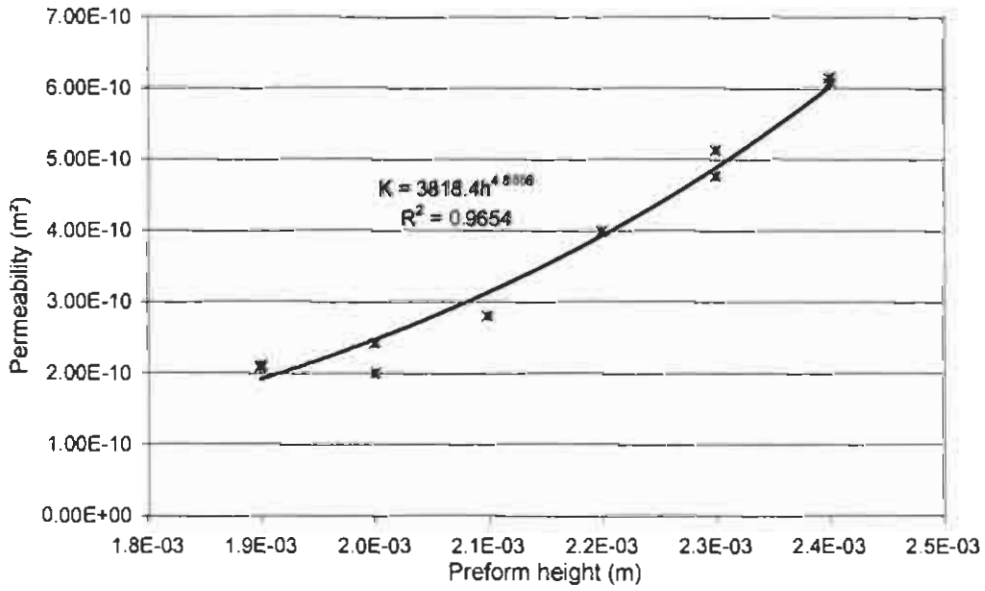

Figure B.3: Permeability as a function of preform height for 10 layers of 280 gr. Glass Twill.

Appendix C

Modelling the Flow Pipes

The physically based flow model of Part I used the centroids of the control volumes to calculate the flow in the preform. The genetically based optimisation tool calculated the optimal flow pipe arrangement along the nodes and edges of the control volumes. In order to use the results of the optimisation routine directly with the physical flow model, the flow model had to be extended to accommodate the 1D flow pipes.

A meshed model of the preform, with on top the flow pipes, is schematically represented in Figure C.1. In this figure, N1 ... N3 are nodes, P1 and P2 are the pipes and E1 and E2 are triangular CVs. Pipe P1 is located on the common edge of E1 and E2.

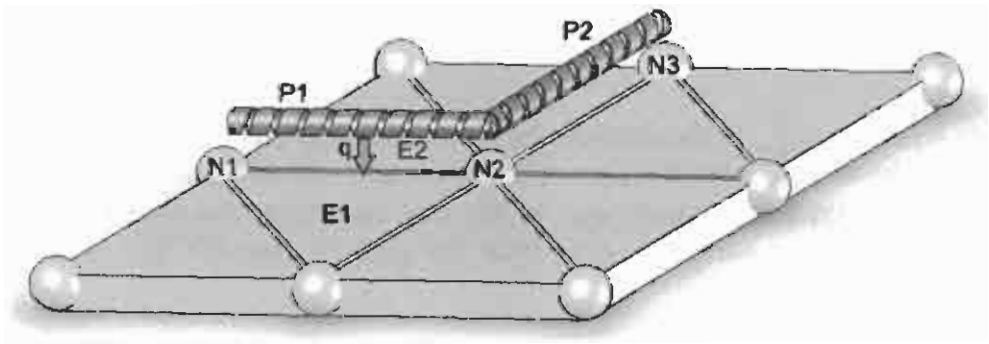

Figure C.1: A model of the preform, meshed with control volumes, with on top the flow pipes.

Figure C.2 shows a more simplified 2D sketch of the flow pipes P1 and P2 and an extra pipe P3.

The flow in the pipe was modelled using Poiseuille's law, as already presented in Chapter 5, Equation 5.1. The application of the finite volume method to

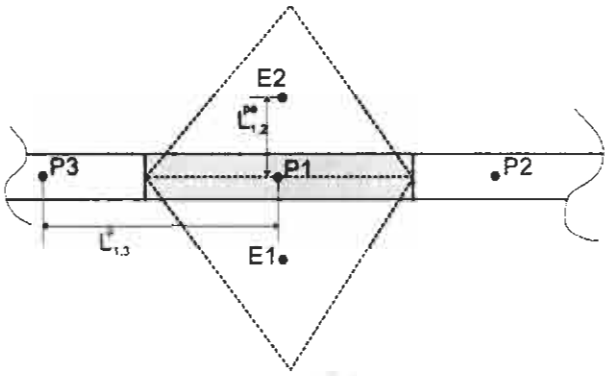

Figure C.2: Top view of the flow pipe P1 with its neighbouring CVs E1 and E2.

the solution of this equation for 1D pipe elements was extensively described by Versteeg & Malalasekera (1995). The discretised equation for the flow in the pipes is very similar to Equation 2.7 of Section 2.3, but instead of a net flow over 3 faces, there is only a flow over 2 faces (hence $n = 1..2$). However, the flow pipes also communicate with the preform. In Figure C.1, this is depicted with an additional resin flux q from pipe P1 to the underlying CVs E1 and E2. Hence the discretised continuity equation for the pressure, P_1^p, in pipe P1 can be written as:

$$C_{1,2}^p(P_2^p - P_1^p) + C_{1,3}^p(P_3^p - P_1^p) - q = 0 \tag{C.1}$$

where

$$C_{1,n}^p = \frac{\pi r^4}{8\mu L_{1,n}^p} \tag{C.2}$$

In this equation, $L_{1,n}^p$ is the distance between the centroids of the flow pipes P1 and Pn. The flux, q, from the pipe into the control volumes has to comply with Darcy's Law (Eq.2.1). A part, $q_{1,1}$, of the flux goes from the pipe P1 into the CV E1 and another part, $q_{1,2}$, goes from the pipe P1 into CV E2. The flux q can hence be written as:

$$\begin{array}{rccc} q = & q_{1,1} & + & q_{1,2} \\ q = & C_{1,1}^{pe}(P_1^e - P_1^p) & + & C_{1,2}^{pe}(P_2^e - P_1^p) \end{array} \tag{C.3}$$

In this equation the superscripts p and e refer to the values in the pipe and the CV respectively. The superscript pe refers to the interaction term between the pipe and the CVs. For example:

$$C_{1,2}^{pe} = \frac{K}{\mu} \frac{A_{1,2}}{L_{1,2}^{pe}} \tag{C.4}$$

This term is similar to the term presented in Equation 2.8. Here, $A_{1,2}$ is the cross-section of the face between E1 and E2, where pipe P1 is located. $L_{1,2}^{pe}$ is the distance between the centroids of pipe P1 and the CV E2, as depicted in Figure C.2.

The discretised continuity equation for the control volumes was already presented in Section 2.3, Equation 2.7. For reasons of simplicity, the preform compaction flux term is omitted. For every control volume which borders to a flow pipe, an extra flux term from the flow pipe has to be added. For example, equation 2.7 for CV E1 becomes:

$$q_{1,1} + \sum_{n}^{1..3} C_{n,e}^{e}(P_n - P_e) = 0 \tag{C.5}$$

The assembly of the continuity equations for all the i CVs and all the j flow pipes leads to the following linearised system:

$$\begin{bmatrix} & & \\ C^{e} & C^{pe} & \\ & & \\ C^{pe} & C^{p} & \\ & & \end{bmatrix} \begin{bmatrix} P_1^e \\ \cdots \\ P_i^e \\ P_1^p \\ \cdots \\ P_j^p \end{bmatrix} = 0 \tag{C.6}$$

This system is solved in the same way as the system of Equation 2.11, knowing that the pressure at the inlet pipe element is equal to the atmospheric pressure and at the flow front equal to the vacuum pressure. The position of the flow front is tracked in the same way as presented in Section 2.4, with an extra fluid presence function for the flow in the pipes.

Bibliography

ACHESON J.A., SIMACEK P. & ADVANI S.G., 2004. The implications of fiber compaction and saturation on fully coupled VARTM simulation. *Composites Part A: Applied Science and Manufacturing*, 35:159–169.

ANDERSSON H.M., LUNDSTRÖM T.S. & GEBART B.R., 2003. Numerical model for vacuum infusion manufacturing of polymer composites. *International Journal of Numerical Methods for Heat & Fluid Flow*, 13(2–3):383–394.

BEASLEY D., BULL D.R. & MARTIN R.R., 1993. An overview of Genetic Algorithms: Part 2, Research Topics. *University Computing*, 15(4):170–181.

BOCCARD A., LEE W. & SPRINGER G., 1995. Model for determining the vent locations and the fill time of resin transfer molds. *Journal of Composite Materials*, 29(3):306–323.

BOOKER L., 1987. Improving search in genetic algorithms. (*In* Davis L., *ed.*, Genetic Algorithms and Simulated Annealing, London: Pitman, Chapter 5, p. 61–73).

BROUWER W., VAN HERPT E. & LABORDUS M., 2003. Vacuum injection moulding for large structural applications. *Composites Part A: Applied Science and Manufacturing*, 34:551–558.

CAI Z., 1992. Analysis of Mold Filling in RTM Processes. *Journal of Composite Materials*, 26(9):1310–1338.

CARMAN P.C., 1937. Fluid Flow Through a Granular Bed. *Transaction of the Institution of Chemical Engineers*, 15:150–166.

CASTILLO L., BALDWIN M., SASSINE M.P. & MERGLER D., 2001. Cumulative exposure to styrene and visual functions. *American Journal of Industrial Medicine*, 39(4):351–360.

CORREIA N.C., ROBITAILLE F., LONG A.C., RUDD C.D., SIMACEK P. & ADVANI S.G., 2004. Use of Resin Transfer Molding Simulation to Predict Flow, Saturation, and Compaction in the VARTM Process. *Journal of Fluids Engineering*, 126:210–215.

CRAEN J.A., GROVE S.M. & SUMMERSCALES J., 1998. The compression response of fibre beds subjected to repeated loading cycles in the *RIFT* manufacturing process. (*In* 7th International Conference on Fibre-Reinforced Composites held in Newcastle-upon-Tyne on 15 until 17 April 1998. Cambridge: Woodhead Publishing, p. 120–127).

DAVIS S.F., 1994. Flux difference splittings and limiters for the resolution of contact discontinuities. *Applied Mathematics and Computation*, 65:3–18.

DE JONG K.A. & SPEARS W.M., 1990. An analysis of the interacting roles of population size and crossover in genetic algorithms. (*In* Proceedings of the First Workshop of parallel Problem Solving from nature. Berlin: Springer Verlag, p. 38–47).

FERZIGER J.H. & PERIĆ M., 1997. Computational Methods for Fluid Dynamics. Springer.

GARCIA J.A., GASCÓN L. & CHINESTA F., 2002. A fixed mesh numerical method for modeling the flow in liquid composites moulding processes using a volume of fluid technique. *Computer methods in applied mechanics and engineering*, 192:877–893.

GEBART B.R., 1992. Permeability of Unidirectional Reinforcements for RTM. *Journal of Composite Materials*, 26:1100–1133.

GOKCE A. & ADVANI S.G., 2004. Simultaneous gate and vent location optimization in liquid composite molding processes. *Composites Part A: Applied Science and Manufacturing*, 35:1419–1432.

GOLDBERG D.E., 1989. Genetic algorithms in search, optimization, and machine learning. Reading, Massachusetts: Addison-Wesley.

GOTCH T., 1978. Improved Production Process for Manufacturing of GRP on British Rail. (*In* 11th Reinforced Plastics Conference. BPF RPG, Brighton, Paper 4. p. 33–39).

GRIMSLEY B.W., HUBERT P., SONG X., CANO R.J., LOOS A.C. & PIPES R.B., 2001. Flow and Compaction in the Vacuum Assisted Resin Transfer Molding Process. (*In* Proceedings of the 33rd International *SAMPE* Technical Conference: held in Seattle, Washington, November 4-8).

GUNNARSSON A.T., 2004. Icelandic boat builders switch to resin infusion. *REINFORCED plastics*, p. 34–36.

GUTOWSKI T., 1997. Advanced composites manufacturing. New York: John Wiley & Sons.

GUTOWSKI T.G., MORIGAKI T. & CAI Z., 1987. The consolidation of laminate composites. *Journal of Composite Materials*, 21:172–188.

HAMMAMI A., 2001. Effect of Reinforcement Structure on Compaction Behavior in the Vacuum Infusion Process. *Polymer Composites*, 22(3):337–348.

HAMMAMI A. & GEBART B.R., 2000. Analysis of the Vacuum Infusion Molding Process. *Polymer Composites*, 21(1):28–40.

HAN K., JIANG S., ZHANG C. & WANG B., 2000. Flow modeling and simulation of *SCRIMP* for composites manufacturing. *Composites Part A: Applied Science and Manufacturing*, 31:79–86.

HIRT C.W. & NICHOLS B.D., 1981. Volume of Fluid (*VOF*) Method for the Dynamics of Free Boundaries. *Journal of Computational Physics*, 39:201–225.

HOLLAND J., 1975. Adaption in natural and artificial systems. The University of Michigan Press, Ann Arbor.

HOU T.H. & JENSEN B.J., 2004. Evaluation of Double-Vacuum-Bag Process for Composite Fabrication. (*In SAMPE* 2004 Symposium & Exhibition , Long Beach, California, May 16-20).

HOUCK C.R., JOINES J.A. & KAY M.G., 1998. A Genetic Algorithm for Function Optimization: A Matlab Implementation. website:www.ie.ncsu.edu/mirage/GAToolBox/gaot/papers/gaot.ps. Last modified: Fri Jun 12 10:22:12 EDT 1998.

HSIAO K.T., DEVILLARD M. & ADVANI S.G., 2004. Simulation based flow distribution network optimization for vacuum assisted resin transfer moulding process. *Modelling and simulation in materials science and engineering*, 12:175–190.

JIANG S., ZANG C. & WANG B., 2002. Optimum arrangement of gate and vent locations for RTM process design using a mesh distance-based approach. *Composites Part A: Applied Science and Manufacturing*, 33:471–481.

KELLY P., UMER R. & BICKERTON S., 2004. Compaction of dry and wet fibrous materials during infusion processes. (*In* SAMPE Technical Conference, held in San Diego, November 2004).

KIM Y., MCCARTHY S. & FANUCCI J., 1991. Compressibility and Relaxation of Reinforcements during Composite Processing. *Polymer Composites*, 12:13–19.

KOOREVAAR A., 2002. Simulation of Liquid Injection Molding. (*In* Proceedings of the *SAMPE* 2002 Conference. Held at JEC in Paris, April).

KOZENY J., 1927. Ueber Kapillare Leitung des Wassers im Boden. *Sitzungsberichte der Akademie der Wissenschaften in Wien*, 136:271–306.

LAWRENCE J.M., BARR J., KARMAKAR R. & ADVANI S.G., 2004. Characterization of preform permeability in the presence of race tracking. *Composites Part A: Applied Science and Manufacturing*, 35:1393–1405.

LEE L.J., YOUNG W.B. & LIN R.J., 1994. Mold filling and cure modeling of *RTM* and *SRIM* processes. *Composite Structures*, 27:109–120.

LIN M., MURPHY M. & HAHN H., 2000. Resin transfer molding process optimization. *Composites Part A: Applied Science and Manufacturing*, 31:361–371.

LOENDERSLOOT R., 2006. The structure-permeability relation of textile reinforcements. PhD Thesis, University of Twente.

LOMOV S. & VERPOEST I., 2000. Compression of woven reinforcements:a mathematical model. *Journal of Reinforced Plastic Composites*, 19(16):1329–1350.

LOOS A.C., 2001. Low-cost fabrication of advanced polymeric composites by resin infusion processes. *Advanced Composite Materials*, 10(2).

LOPATNIKOV S., SIMACEK P., GILSSEPIE J. JR & ADVANI S.G., 2004. A closed form solution to describe infusion of resin under vacuum in deformable fibrous porous media. *Modelling and Simulation in Materials Science and Engineering*, 12(3):191–204.

LUO J., LIANG Z., ZHANG C. & WANG B., 2001. Optimum tooling design for resin transfer molding with virtual manufacturing and artificial intelligence. *Composites Part A: Applied Science and Manufacturing*, 32:877–888.

MALLICK P., 1988. Fiber-reinforced composites:materials, manufacturing, and design. New York: Marcel Dekker, Inc.

MAN K., TANG K. & KWONG S., 1999. Genetic Algorithms, Concepts and Designs. London: Springer Verlag.

MARCO, 1950. Marco Method. US Patent no. 2495640, filed January 24.

MIRAVETE A., 1999. 3-D textile reinforcements in composite materials. Cambridge: Woodhead Publishing Limited.

MODI D., SIMACEK P. & ADVANI S., 2003. Influence of injection gate definition on the flow front approximation in numerical simulations of mold filling processes. *International Journal for Numerical Methods in Fluids*, 42:1237–1248.

PATANKAR S.V., 1980. Numerical Heat Transfer and Fluid Flow. McGraw-Hill.

POHLHEIM H., 1995. Ein genetischer Algorithmus mit Mehrfachpopulationen zur Numerischen Optimierung. *Automatisierungstechnik*, 3:127–135.

ROBITAILLE F. & GAUVIN R., 1998. Compaction of textile reinforcements for composites manufacturing. I:review of experimental results. *Polymer Composites*, 19(2):198–216.

ROBITAILLE F. & GAUVIN R., 1999. Compaction of textile reinforcements for composites manufacturing. III:Reorganization of the fiber network. *Polymer Composites*, 20(1):48–61.

ROBITAILLE F., LONG A.C. & RUDD C.D., 2002. Permeability prediction for industrial preforms. *Plastics, Rubber and Composites*, 31(6):238–248.

SCHEIDEGGER A.E., 1974. The Physics of Flow Through Porous Media. University of Toronto Press, third edition.

SEEMANN W., 1989. Plastic Transfer Molding Techniques for the production of fiber reinforced plastic structures. US Patent No. 4,902,215, filed Mar. 30.

SONG X., LOOS A.C., GRIMSLEY B.W., CANO R.J. & HUBERT P., 2004. Modeling the VARTM Composite Manufacturing Process. (*In* Proceedings of SAMPE 2004 - Long Beach, CA May 16 - 20).

SUMMERSCALES J., 2002. Clean efficient manufacture of composites using resin infusion under flexible tooling (*RIFT*). (*In* Composites Processing Association. Papers read at the Composites Processing 2002 Congress, held in Birmingham Airport, 24 January 2002. Birmingham. Paper 4).

SUTERA S.P. & SKALAK R., 1993. The history of Poiseuille's law. *Annual Review of Fluid Mechanics*, 25:1–19.

TERZAGHI K. & PECK R.B., 1963. Soil Mechanics in Engineering Practice. John Wiley & Sons, Inc, second edition.

THAGARD J.R., OKOLI O.I., LIAN Z., WANG H.P. & ZHANG C., 2003. Resin infusion between double flexible tooling: prototype development. *Composites Part A: Applied Science and Manufacturing*, 34:803–811.

VAN WIJK C., 1946. Note on the compressibility of wool. *Journal Textile Inst.*, 37:285–292.

VERSTEEG H.K. & MALALASEKERA W., 1995. An introduction to Computational Fluid Dynamics. Longman Group Ltd.

WHITE D.M., DANIELL W.E., MAXEWELL J.K. & TOWNES B.D., 1990. Psychosis Following Styrene Exposure: A Case Report of Neuropsychological Sequelae. *Journal of Clinical and Experimental Neuropsychology*, 12(5):798–806.

WILLIAMS C., GROVE S. & SUMMERSCALES J., 1998. The compression response of fibre-reinforced plastic plates during manufacture by the resin infusion under flexible tooling method. *Composites Part A: Applied Science and Manufacturing*, 29A:111–114.

WILLIAMS C., SUMMERSCALES J. & GROVE S., 1996. Resin Infusion under Flexible Tooling (*RIFT*) a review. *Composites Part A: Applied Science and Manufacturing*, 27A:517–524.

YOUNG W., 1994. Gate location optimization in liquid composite molding using genetic algorithms. *Journal of Composite Materials*, 28(12):1098–1113.

Index